NAVAL POSTGRADUATE SCHOOL
Monterey, California

THESIS

SIMULATION OF A ROTORCRAFT IN TURBULENT FLOWS

by

Robert D. Moran, Jr.

September 1991

Thesis Advisor J. V. Healey

Unclassified

security classification of this page

REPORT DOCUMENTATION PAGE

1a Report Security Classification Unclassified			1b Restrictive Markings
2a Security Classification Authority			3 Distribution Availability of Report
2b Declassification Downgrading Schedule			Approved for public release; distribution is unlimited.
4 Performing Organization Report Number(s)			5 Monitoring Organization Report Number(s)
6a Name of Performing Organization Naval Postgraduate School	6b Office Symbol *(if applicable)* 31		7a Name of Monitoring Organization Naval Postgraduate School
6c Address *(city, state, and ZIP code)* Monterey, CA 93943-5000			7b Address *(city, state, and ZIP code)* Monterey, CA 93943-5000
8a Name of Funding Sponsoring Organization	8b Office Symbol *(if applicable)*		9 Procurement Instrument Identification Number
8c Address *(city, state, and ZIP code)*			10 Source of Funding Numbers

Program Element No	Project No	Task No	Work Unit Accession No

11 Title *(Include security classification)* SIMULATION OF A ROTORCRAFT IN TURBULENT FLOWS

12 Personal Author(s) Robert D. Moran, Jr.

13a Type of Report	13b Time Covered	14 Date of Report *(year, month, day)*	15 Page Count
Master's Thesis	From To	September 1991	103

16 Supplementary Notation The views expressed in this thesis are those of the author and do not reflect the official policy or position of the Department of Defense or the U.S. Government.

17 Cosati Codes			18 Subject Terms *(continue on reverse if necessary and identify by block number)*
Field	Group	Subgroup	Computer Simulation, Rotorcraft,turbulent flow, tunnel strikes

19 Abstract *(continue on reverse if necessary and identify by block number)*

Accurate simulation of helicopters in an at-sea-shipboard environment is desired to provide realistic operating envelopes without incurring the enormous cost of real-time flight tests. This study examines the simulation of rotorcraft in turbulent flow by looking at previous attempts at helicopter-ship interfacing, current efforts in this area, and what will be needed in the future. Part of this study is devoted to the construction of an analytic model of the "tunnel strike" problem of the CH-46 Sea Knight helicopter that is based on measurements made over the flight deck of a model ship. A computer model was constructed, with the aim of modeling the "tunnel strike" during engagement aboard AOR type ships. The remainder of the study is concerned with the simulation of the motion of a helicopter in the turbulent wake of a DD-963 class ship. Results show that a sixth order transfer function can filter white noise to accurately model the turbulence spectra at specific points along a helicopter glide path in the wake. While a tunnel strike could not be successfully modeled using DYSCO software, a simple blade-element program was developed to show the aerodynamic forces on the rotor blades in a specific flow field over an AOR class ship flight deck. That program shows the location and magnitude of the aerodynamic forces contributing to the flapping of the rotor blades, which results in the rotor blades impacting the fuselage.

20 Distribution/Availability of Abstract	21 Abstract Security Classification	
☒ unclassified unlimited ☐ same as report ☐ DTIC users	Unclassified	
22a Name of Responsible Individual I. V. Healey	22b Telephone *(include Area code)* (408) 646-2804	22c Office Symbol 67He

DD FORM 1473,84 MAR 83 APR edition may be used until exhausted
All other editions are obsolete

security classification of this page

Unclassified

Approved for public release; distribution is unlimited.

Simulation of a Rotorcraft in Turbulent Flows

by

Robert D. Moran, Jr.
Captain, United States Marine Corps
B.M.E., Villanova University, 1979

Submitted in partial fulfillment of the
requirements for the degree of

MASTER OF SCIENCE IN AERONAUTICAL ENGINEERING

from the

NAVAL POSTGRADUATE SCHOOL
September 1991

Author: 
Robert D. Moran, Jr.

Approved by: 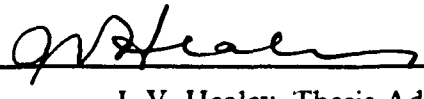
J. V. Healey, Thesis Advisor

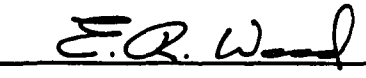
E.R. Wood, Second Reader

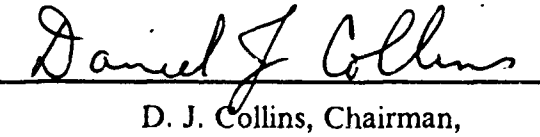
D. J. Collins, Chairman,
Department of Aeronautics and Astronautics

ABSTRACT

Accurate simulation of helicopters in an at-sea-shipboard environment is desired to provide realistic operating envelopes without incurring the enormous cost of real-time flight tests. This study examines the simulation of rotorcraft in turbulent flow by looking at previous attempts at helicopter-ship interfacing, current efforts in this area, and what will be needed in the future. Part of this study is devoted to the construction of an analytic model of the "tunnel strike" problem of the CH-46 Sea Knight helicopter that is based on measurements made over the flight deck of a model ship. A computer model was constructed, with the aim of modeling the "tunnel strike" during engagement aboard AOR type ships. The remainder of the study is concerned with the simulation of the motion of a helicopter in the turbulent wake of a DD-963 class ship. Results show that a sixth order transfer function can filter white noise to accurately model the turbulence spectra at specific points along a helicopter glide path in the wake. While a tunnel strike could not be successfully modeled using DYSCO software, a simple blade-element program was developed to show the aerodynamic forces on the rotor blades in a specific flow field over an AOR class ship flight deck. That program shows the location and magnitude of the aerodynamic forces contributing to the flapping of the rotor blades, which results in the rotor blades impacting the fuselage.

THESIS DISCLAIMER

The reader is cautioned that computer programs developed in this research may not have been exercised for all cases of interest. While every effort has been made, within the time available, to ensure that the programs are free of computational and logic errors, they cannot be considered validated. Any application of these programs without additional verification is at the risk of the user.

TABLE OF CONTENTS

LIST OF TABLES

LIST OF FIGURES

ACKNOWLEDGEMENTS

I would like to thank Professor J. Val Healey for his guidance, patience, and countless suggestions which made this project a success. Many thanks to Professor Dan Collins for his invaluable assistance with control theory concepts. My deepest gratitude to Tony Cricelli for his help on the VAX, and for his time spent working with DYSCO and Kaman Industries so that DYSCO could be used for this project. Thanks also to Dean Carico at the Naval Air Test Center for assistance. This project could not have been done without the encouragement, love and friendship of my wife, Nancy. I am deeply indebted to her for the sacrifices she has made.

I. INTRODUCTION

Interface flight tests are used to determine the operating envelopes for various helicopters on the various classes of U.S. Navy ships. The high cost of ship-helicopter interface flight tests indicate the need for a faster and less expensive method to determine the safe operating envelopes of the fleet's helicopters on aviation capable ships. One solution to this is to attempt to develop an accurate, real-time computer simulation of various ship-helicopter combinations [Ref. 1]. In order to accomplish this a computer model must include a sufficiently accurate math model of the dynamics and aerodynamics of the helicopter, and the operating environment. Several attempts have been made to model the aerodynamic wake turbulence for various class ships, all of which have resulted in simulations that bear no relation to the real flight. One such attempt, made by Fortenbaugh, was the use of Strouhal number scaling to extrapolate the ship air-wake model of a FF-1052 for a DD-963 class [Ref. 2].

For aircraft simulations in land based flight, the current MILSPEC dictates the use of a Dryden stochastic model [Ref. 3]. Since the wake of each class of ship is different no such standardization is possible. This turbulence has a great influence on the operation of helicopters aboard Navy ships, and needs to be modeled correctly in order to provide an accurate simulation for pilot training. The greatest concerns at the present time are methods used to combine ship air-wake turbulence models, such as those developed by Fortenbaugh [Ref. 2] and Hanson [Ref. 4] with an accurate helicopter math model that gives a true representation in real-time of the helicopter's motion in all flight profiles. This is extremely difficult to do in any quantitative way, considering the numerous stability derivatives present in a six degree-of-freedom helicopter model.

Another area of particular interest at the present time is the rotor engage/disengage envelope of Navy/Marine helicopters on aviation capable ships at sea. This interest is due to the occurrence of rotor blade strikes to the fuselage during rotor engagement and disengagement. This problem has occurred on the AOR and LHA class ships frequently enough to warrant investigations into their cause. In order to complement completed studies of airwake aerodynamics of the flight deck of the AOR class ships [Ref. 5], this study will concentrate on the AOR class ship. Current limitations are illustrated in Figure 1 on page 2.

AOR CLASS SHIPS ROTOR ENGAGE/DISENGAGE WIND LIMITS		
All Wind Azimuths Relative to Ship's Centerline/		Maximum Wind Speed (Knot)
Aircraft Parallel To Ship's Centerline	Aircraft Parallel To Port-To-Starboard Landing Lineup Line	Aircraft Parallel To Starboard-To-Port Landing Lineup Line
345 to 015/35 016 to 040/30 041 to 180/45 181 to 235/25 236 to 320/15 321 to 344/25	340 to 005/45 006 to 035/35 036 to 050/30 051 to 070/20 071 to 080/30 081 to 180/45 181 to 235/25 236 to 310/15 311 to 339/35	345 to 005/45 006 to 025/40 026 to 040/30 041 to 180/45 181 to 255/20 256 to 325/25 326 to 344/40

Figure 1. CH-46 Rotor Engage/Disengage Limits for AOR Class Ship.
Source: NAVAIR A1-H46D-NFM-000, H-46D NATOPS Manual

Due to both the atmospheric turbulence and that caused by the airflow around the various superstructure elements of the ship, a highly turbulent recirculating flow exists on the helicopter landing deck, typically located on the aft end of the ship. Previous work by Anderson has attempted to measure these flows in a wind tunnel environment that simulates the air-wake turbulence of a DD-963 class ship [Ref. 6]. These unsteady turbulent flows restrict the starting and stopping of rotor systems due to excessive flapping of the blades. One of the most severe restrictions apply to the CH-46 Sea Knight tandem rotor helicopter, built by Boeing Helicopter Company (Boeing Vertol). The "tunnel strike" occurs when the blades of the aft rotor head bend down far enough to strike the fuselage and housing or "tunnel" that covers the interconnecting shaft between the aft and forward rotor systems, near the $\Psi = 180°$ position, with $\Psi = 0°$ located along the longitudinal axis as shown in Figure 2 on page 3.

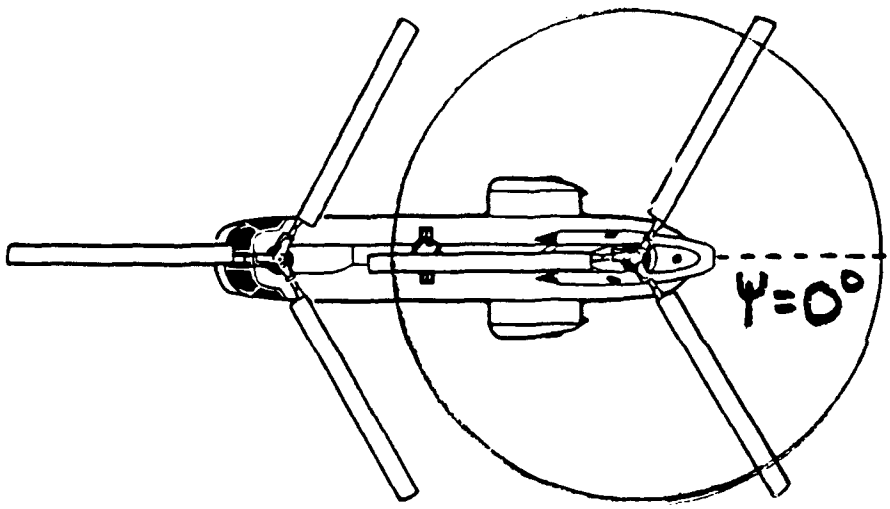

Figure 2. CH-46 Sea Knight Relative Blade Position.
Source: NAVAIR A1-H46D-NFM-000, H-46D NATOPS Manual

Analytical studies by Leone at Boeing have indicated a possible source of the problem, but no solution or safe operating envelope has been found without using actual flight tests [Ref. 7]. If a computer model of the "tunnel strike" could be made using either math models or physical models of various ships, determination of safe envelopes could be done faster and cheaper. One possible solution is to construct a computer model of the H-46 and expose it to a physical model of the flow over the flight deck in an attempt to create tunnel strikes constructed from current mishap data. One potential modeling tool is DYSCO, a dynamic system coupling program produced by Kaman Aerospace. The details of this system will be discussed later. By introducing velocities obtained from Computational Fluid Dynamics (CFD) programs or wind tunnel tests, it may be possible to simulate strikes for various helicopter positions on the flight deck, as well as for different class ships. A limitation of using the velocities from CFD programs is that the power spectra of the velocity fluctuations cannot be predicted at present, and thus cannot account for other than mean airflow velocities. If successful, such a method could replace the expensive and time consuming flight tests now used to determine safe rotor engagement/disengagement envelopes.

Thus, the goals of this project are twofold. First, to investigate the steps that would need to be taken to incorporate a stochastic ship air-wake turbulence model into a helicopter math model capable of reacting accurately to the multi-directional, multi-valued velocities and produce a real-time simulation with sufficiently fast computation time. Second, to use the wind component velocities obtained from a CFD program (not yet developed) or from tunnel tests at the Naval Postgraduate School in an analytic code to duplicate actual tunnel strike incidences, and then investigate with this model possible safe engagement/disengagement envelopes for specific ship classes.

A. PREVIOUS STUDIES

1. Air Wake Studies

Studies of the airwakes of ships were done at Boeing Vertol Company in 1976 for a FF 1052 class frigate and 1980 for a DD-963 Class destroyer. These air-wake models were obtained using scaled models of the ships in a uniform-flow wind tunnel [Ref. 8] [Ref. 9]. The details of how the models were obtained are explained by Anderson [Ref. 6: p. 4.]. The FF-1052 model was used in 1978 by Fortenbaugh, in an attempt to generate data for the DD 963 class destroyer and used Strouhal scaling to relate the frequencies. This scaling procedure is valid for relationships between different sizes of the same ship, not for ships of different configurations.

Based on the recommendation of Fortenbaugh, the airwake of a scale model of the DD 963 class destroyer was mapped in a wind tunnel by Boeing in 1980 [Ref. 9]. Again, the same assumption of no environmental turbulent boundary layer was used.

A study by Nave produced several algorithms with which to mathematically model the ships' airwakes for incorporation into a motion simulator [Ref. 10: p. 6.]. As with all simulators studied, Nave's turbulence model assumes a point mass aerodynamic model in which all aerodynamic forces and moments are calculated from the mean value of airspeed, angle of attack, and sideslip at the aircraft center of gravity [Ref. 10 : p. 16]. This is due to the availability of single point data only, as noted by Anderson [Ref. 6: p. 2.], since no multi-point model for helicopters exists. Using a second order filter equation, Nave investigated several variations of damping and filter frequency. The filter helps shape the straight line Gaussian noise to the values required to represent the power spectral density of the velocity fluctuations in the ship's airwake. The form of the filter is:

$$F(S) = \frac{K(S + a)}{S^2 + 2\zeta\omega_n S + \omega_n^2}$$

using the baseline of $\omega_n = \frac{1.9V}{59}$ and $\zeta = 0.4$, where K is the filter gain, ω_n is the system frequency, a is the minimum phase zero of the transfer function and V is the airflow mean velocity, as suggested by Garnett. [Ref. 10: p. 28.] [Ref. 8] This configuration matched the characteristics of the measured data. Unfortunately, these relations are derived from wind tunnel data in a uniform flow, and without the use of an environmental boundary layer and they must be viewed with some skepticism.

Hanson [Ref. 4] also developed a turbulence model, based initially on the airwake data from the DD-963 model developed by Fortenbaugh. Hanson refined Nave's analysis of processing the output of the random number generators prior to being input into first order shaping filters. This was done by generating the random numbers at intervals other than the time frame of the simulation and linearly interpolating the random number sequence for time values between the successive calls to the random number generator, in order to give a smoothly varying number sequence. This method is shown in Figure 3, where η_I is the interpolated Gaussian white noise input, and v_i is the filtered white noise output [Ref. 4: p.11]

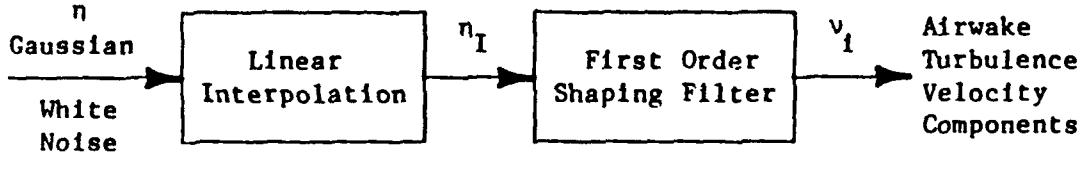

Figure 3. Block Diagram of Linear Interpolation Scheme
Source: Hanson, G.D., *Airwake Analysis*

Nave's method [Ref. 10] produced turbulence levels that were too high, according to pilot reports on the flight characteristics of the model as installed in the NASA Ames H-2 simulator model, and thus required modifications. These modifications included changing the means and variances of the FF-1052 data base to a DD-963 data base, elimination of the Strouhal scaling relations with development of a DD-963 wind tunnel data base [Ref. 9], and changing the extrapolation of the shaping functions to exponential versus the cosine type functions used by Nave [Ref. 4 : p.31.].

Anderson's study of DD-963 Airwake Turbulence [Ref. 6] at the Naval Postgraduate School included measurements along three typical helicopter landing paths, but the data was defective due to a hot-wire system malfunction. These data points have since been retaken and are discussed in this study and presented in Reference 11.

2. Helicopter Models

a. GENHEL

One helicopter simulator in use today is GENHEL, developed by Sikorsky Helicopters, and run on a CDC 7600 machine. This is a six degree of freedom (DOF) system, and was used in the development of the UH-60 Black Hawk. The flow diagram for this simulator is illustrated in Appendix C. The atmospheric turbulence model used is the Dryden model, as required by current military specifications [Ref. 3: p. 45.]. This model is represented by the algorithm:

$$\frac{n\,S(n)}{\sigma^2} = \frac{4\,\tilde{n}}{1+(2\pi\tilde{n})^2}$$

where $\tilde{n} = n\frac{L}{U}$, n being the frequency, L turbulence length scale and U the mean component velocity. This function is used frequently because of its simplicity; however, the accuracy of this function falls off with increasing frequency [Ref. 1: p. 14.].[Ref. 12: p.2]. Inputs required for the GENHEL program include:

Aircraft velocity relative to the airmass

Longitudinal turbulence length scale

Root mean square (rms) gust velocities

These inputs provide the environment for calculating the effects of the turbulence on the fuselage and rotor blades. The blade forces are found by strip theory, summing up the contributions of each blade for forces and moments. The rotor forces and moments are obtained in a wind-hub coordinate system, then transformed to a hub-body system.

These forces and moments are then given in reference to the body CG by transforming all forces and moments to body axes.[Ref. 12: p. 4.]

b. Parallel Processing

One of the problems with introducing non-steady flows to rotary wing aerodynamics is the large amount of computation necessary to achieve an accurate solution. Most of these effects require implementation of the Navier-Stokes equations, which are expensive to solve. Such a solver was introduced by Wake and Sankar, but full scale Navier-Stokes are not yet feasible on the CRAY-2 supercomputer due to the extremely fine grid system required to resolve the boundary layer [Ref. 13]. Since supercomputers are expensive, and the Navier-Stokes equations cannot be solved in real time, both are impractical for simulator use.

One approach is to simplify the entire model. This has been accomplished by Messerschmitt-Belkow-Blohm GmbH (MBB) in West Germany. The rotor aerodynamic model is based on blade-element theory, including the effects of compressibility, stall, and reverse flow effects. Also included are rotor downwash (by modified momentum theory) and the influence of ground effect on the rotor. This, along with rotor flapping dynamics are considered for each blade separately. All blade forces are computed simultaneously by a separate processor for each blade, and when each processor is finished, the total rotor forces are computed. See Figure 4 on page 8 for the flow diagram of this process. The total simulation model is presented in Figure 5.[Ref. 14]

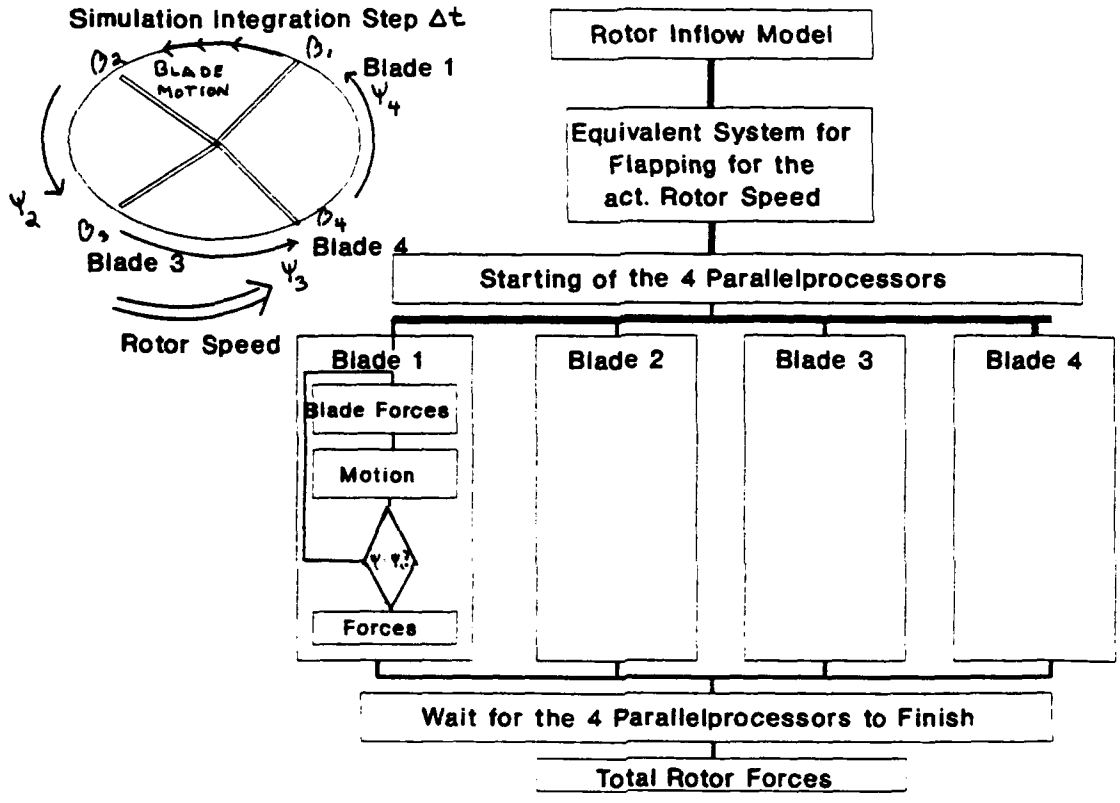

Figure 4. Parallel Calculation of Blade Dynamics (4 blades)

Source:Huber, H., *AGARD CP 359*

While modeling the unsteady aerodynamics is difficult, modeling a helicopter in atmospheric turbulence only complicates the problem, and dims the prospect for a real-time solution. MBB, using their parallel processors, introduce discrete gusts and continuous stochastic disturbances in accordance with MIL-F-8785C [Ref. 3: p. 45.]. The stochastic disturbances are simulated by passing a random signal (white noise) through a first order lag function, and adjusting the filter gain and time constant to produce a power spectrum match with the Dryden model [Ref. 15: p. 68.]. That lag function is:

$$G_f(S) = \frac{A}{1 + B\,S}$$

where A is the filter gain, and B is the location of the single pole of the system. Taking into consideration the Dryden model for the horizontal gust component, the horizontal turbulence power spectra model would be:

$$F_u(S) = \sqrt{\frac{2\,\sigma_u^2\,L_u}{a^2\,\Delta t\,v}}\;\frac{1}{1 + L_u/vs}$$

where $F_u(S)$ is the power spectra, with the sampling frequency Δt and the factor "a" to adjust the standard deviation of the noise source. Here, L_u is the horizontal length scale, σ_u is the horizontal variance of the noise, and v is the magnitude of the velocity vector of the wind disturbance. This method is employed in this study to obtain suitable models for the power spectra in the wake of a ship. [Ref. 15: p. 69.]

B. A PREVIOUS TUNNEL STRIKE STUDY

Early investigation of the excessive flapping of CH-46 rotor blades was conducted in 1964 by Peter Leone [Ref. 7]. He studied the transient aero-elastic response of the helicopter blade, and the excessive flapping and droop-stop impact. This study was done with the rotor RPM at one hundred percent, with a step input to the rotor system from the cyclic pitch controls. Using the Myklestad finite difference equations, Leone calculated the fundamental and first modes in flapping [Ref. 7 : p.36.]. This assumes only cantilever flapping motion, without consideration of coupling with the lead-lag and torsion modes. This approach also used only mean wind flows, and did not account for discrete or random wind gusts. In 1982, at the request of NAVAIR, Boeing Helicopter conducted an analytical study of excessive flapping at low rotor RPM [Ref. 16]. This report noted that upflow through the rotor disk contributed to the high bending de-

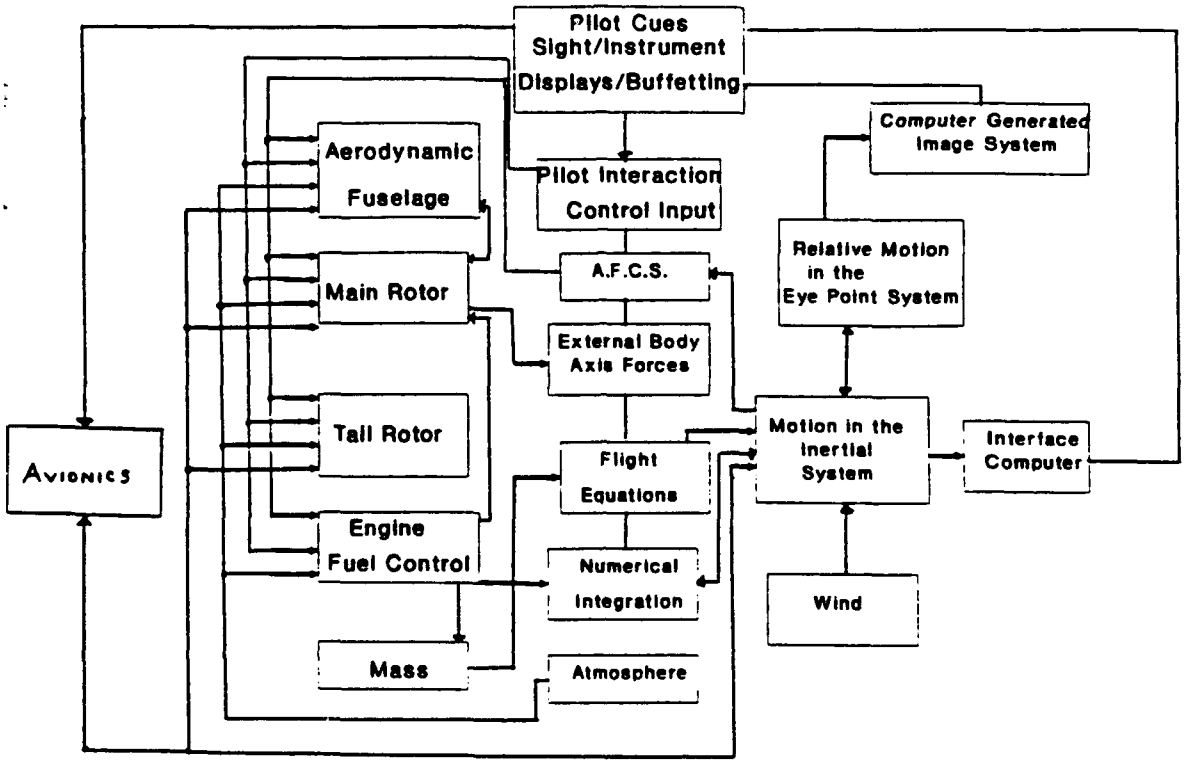

Figure 5. Total Simulation Model (MBB)
Source: Huber, H., *AGARD CP 359*

flections with the blades. Using a company program labeled as LO2 and a RPM acceleration rate similiar to that on page 31, the maximum bending deflections to hit the

fuselage occurred at 16 RPM, which agree with tunnel strikes reported before and after Leone's study. Leone's assumptions of the angle of attack of the wind through the rotor system were based on wind tunnel flow visualization techniques of an oil rig [Ref. 7 : p.5.]. Figure 6 on page 12, Figure 7 on page 13, and Figure 8 on page 14 illustrate the results of Leone's investigation. Figure 6 shows the position of the rotor disk with respect to the flight deck and incoming wind vector, and the rationale for the angle of attack of 15°. Figure 7 illustrates the upward blade displacement as a function of main rotor RPM, while Figure 8 shows the downward blade displacement as a function of main rotor RPM. Using this angle of attack, he broke down the wind to vertical and horizontal components, addressing only the mean velocity for each component. Using the assumption that this vertical flow from the side of the ship would cause the rotor blade to "sail" up until it impacted the upper flap restraint, he computed the blade tip deflection using the first bending mode.

Unfortunately, the geometry of the oil rig is a poor representation of the landing deck of a ship. Thus, the low (15°) angle of attack assumption made here causes Leone's results to be suspect. While there is no argument of the existence of an upflow as the wind meets the side of the ship, flow visualizations by Johns [Ref. 17] indicate that turbulence levels exist that would require the use of more than just the mean velocities to compute the effects of the vertical relative wind component on the exposed rotor blade. The behavior of the upflows on the AOR were investigated by Rhoades [Ref. 5] who made measurements at four points around the blade-tip trajectory of the aft CH-46 rotor for a range of ship-wind relative velocity vectors. Mean values of the velocities are used in Chapter III due to the unavailability of more suitable values and the simplicity of the model developed.

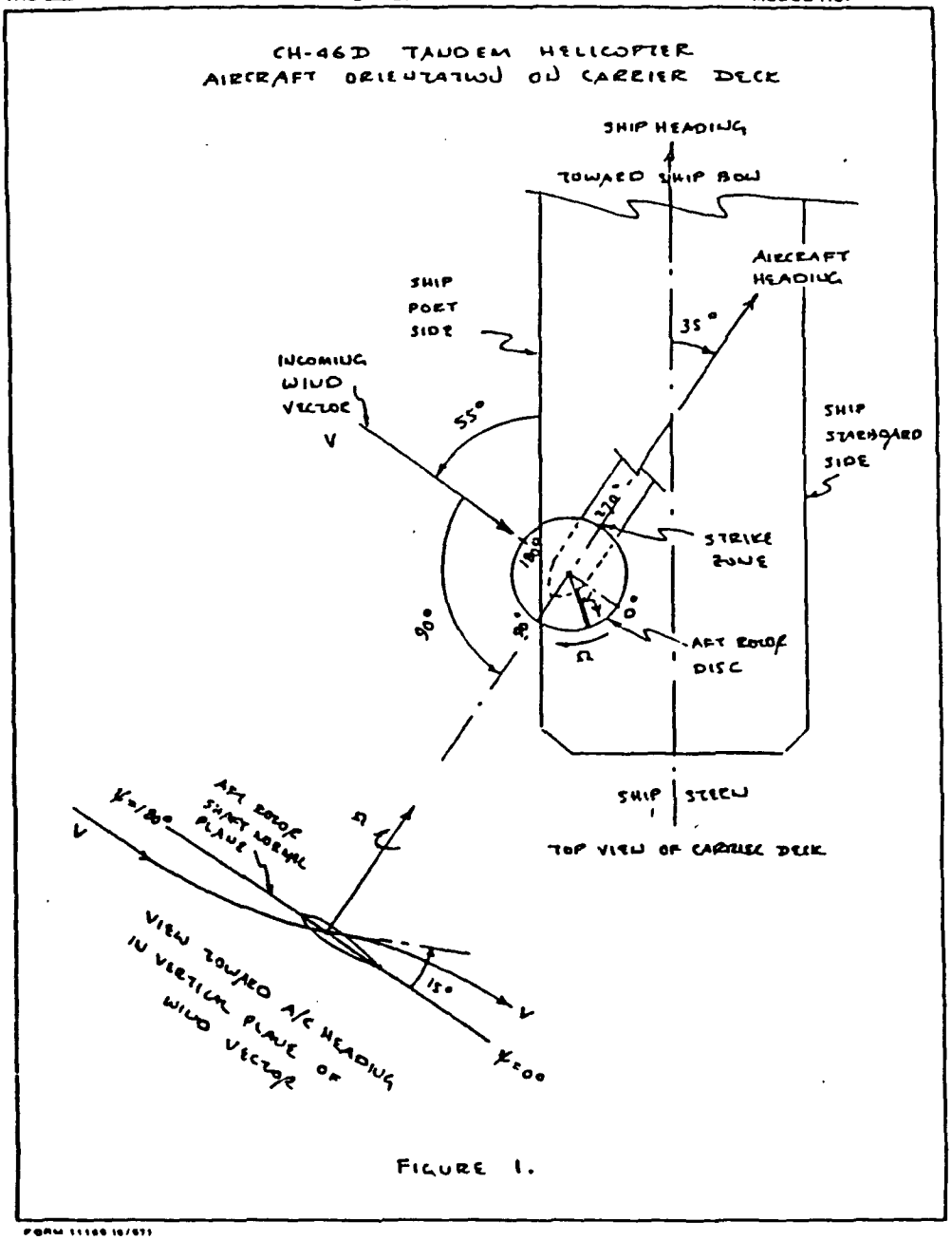

FIGURE 1.

Figure 6. Tunnel Strike Analysis

Source: Leone, P.F., Boeing Rpt. 8-7450-PFL-06

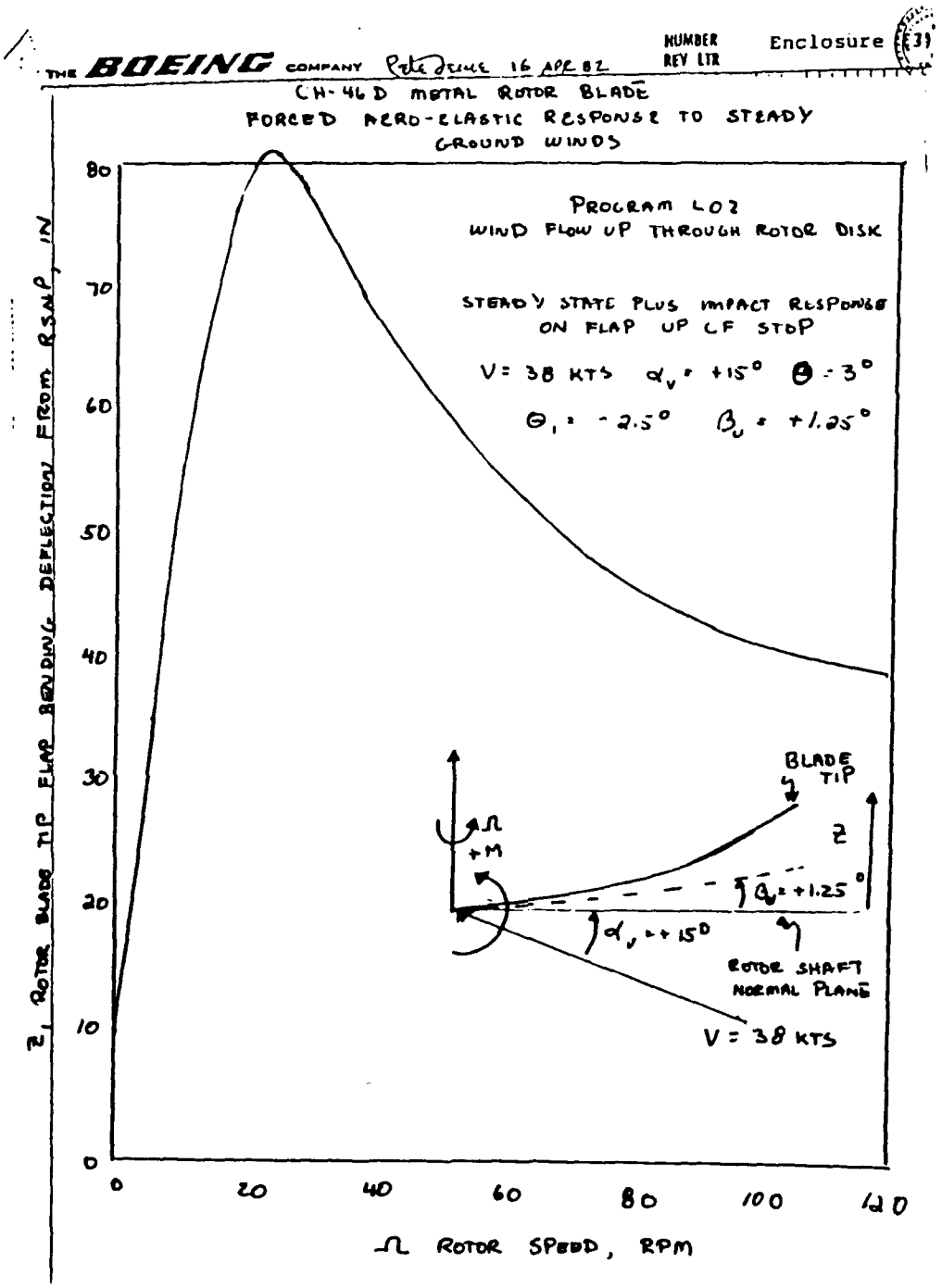

Figure 7. Tunnel Strike Analysis

Source: Leone, P.F., Boeing Rpt. 8-7450-PFL-06

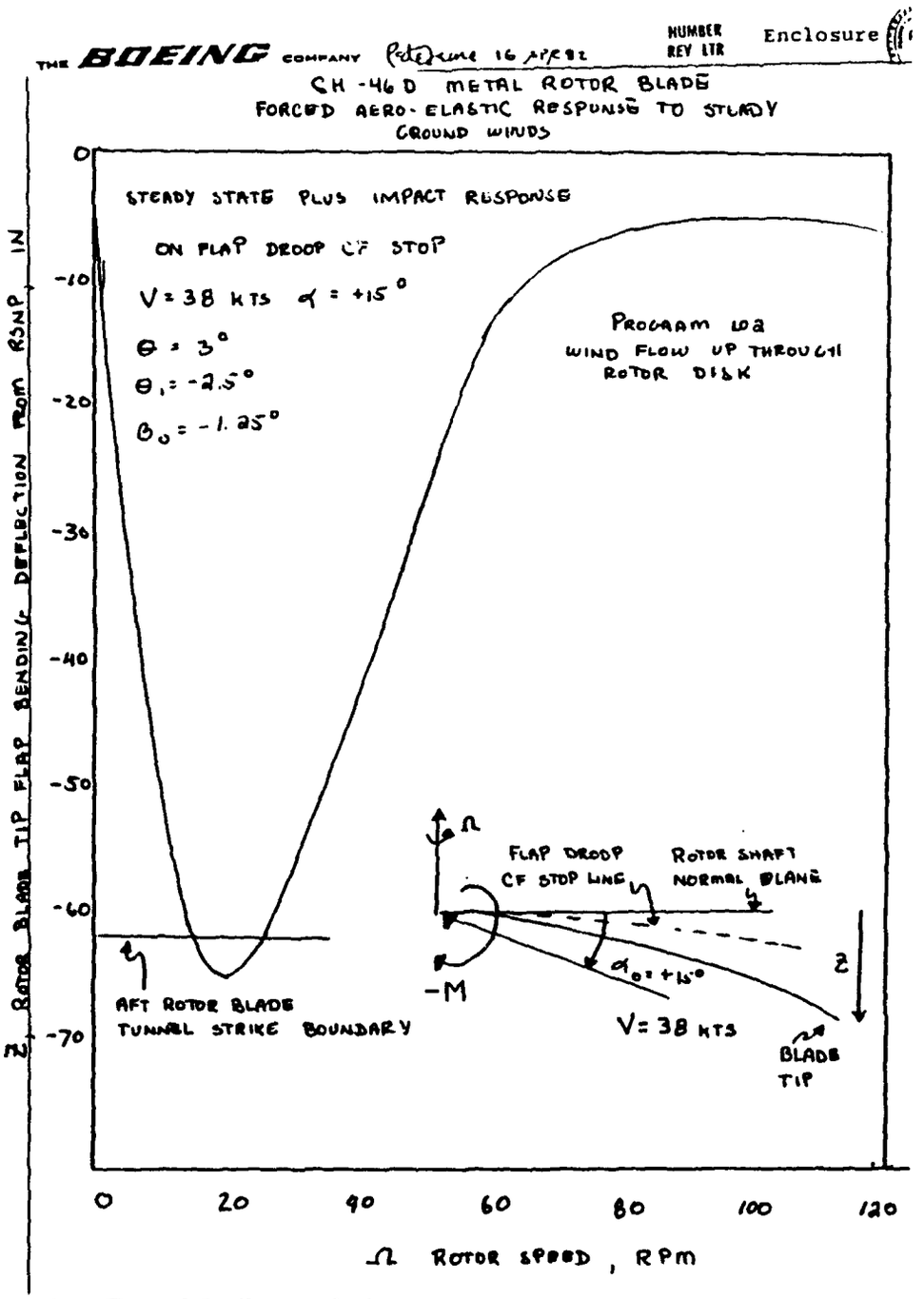

Figure 8. Tunnel Strike Analysis

Source: Leone, P.F., Boeing Rpt. 8-7450-PFL-06

II. THEORY OF TUNNEL STRIKE AND AIR-WAKE TURBULENCE MODELS

A. DYNAMIC SYSTEM COUPLER PROGRAM (DYSCO)

The program DYSCO is used in this study to model the flapping behavior of the main rotor blades of the CH-46 helicopter. DYSCO is installed on a Digital Electronics Corporation VAX 2000. It is an interactive computer program which allows the user to model the dynamic and aerodynamic behavior of rotorcraft and other aerospace structures [Ref. 18: p.1]. This is done using component modules to represent the second-order ordinary differential equations which may have constant, time-dependant, or non-linear coefficients. For the CH-46 Tunnel Strike model, the following components were used:

CFM2	Two Dimensional Modal Fuselage
CRE3	Elastic Rotor Blades
CSF1	Finite Element Structure (Landing Gear and Blade Weight)
CES1	Elastic Stop (Droop and Flap Restraints)
FRA3	General Aerodynamic Force Module
STH4	Time History Solver (Integrator)

The following assumptions apply to the use of DYSCO [Ref. 18]:

1. All angles are small, which allows approximations.
2. The relevant physics of a system may be modeled as a set of second-order differential equations in the time domain. The equations are of the form:

$$M\ddot{X} + C\dot{X} + KX = F$$

   where X is the vector of the displacements, M, C, and K are coefficient matrices, and F is the force vector.
3. It is possible to formulate the equations of a system based on the equations of the components of the system.
4. It is possible to compute the state vector $(X, \dot{X})$ of each component based on the state vector of the system.

1. **Rotor Blade Model**

Since the main concern of this study is the flapping of the rotor blades, the flapping equations will be examined in detail. Figure 9 shows the various components assembled to make the model of the H-46.

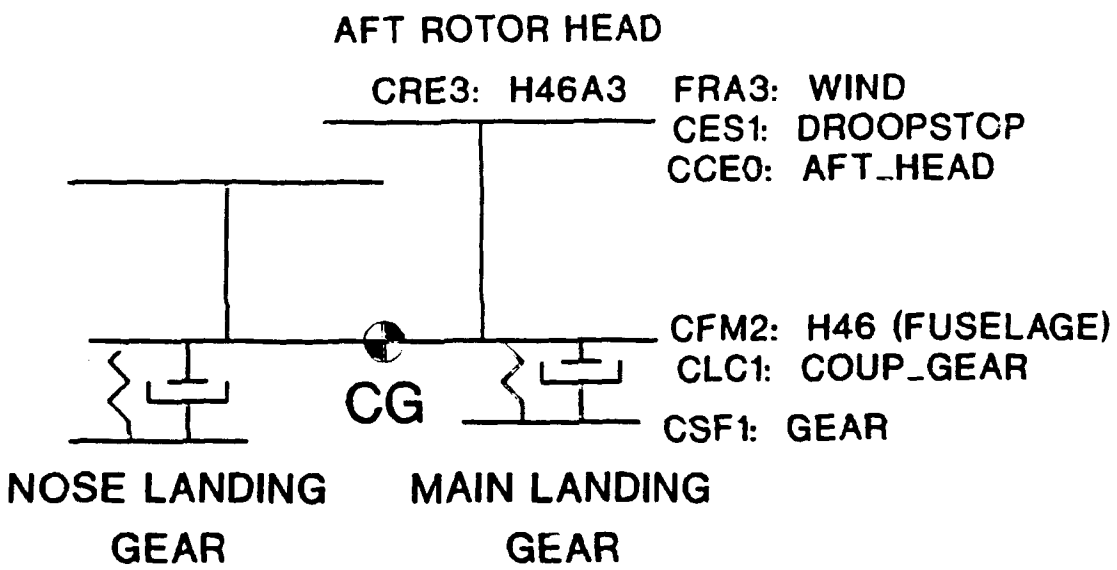

Figure 9. DYSCO Model of CH-46

Figure 10 on page 17 shows the three primary degrees of freedom that are of interest in this study. Hamiltons's law of varying action has

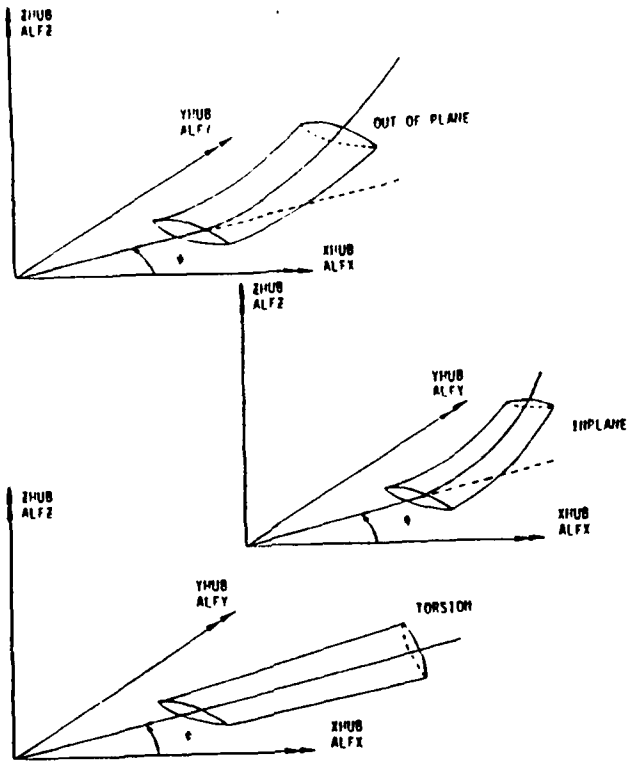

Figure 10. Degrees of Freedom for Rotor Blade Element.
Source: DYSCO Theoretical Manual

been used to derive the equations of motion in a generalized coordinate system which allows a direct solution without the consideration of force equilibrium [Ref. 18: p.12]. To avoid higher order terms that might complicate the equations of motion, an ordering scheme was adopted to determine which terms should be ignored. The following scheme was employed in DYSCO:

Table 1. ORDERING SCHEME USED IN DYSCO.

$u/R = O(\varepsilon^2)$	$\eta, \zeta/R = O(\varepsilon)$
$v/R = O(\varepsilon)$	$c, t/R = O(\varepsilon)$
$w/R = O(\varepsilon)$	$e/R = O(\varepsilon)$
$x/R = O(1)$	$\beta_{pc} = O(\varepsilon)$
$\phi = O(\varepsilon)$	

$$X_H, Y_H, Z_H, \alpha_x, \alpha_y, \alpha_z = O(\varepsilon)$$

where the following are:

R	Rotor blade length, also inertia frame
u,v,w	elastic displacement in the x,y,z directions.
ϕ	Pitch angle of blade element
ζ, η	principal axes of local cross section of blade
c	chord length of blade element.
t	thickness of blade element
α	local angle of attack of blade element
e	mass centroid offset from elastic axis
β_p	precone angle of the blade

The references for these variables are shown in Figure 11 on page 19, and Figure 12. In Figure 11, the X,Y,Z coordinates are in inertial frame, R. The R system coordinates are the rotor shaft axes when there is no hub motion, while x_p, y, s coordinates are fixed in the reference frame B_1 which rotates with respect to R frame at a constant angular velocity Ω. The coordinates x', y', z' are the coordinate axes of the deflected blade element.

As mentioned earlier, the Hamilton's Law of Varying Action is employed to derive the equations of motion for the rotor blade. "Hamilton's Principle", can be expressed as:

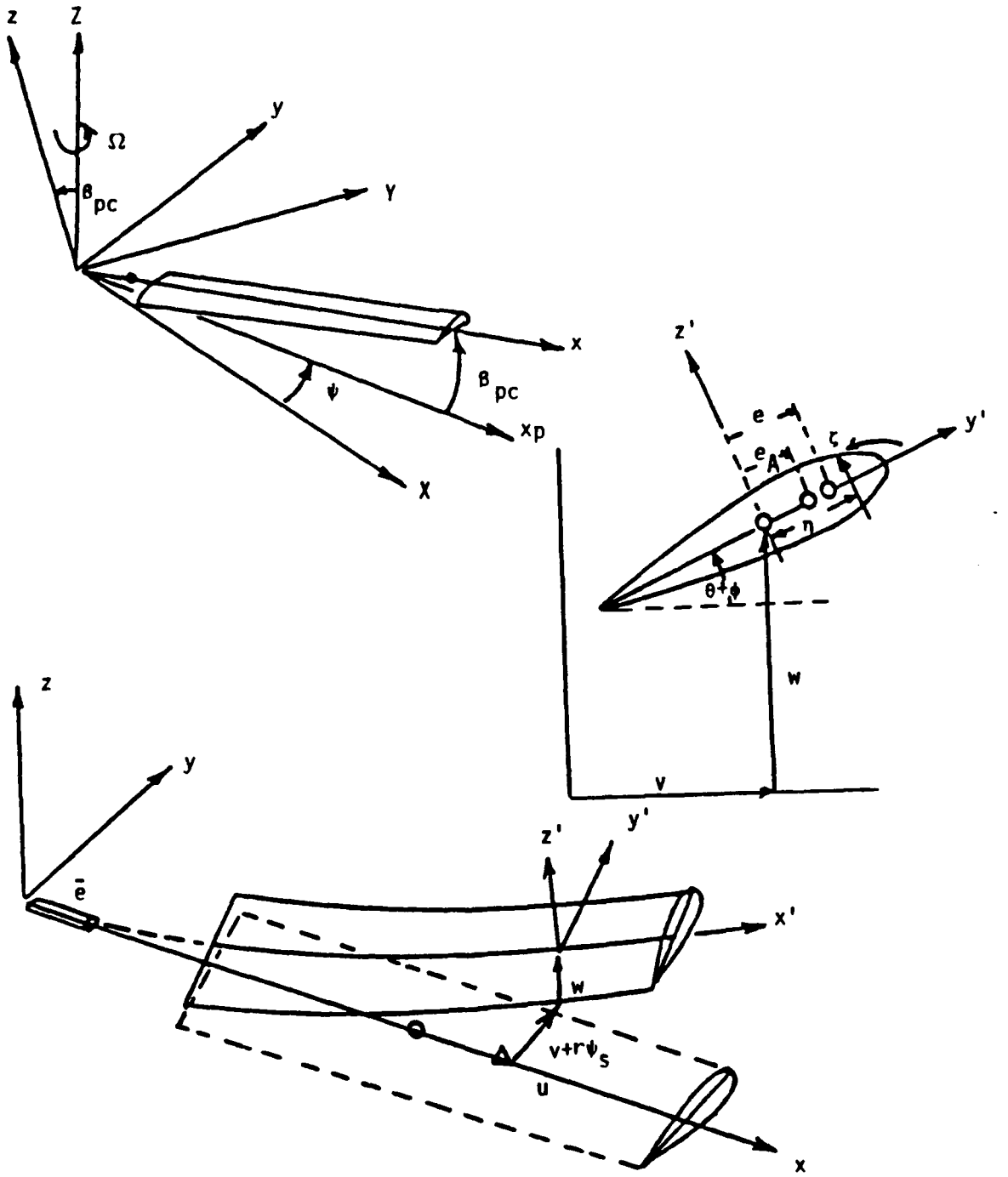

Figure 11. Blade Coordinate System for DYSCO

Source: DYSCO Manual, Vol. I

$$\int_{t1}^{t2}[\delta(U-T)-\delta W]dt=0$$

where U is the strain energy, T is the kinetic energy, and δW is the virtual work of the external forces. Hamilton's law is a special case of Hamilton's Principle, and is [Ref. 18:. p.16]

$$\int_{t_1}^{t_2}[\delta(U-T)-\delta W]dt-\frac{\partial T}{\partial \dot{q}_i}\delta q_i\Big|_{t_2}^{t_1}=0$$

Further developments of strain energy, kinetic energy and the virtual work of the external forces are made in Reference 18, and are applied to the blade elastic displacement through the Raleigh-Ritz method. For this, arbitrary functions for the blade displacement can be separated into a sum of products of functions of **r** and **t** only:

$$v(r,t)=\sum_i y_i(t)Y_i(r)=\sum y_iY_i$$

$$w(r,t)=\sum_j z_j(t)Z_j(r)=\sum z_jZ_j$$

$$\phi(r,t)=\sum_k \phi_k(t)\Phi_k(r)=\sum \phi_k\Phi_k$$

where $Y_i(r)$, $Z_j(r)$, $\Phi_k(r)$ are modal functions and y_i, z_j, and ϕ_k are generalized coordinates. These sums are substituted into the displacement equations for u, v, and w to yield equations of motion for all the generalized degrees of freedom.[Ref. 18: p.49]

These methods are incorporated in the elastic blade module, named CRE3. The module allows out-of-plane bending (flapping), in-plane bending (lead-lag), and torsion (pitch change)[Ref. 18: p.50]. Mode shape data is also defined, based on the normal modes of a non-rotating beam for given boundary conditions[Ref. 19: p.70]. Rotor hub degrees of freedom are user defined, and will automatically couple to the fuselage component degrees of freedom through a detailed set of transformation matrices.

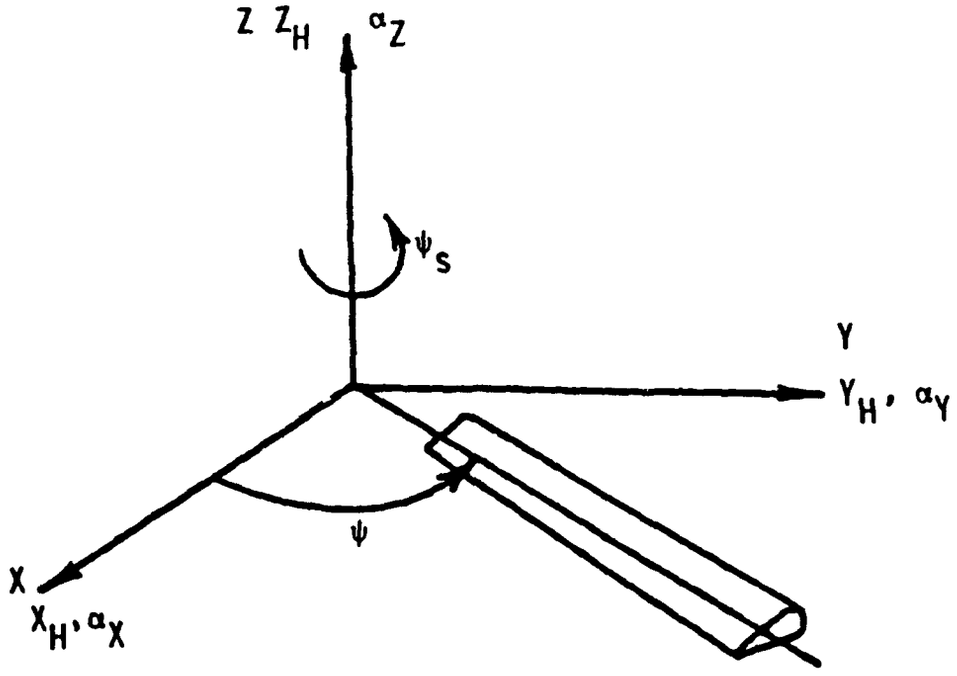

Figure 12. Hub and Perturbation Rotational Degrees of Freedom.
Source: DYSCO Manual, Vol. I

2. Rotor Blade Aerodynamic Model

As discovered by Johns in flow visualizations [Ref. 17] and by Anderson in velocity measurements [Ref. 6], the airflow in the vicinity of the flight deck of a ship is extremely turbulent and unsteady. Rhoades [Ref. 5] study is the best effort to obtain airflow velocity measurements so far, and his data were used as input to the FRA3 module. The aerodynamics of the rotor blade are further complicated by the low RPM of the rotor blades during rotor engagement, thus introducing Reynolds numbers far below those encountered in normal flight. While simple linear aerodynamics (component FRA0) was used for the DYSCO model test runs, a more comprehensive approach is needed to accommodate the changing aerodynamics that exist on the ship flight deck. This can be accomplished with the FRA3 component of DYSCO. Using this component implies that linear aerodynamics does not accurately model the flow over the deck of the AOR. Figure 13 on page 23 illustrates the rotor aerodynamic logic for DYSCO.

All of the steady state aerodynamic coefficients for the rotor blade (C_L, C_D, C_M) can be either calculated or looked up from tables external to the DYSCO program. For either option, the angle of attack (α) and Mach number (M), based on the two-dimensional strip theory, are modified by yaw flow angle to account for the three-dimensional aerodynamic effect.[Ref. 18 : p.52]

As observed by Rhoades [Ref. 5], angles of attack for the upflows from the side of the ship and downflows from the forward superstructure are all greater than the low Reynolds number stall angles in Reference 20. This indicates that drag forces on the flat plate area of the rotor blade are likely to be the largest contributor to forcing the blades to such high flapping angles. This view is reinforced by the results of the computer simulations and by the blade element program in Appendix A, which shows the lift and drag forces as a function of blade position in the rotor disk. The modified drag coefficient is

$$C_{DN} = C_D(\alpha_{RD}, M_{eff})$$

where α_{RD} is the angle of attack corrected for compressibility effects.

B. MATHEMATICAL MODELING OF AIR-WAKE TURBULENCE

In order to fully understand the modeling methods used for representing the ship airwake turbulence, one must understand the use of stochastic control theory. In brief terms, the modeling is done by shaping Gaussian white noise through the use of first or

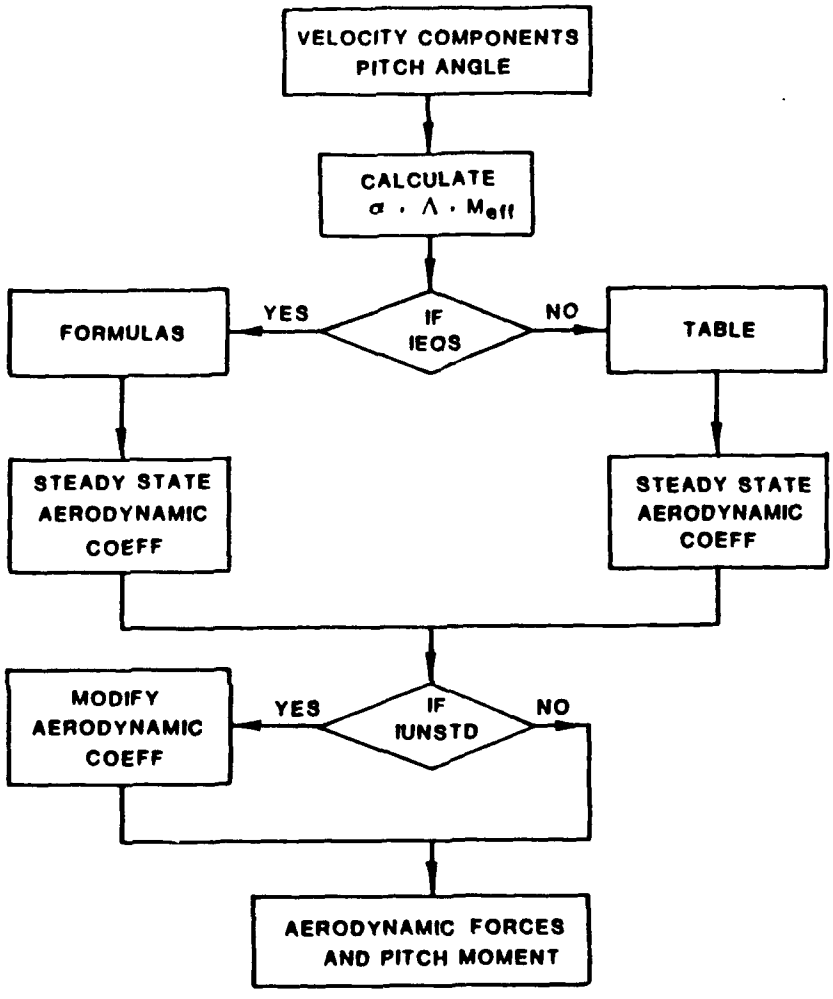

Figure 13. Rotor Aerodynamic Logic.
Source: DYSCO Theoretical Manual

second order lag functions so that the output closely resembles the spectral densities of the velocity components at each point in the wake of the ship.

White noise is a theoretical abstraction used to simplify calculations. It is simply a random process with an expected value (mean) of zero and an absolutely flat power spectrum.

$$S(\omega) = W = \text{constant for all } \omega$$

where $S(\omega)$ is the power spectral density function with respect to frequency ω. Because the mean square value ($\rho(0)$) of any random process is the integral of the spectral density over all frequencies,

$$\rho(0) = \frac{1}{2\pi} \int_{-\infty}^{\infty} S(\omega)\, d\omega$$

and since white noise has a constant spectral density for all frequencies, white noise theoretically has an infinite mean square value. This bothersome feature means that the power spectral density does not decrease with increasing frequency. Thus shaping functions are needed to represent real-life processes. [Ref. 21]

The best examples of the modeling of atmospheric turbulence are the Von Karman and Dryden models, which are briefly discussed in Reference 1. The models resemble free-air turbulence closely enough to be used in the military aircraft design process [Ref. 3]. According to the Dryden model the spectrum of the vertical component of random wind velocity in turbulent air is

$$S(\omega) = \sigma_z^2 T \frac{1 + 3(\omega T)^2}{[1 + (\omega T)^2]^2}$$

where σ_z^2 is the variance in the z component, and T is the time constant. This spectral density function is shown in Figure 14 on page 25. Figure 15 on page 26 illustrates the realization of a signal with a Dryden spectrum.

The two functions being considered here are first and second order lag functions. They are

$$G_f(S) = \frac{A}{1 + BS} \quad \text{and}$$

$$F(S) = \frac{K(S + a)}{S^2 + 2\zeta\omega_n S + \omega_n^2}$$

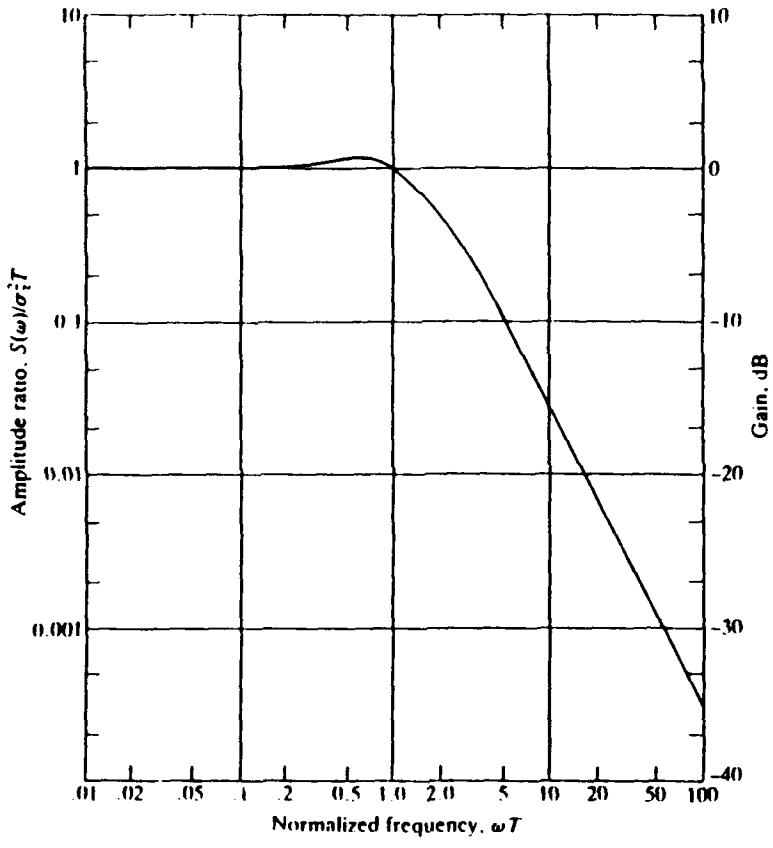

Figure 14. Dryden spectrum of air turbulence.
Source: Freidland, B., *Control System Design*

where K and A are filter gains, "a" is the location of the minimum phase zero, B and ω are the frequencies, and ζ is the system damping coefficient. By adjusting the bandwidth, a model representing the measured data can be found. Once the model is formed, the transfer functions representing the model may be used to input turbulent disturbances into the plant matrices of a flight simulator. To obtain the simplest possible simulator model of the turbulent flow, transfer functions must be developed for the u, v, and w velocity components.

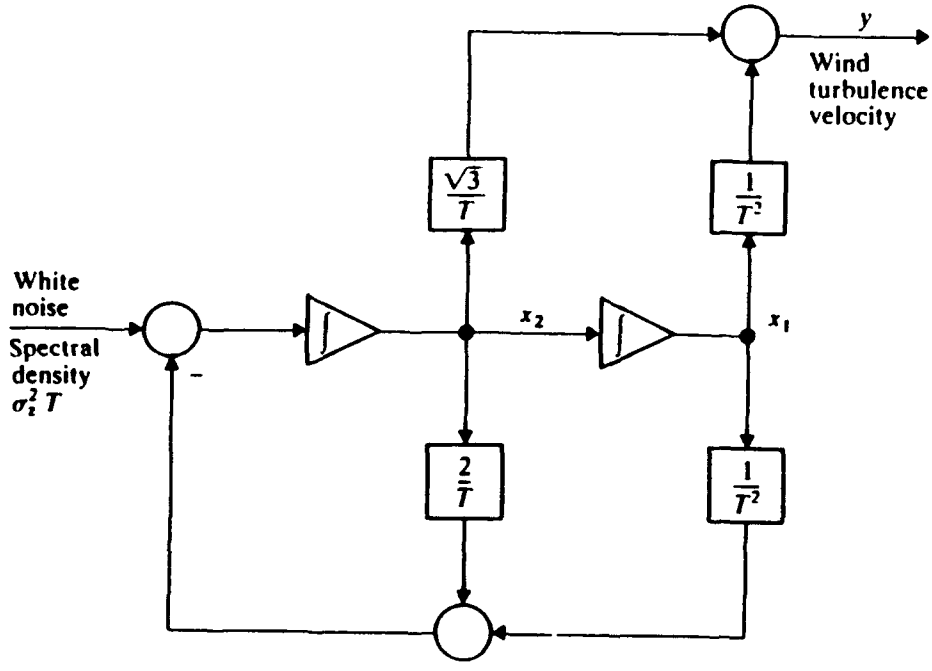

Figure 15. Realization of signal having Dryden spectrum.

Source: Freidland, B., *Control System Design*

III. CONSTRUCTION OF TUNNEL STRIKE AND AIR-WAKE TURBULENCE MODELS

A. AIR-WAKE TURBULENCE MATH MODEL

The goal of the air-wake model is to mathematically simulate the turbulence felt by a helicopter flying downwind of a ship. The methods used to do this involve finding the spectral densities of the air-wake at discrete points along some glidepath, and then developing filters to shape random or Gaussian white noise to them. The filter will be of the form:

$$H(s) = \frac{z(s)}{p(s)} = \frac{K(s - z(1))(s - z(2)) \ldots (s - z(n))}{(s - p(1))(s - p(2)) \ldots (s - p(n))} .$$

Filter design is accomplished here using the *Signal Processing Toolbox* of MATLAB.

For this project, an infinite impulse response digital lowpass filter is used, and presented in the form given above. The algorithms used by MATLAB take the spectrum shape specifications given by the user and produce vectors for the numerator and denominator, yielding a transfer function in the first canonical form. The software can then be programmed to produce random white noise, and pass this noise through the filter. The digital domain representation is

$$\frac{Y(z)}{X(z)} = \frac{b(1) + b(2)z^{-1} + \ldots + b(n+1)z^{-n}}{1 + a(2)z^{-1} + \ldots + a(n+1)z^{-n}},$$

where $a(i)$ and $b(i)$ are the transfer function coefficients.

This filtered white noise is then processed to find the spectral density, using break frequencies input by the designer. This effort is directed to providing a transfer function for the DD-963 class ship, with data obtained from the Naval Postgraduate School wind tunnel measurements being used as the baseline. To obtain the math model, the gains, poles and minimum phase zeros are derived for points along helicopter glide paths.

Appendix D contains the file used to transform the transfer functions to power spectra models. The simulated spectra contrast with those offered by Nave [Ref. 10: pp.29-32.] and Hanson [Ref. 4: pp.12-29.] in that the curves are smoother, due to Healey's data[Ref. 11] for the spectra containing 66,000 samples, acquired at 2.5 kHz. vice 256 samples acquired at 164 Hz for Nave's FF 1052 model and 131 samples at 164

Hz. for Garnett's DD-963 model. The lower number of samples and lower sampling rate produces a very jagged power spectral density curve, while the higher number of samples will give a more accurate variance and mean, and the higher sampling rate will smooth out the curve somewhat. Scaling of the bandwidth is accomplished by computing the ratio between model and prototype size. Garnett used the scale factor of the ship model to scale the frequencies of the turbulence up to the prototype. This was justified by the use of real-world wind velocities in the wind tunnel. Thus, the 1:50 FF-1052 model's frequencies were divided by fifty [Ref. 10: p.23.], and the 1:80 DD-963 model's frequencies were divided by eighty [Ref. 9: p.20.]. NPS's model employed much slower tunnel velocities than real-world values, hence the frequencies are scaled using velocities and characteristic lengths, in this case the beam of the ship. By comparing the Strouhal number for the prototype and wind tunnel model, a scaling factor of fourteen was found.

B. DYSCO CH-46 TUNNEL STRIKE MODEL

As mentioned in Chapter II, various modules were used to construct the math model of a complete CH-46 helicopter. Rotor blade properties were obtained from the Dynamics Group of Boeing Helicopter Company, and are provided in Appendix B. Appendix E contains the information entered into each of the DYSCO modules. To ease the complexity of the system, only a two-dimensional rigid body representation was used for the fuselage. Parameters such as C.G. location and locations and inclinations of the rotor masts were obtained from the CH-46 Maintenance Information Manual [Ref. 22].

Another simplification involved eliminating the forward rotor head. Since there have been no incidences of tunnel strikes of the forward head, due mainly to its tilt away from the fuselage, such a simplification was justified, and lessened the computation time.

Degrees of freedom deemed important for the aft rotor head are the out-of-plane or flapping (OP) degree of freedom, in-plane or lead-lag (IP) degree of freedom and torsional or blade pitch (TOR) degree of freedom. All three basic degrees of freedom were included to allow for any coupling that may occur between the three. Two modes were allowed in the flapping degree of freedom to insure an accurate description of the bending modes of the rotor blades.

To model the flap stops incorporated in the CH-46 to restrict the amount of flapping at the hub, the DYSCO module CES1 was used. The module not only imposes restrictions on the flapping, but also was used to model the lead-lag dampers for each blade in the in-plane degree of freedom. Values for the damping, obtained from Boeing

Helicopter Co., are included in the DYSCO input list in Appendix D. Figure 16 on page 30 illustrates a sample model using CES1.

Another constraint was needed for the pitch or torsion degree of freedom. This was accomplished by using the simple module CCE0. This module helps model the pitch change control rod for each rotor blade. Failure to add this constraint would result in a rotor blade that theoretically could twist 360° in torsion. By adding a control rod with a very large stiffness value, such twisting is prevented mathematically.

Linear constraints are added to the fuselage model to simulate landing gear. Using CSF1, simple spring damper systems are constructed to model the nose and main landing gear. Stiffness and damping coefficients are used to ensure that high oscillations do not occur that would affect the movement of the rotor blades. These simple spring-damper systems are then coupled linearly to the fuselage degree of freedom ZCG, which is the CG degree of freedom in the Z direction. A sinusoidal forcing function is added to the landing gear system to simulate wave action on the ship, but has been set to zero for this study. Future studies could incorporate this forcing function.

Modeling the air flow from the side of the ship up through the rotor system has been difficult. As covered in Chapter II, the module FRA3 will compute aerodynamic forces of airflows. A look-up table of low Reynolds's Number airfoil data was obtained from Reference 20, based on a Reynolds number of 660,000. This was used based on the computed Reynolds Numbers for each blade at each time step using the algorithm in Appendix A, which was based on wind tunnel measurements by Rhoades [Ref. 5], and scaled to the prototype. Values of wind-tunnel velocities from Rhoades are given in Appendix F. Rhoades' flow visualization on the windward side also indicated that angles of the flow ranged from 15° to 25°, relative to the rotor disk. Since these angles are well above the stall angle of attack for the airfoil used (12°) the predominant force acting on the rotor blade is expected to be the drag force caused by the updraft or downdraft of the vertical component of the wind. Appendix G contains the values used in the look up table and the inputs for the FRA3 module.

C. SIMPLE CH-46 BLADE ELEMENT PROGRAM

The blade element program in Appendix A is an extremely basic program and was developed to describe the flowfield around the rotor disk and over the flight deck of an AOR class ship. The program was further modified to compute the aerodynamic forces acting on each rotor blade. This program assumes that the blade is a rigid beam, that is, no bending is allowed. The algorithm was developed from wind tunnel measurements

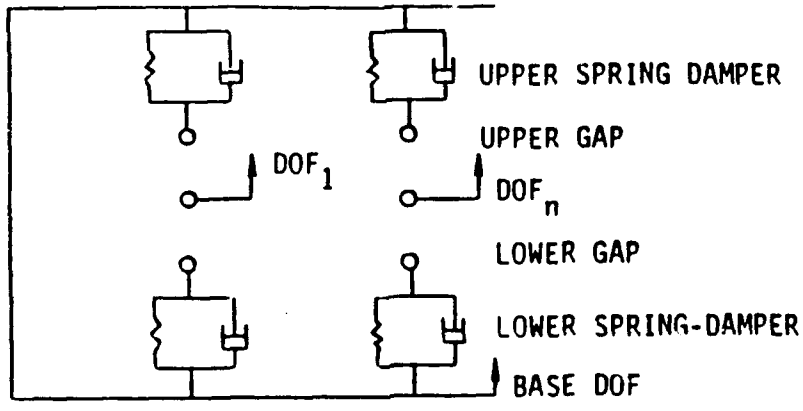

Figure 16. CES1 Model (example)
Source: *DYSCO Users Manual*

made by Rhoades [Ref. 5], which are presented in Appendix F. Using the rotational acceleration obtained from a videotaped Dynamic Interface wind limitation flight test, the varying linear velocities are computed as a function of one-half second time steps for three revolutions of the rotor head. These velocities were combined with the flow field to obtain the relative wind to the blade element, and the angle of attack at each blade element. The following simple calculations illustrate the steps incorporated in the program.

For $\Psi = 3°$, Rotor traveling clockwise,

Point 1 at Blade Root

Point 5 at Mid-Span of Blade

Point 10 at Blade Tip

The curve fit for the rotor RPM acceleration, and subsequent integration to find blade position is as follows,

$$\text{RPM} = 4.2675E-02 + 3.5366t - 0.45788t^2 + 2.3410E-02t^3$$

$$\text{POS} = 0.0071t + 0.02947t^2 - 0.002543t^3 + 0.000098t^4 + 0.151325,$$

where POS is the number of revolutions completed by that blade. For the 15th time step, the time is 7 seconds, which yields a RPM of 10.41, and a blade position of 2.92 degrees. The horizontal (u) and vertical (w) components of the wind over the flight deck, relative to the rotor disk plane, are determined at each position of the rotor blade. For this instance, they are found to be 2.0429 m/s and 0.9377 m/s respectively. These values are then scaled to represent the 40 knot wind represented by the wind tunnel, which yields a horizontal component of 58.6 feet per second and a vertical component of 26.87 feet per second.

The circumferential velocities due to rotation are determined by the RPM and the position of the blade element from the center of rotation. The following values were obtained for time step 15,

$\text{Radius}_1 = 33.255$ inches, $V_{Rotational\,1} = 3.025$fps

$\text{Radius}_5 = 148.1$ inches, $V_{Rotational\,5} = 13.45$ fps

$\text{Radius}_{10} = 291.64$ inches, $V_{Rotational\,10} = 26.49$ fps

Adjustments are made for the position of the leading edge of rotor blade with respect to the direction of the flow field, so that only the components of the flowfield normal to the leading edge of each blade element and normal to the chordline of each blade element are considered. This is accomplished by

$$u_{blade} = V_{rotation} - u_{wind} \cos \psi$$

where u_{blade} is the horizontal wind component normal to the leading edge. For example, for the 10th blade element, u_{blade} is -32.02 fps, indicating that the horizontal component is flowing up the trailing edge of the blade element.

The inflow angle to the blade element is then determined by computing the arctangent of the vertical and horizontal flows at the blade element. Since the CH-46 rotor blade has a linear geometric twist built in, this twist is also computed and added to the inflow angle for each blade element. The program then uses the angle of attack to search the look-up table presented in Appendix G and obtain the correct lift and drag coefficients each blade element. From this, lift and drag forces are computed with respect to the relative wind, and finally each are resolved into a vertical component. Results of this process are presented in Chapter IV and Appendix A.

IV. RESULTS

A. AIR-WAKE TURBULENCE MATH MODEL

In order to obtain the best physical fit of the computer generated power spectra, several orders of transfer functions were attempted. Basing the breakpoints on the slope changes of the measured power spectra, a sixth order transfer function was finally used to model the measured spectra. The parameters used in the "yulewalk" algorithm in "MATLAB" for the modeling of the DD-963 spectrum at a point twenty-five percent of the ship length away from the flight deck, and with the ship pointed thirty degrees to the right of the wind are as follows for each component of the velocity in the air-wake:

$$\bar{m}_u = [10.0 \;\; 1.0 \;\; -2.0 \;\; -32.0 \;\; -72.0 \;\; -82.0]$$

$$\bar{f} = [0 \;\; 3/1000 \;\; 35/1000 \;\; 600/1000 \;\; 999/1000 \;\; 1]$$

$$\bar{m}_v = [0.0 \;\; 0.5780 \;\; -4.0462 \;\; -27.1676 \;\; -41.6185 \;\; -58.9595]$$

$$\bar{f} = [0 \;\; 3/1000 \;\; 35/1000 \;\; 600/1000 \;\; 999/1000 \;\; 1]$$

$$\bar{m}_w = [0.0 \;\; 1.0 \;\; -3.0 \;\; -27.0 \;\; -45.0 \;\; -65.0]$$

$$\bar{f} = [0 \;\; 3/1000 \;\; 35/1000 \;\; 600/1000 \;\; 999/1000 \;\; 1]$$

where $\bar{m}$ is a vector containing the desired magnitude response at the points specified in $\bar{f}$(breakpoints) for each of the components (u, v, and w) and $\bar{f}$ is a vector of frequency points, specified in the range between 0 and 1, where 1.0 corresponds to half the sample frequency (the Nyquist frequency). The transfer function coefficients (see p. 28) from those models are:

$$\bar{b}_u = [22.6588 \;\; -13.0029 \;\; -9.0971 \;\; -4.4572 \;\; -0.1487 \;\; 6.3585 \;\; -0.4214]$$

$$\bar{a}_u = [1.0 \;\; 0.5978 \;\; -0.1317 \;\; -0.3804 \;\; -0.3665 \;\; -0.0400 \;\; 0.0205]$$

$$\bar{b}_v = [19.0600 \;\; -6.0289 \;\; -9.0813 \;\; -2.9458 \;\; -1.5902 \;\; 2.8828 \;\; 0.4594]$$

$$\bar{a}_v = [1.0 \;\; 0.5388 \;\; -0.1256 \;\; -0.2584 \;\; -0.2770 \;\; -0.0516 \;\; 0.0040]$$

$$\bar{b}_w = [18.5670 \quad -3.7482 \quad -5.4913 \quad -8.4648 \quad -4.1090 \quad 5.0879 \quad 0.8924]$$

$$\bar{a}_w = [1.0 \quad 0.7695 \quad 0.2652 \quad -0.2462 \quad -0.4730 \quad -0.1138 \quad 0.0031] \ .$$

These are placed in the following canonical form of a transfer function, with Y(z) as the output and U(z) as the input.

$$\frac{Y(z)}{U(z)} = \frac{b(1) + b(2)z^{-1} + \ldots + b(n+1)z^{-n}}{1 + a(2)z^{-1} + \ldots + a(n+1)z^{-n}}$$

Having modeled the power spectrum of the wind tunnel measurements, the model was then scaled to the prototype using a Strouhal scaling factor of fourteen. This was further reduced to a pole, zero, gain format transfer function, using conversion algorithms in MATLAB. This format is useful in determining the inputs needed for digital simulation. The measurements used for this simulation were the u, v, and w components of the velocities of the air-wake at a point twenty-five percent of the ship length away from the touch-down point on the flight deck. These measurements are shown in Figure 17 on page 35. The transfer coefficients, when used to filter random generated noise, produce the spectra shown in the following figures. The solid line in each spectra is the MATLAB generated model, while the dashed line power spectra is the measured spectrum by Healey [Ref. 11]. Both the wind tunnel and Strouhal scaled models are presented.

When comparing the measured and simulated spectra, the smoother nature of the former is noted. This could be attributed to the very large size of the samples of measured data, which were then averaged in groups of sixty-four, while the simulated spectrum curve was formed with a random signal generator that had no way to control the variance of the signals. The larger variance in the simulated spectra could be a source of higher than normal turbulence, but should be evaluated by a real-time simulator flight prior to adjustments. The MATLAB predicted spectra are much smoother than those obtained by Fortenbaugh and Hanson. For example, the power spectral density curves derived by Hanson for yaw angle of 330° shows very large variances. The very wide variance presented by Hanson could be due to his small data size and small sample rate [Ref. 4: p.30.]. Figure 24 on page 42 is presented only to illustrate the greater variance (more "spikey") at the lower frequencies in the Hanson and Fortenbaugh models. In the NPS wind tunnel, frequencies lower than three radians per second were not measured, but the overall smoothness Healey's measured spectrum indicates a lower variance. The

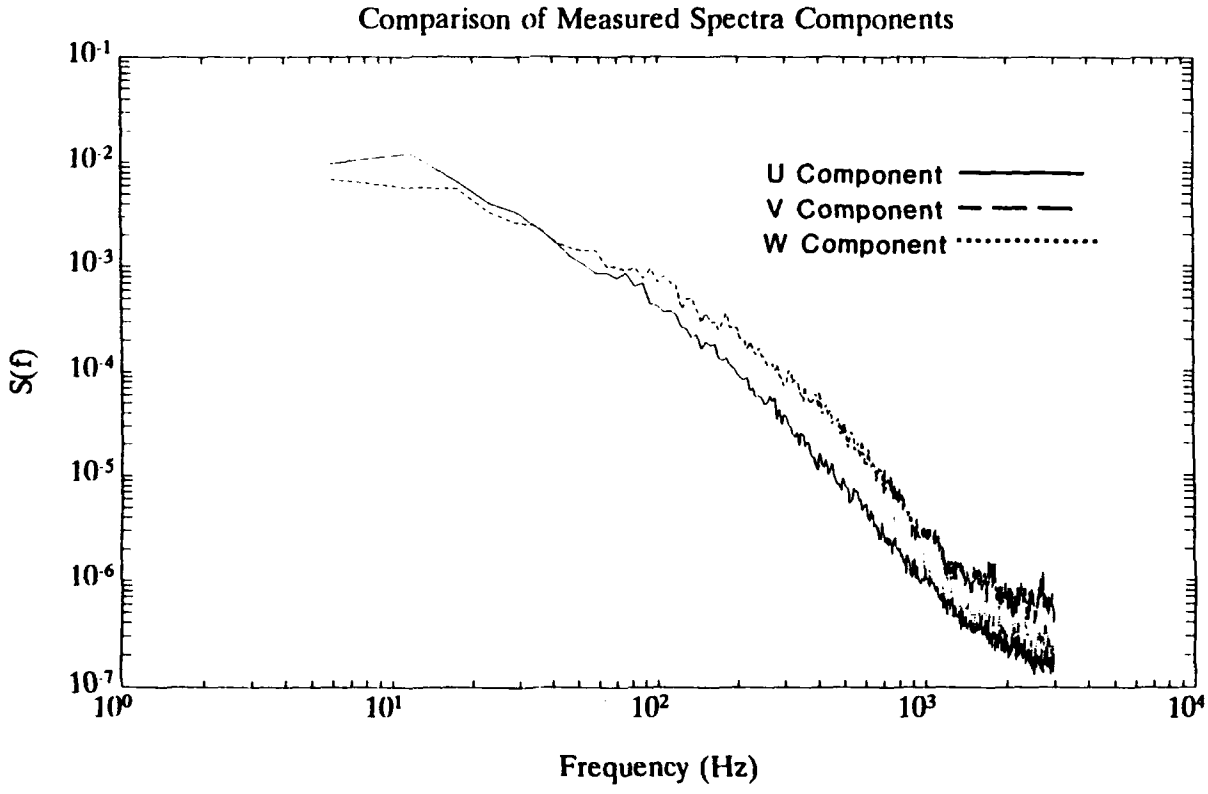

Figure 17. Wind Tunnel Spectra - U, V, and W Components

algorithm used by Hanson allowed for changing the variance of the air wake component velocities, thus permittig him to reduce the variance by the sixty to seventy percent needed to comply with pilot's reports of the simulator trials [Ref. 4: p.30.].

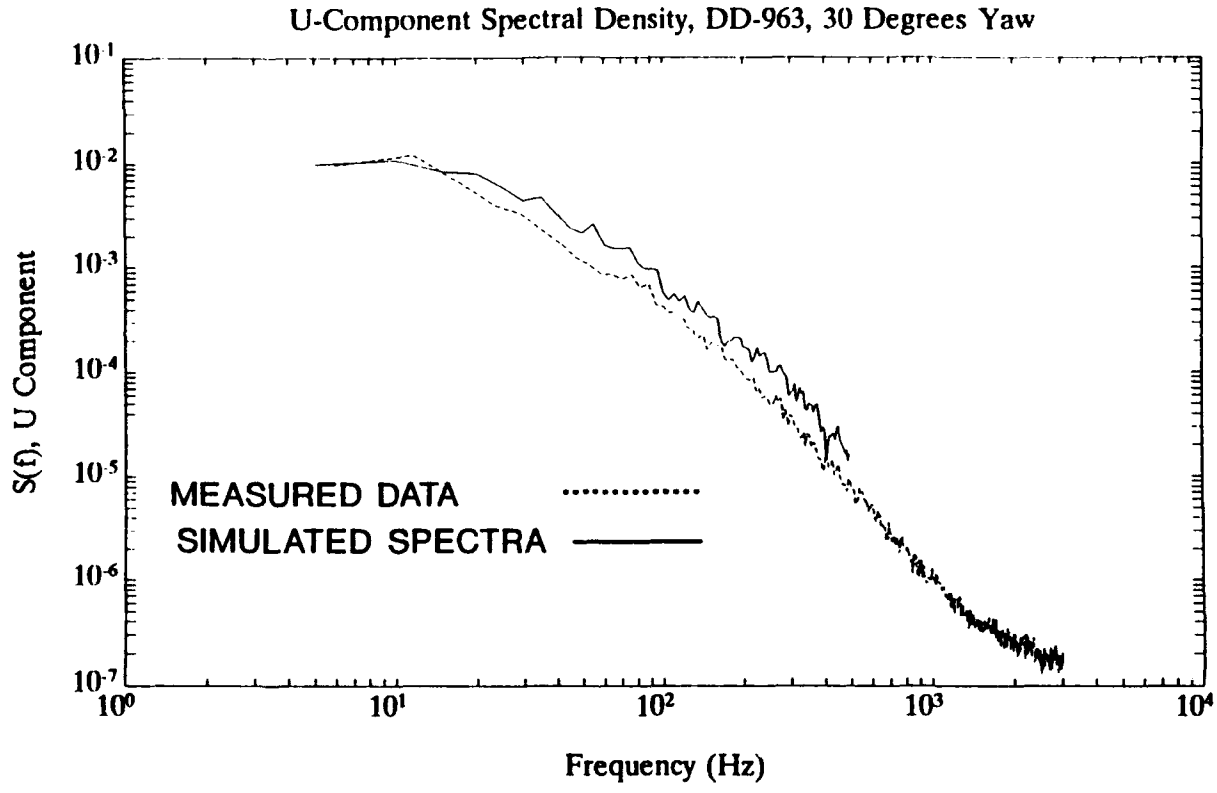

Figure 18. Filtered Noise for U Component Simulation.

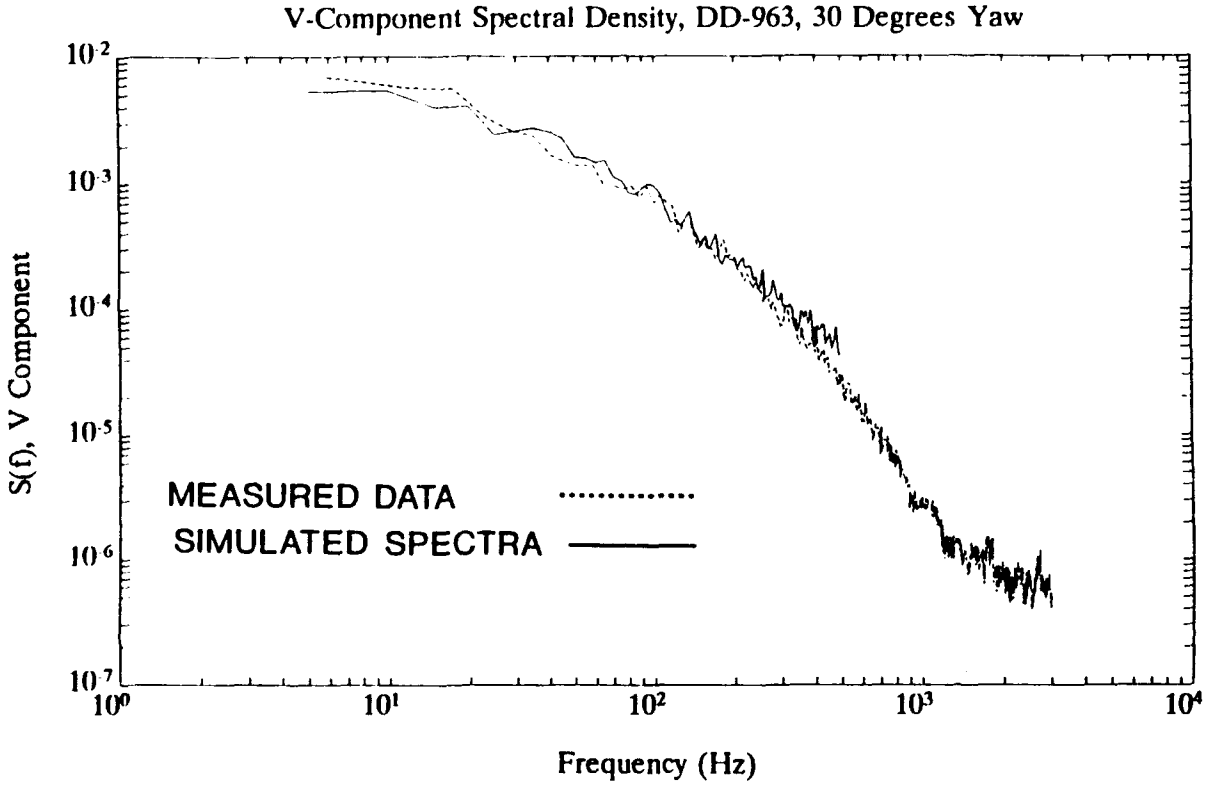

Figure 19. Filtered Noise for V Component Simulation.

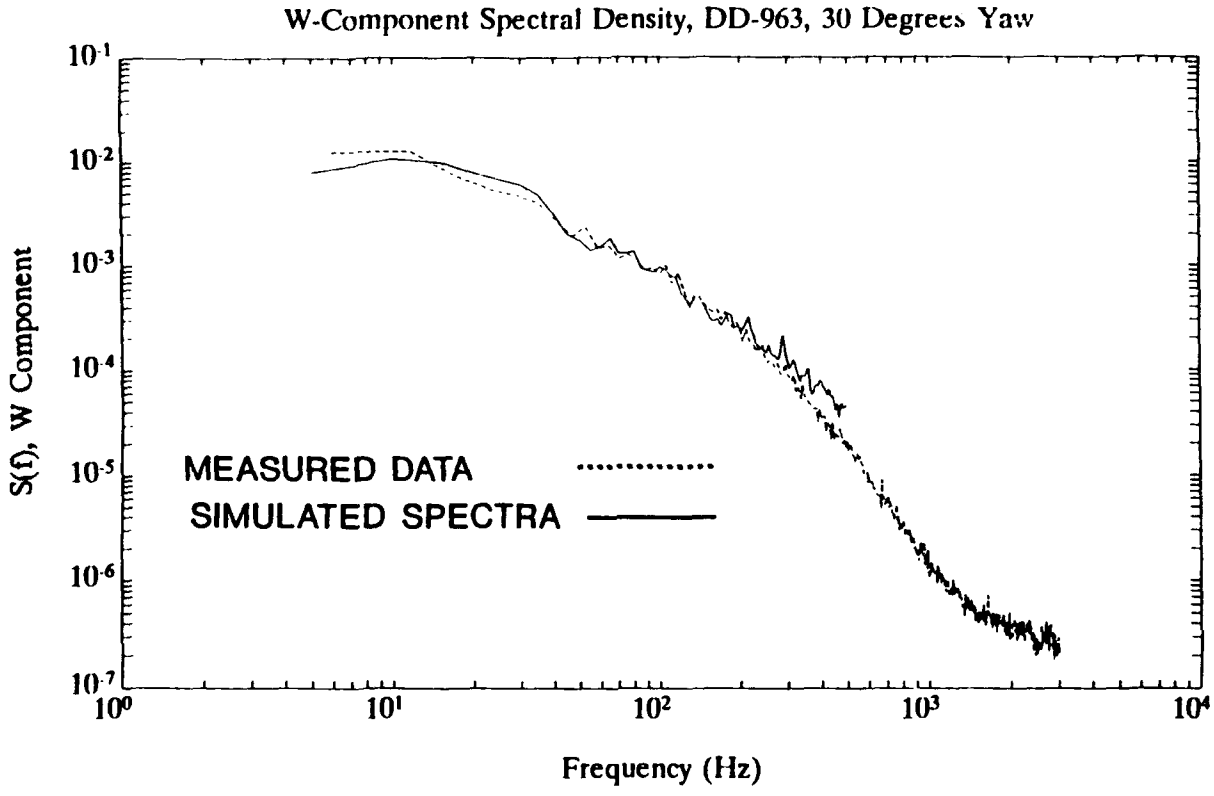

Figure 20. Filtered Noise for W Component Simulation.

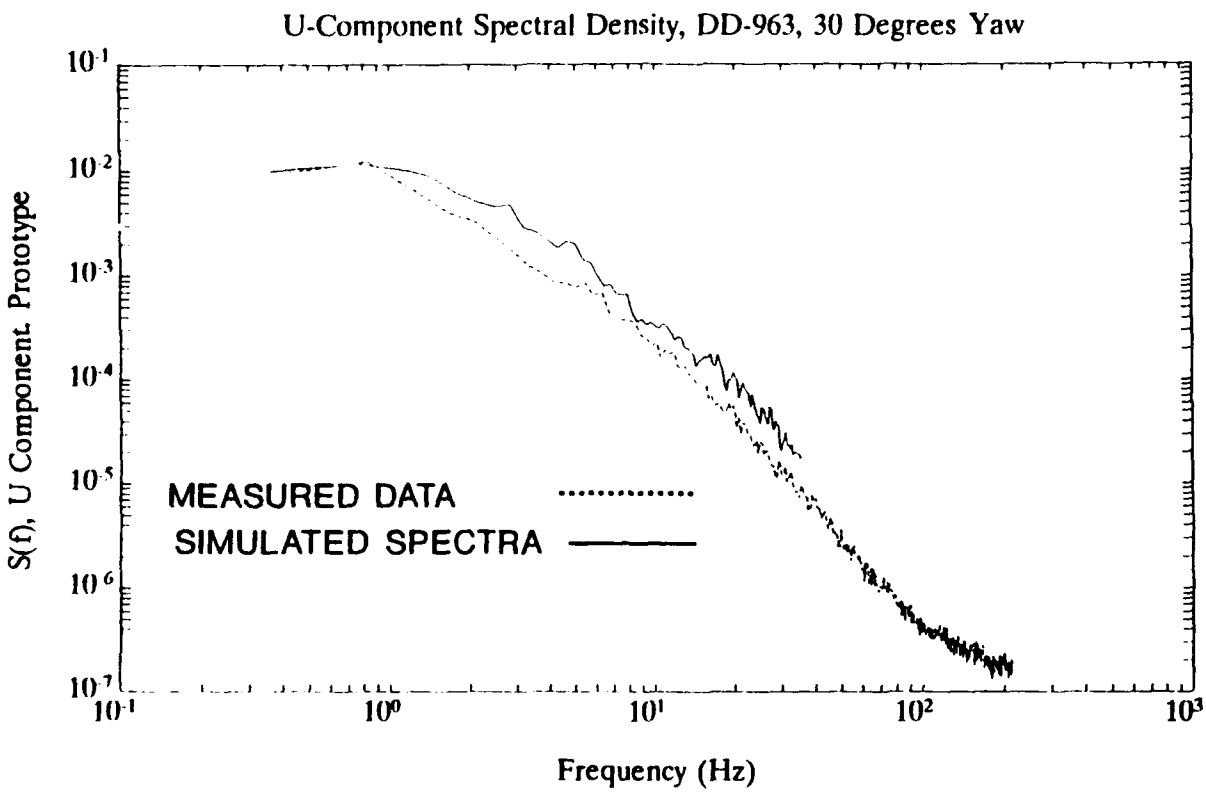

Figure 21. Filtered Noise for U Component Prototype.

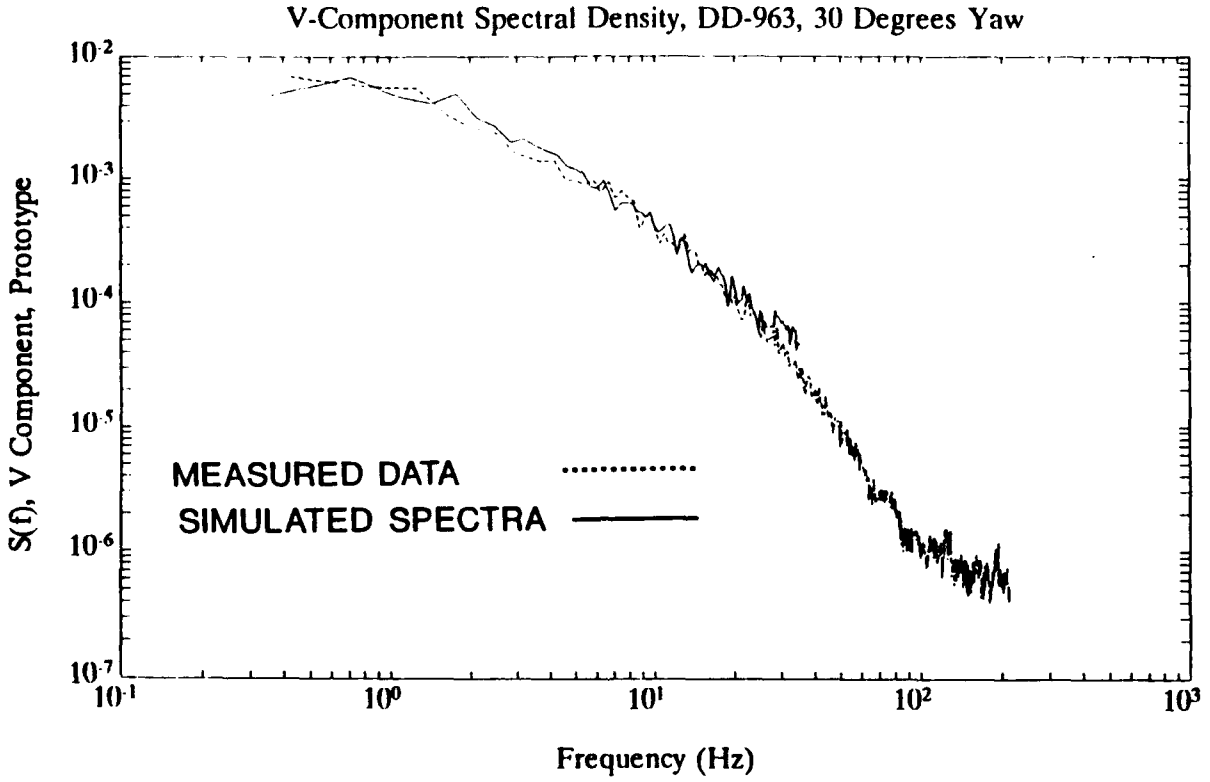

Figure 22. Filtered Noise for V Component Prototype.

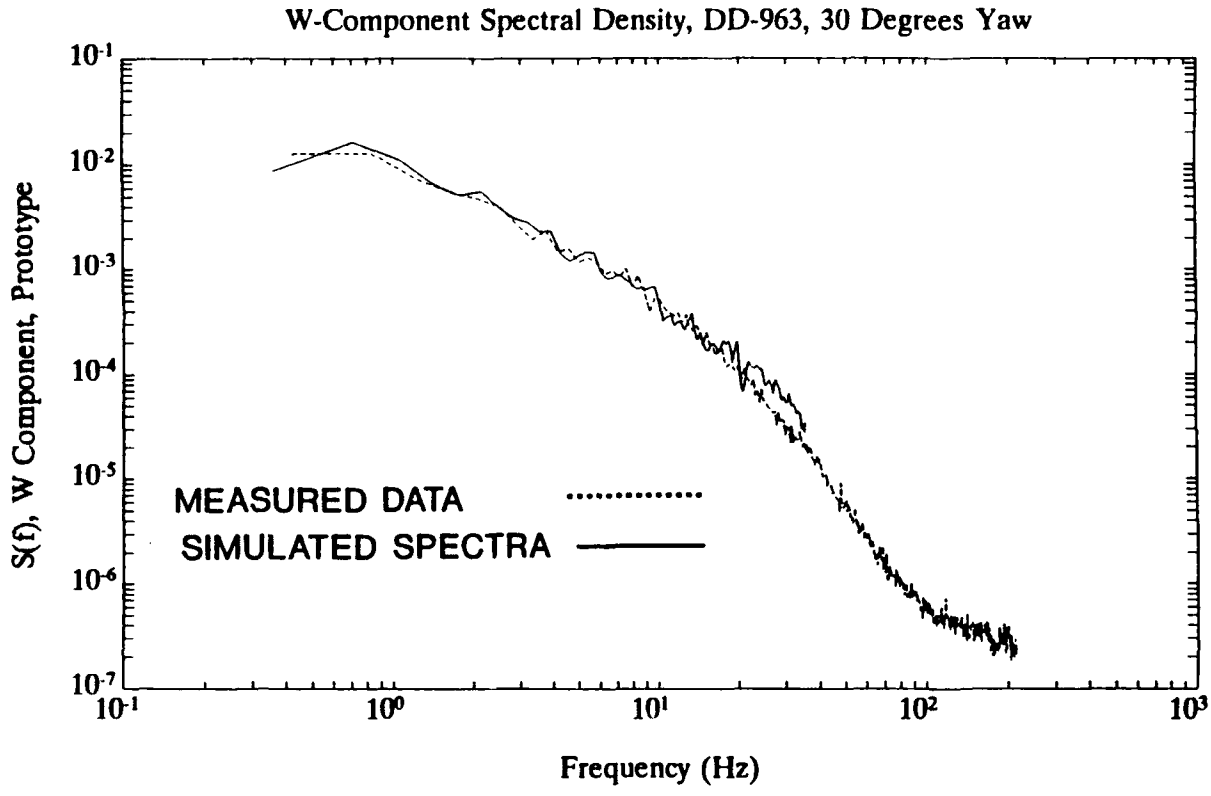

Figure 23. Filtered Noise for W Component Prototype.

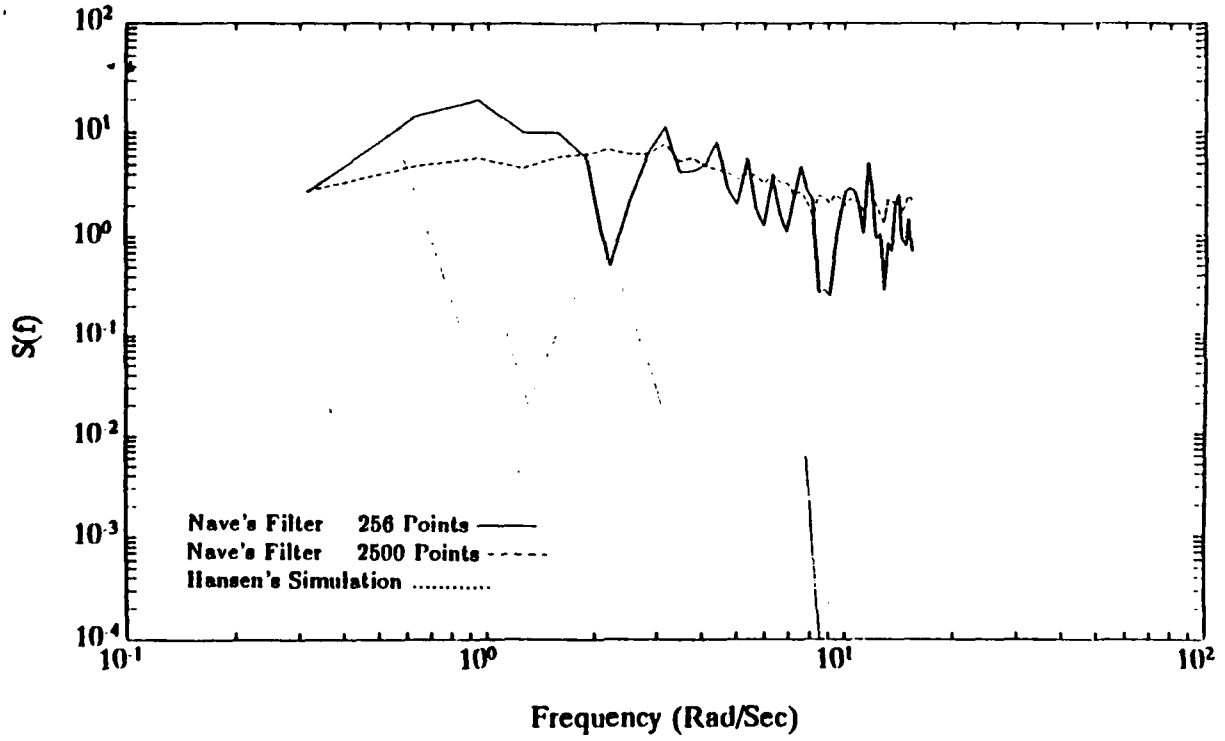

Figure 24. Comparison of Hanson's and Fortenbaugh's Models.

The high variance values found in the MATLAB simulation could also be reduced by increasing the number of points used in the random signal generator. For this model, 4000 points were used. Larger sizes of white noise sets could not be generated due to memory limitations with the PC version of MATLAB. Higher functioning versions of MATLAB, on systems with much larger memory could produce sets one or two orders of magnitude higher, thus reducing the problem of higher variance in the simulated spectra. To test this assumption, the same algorithm was run on *PRO-MATLAB*, installed on the VAX Mini-2000 using VAX/VMS. Since the memory available was considerably greater than that of a PC, the number of white noise points was increased by an order of magnitude, to 25,000. The power spectra obtained were much smoother, and gave an improved representation of the wind tunnel flowfield. This approach also confirms Hanson's theory that the frequency used to generate the white noise signal will affect the quality of the simulation [Ref. 4: p.11]. By varying the number of discrete white noise points generated, it may be possible to eliminate the need to interpolate the

white noise prior to filtering when using Hanson's model. The improved computer simulation for the full scale prototype is shown in Figure 25.

The poles, zeros and gains obtained from MATLAB for the wind tunnel model are given in Table 2 through Table 4.

Since the random signal changes with each computer simulation, the portrayed spectral densities can be assumed to change somewhat with each real-time run. Further study in conjunction with real-time simulator flights are needed to further refine this approach to air-wake simulation. Results of filters designed for the complete glidepath for a 330° yaw angle are presented in Appendix H.

Table 2. POLES, ZEROS AND GAINS FOR U COMPONENT OF THE WIND TUNNEL MODEL

Poles	Zeros	Gain
0.8213	-0.7259	22.6588
-0.2352 + 0.6707i	-0.2340 + 0.6886i	
-0.2352 - 0.6707i	-0.2340 - 0.6886i	
-0.7520	0.8506 + 0.0600i	
-0.3728	0.8506-0.0660i	
0.1761	0.0666	

Table 3. POLES, ZEROS AND GAINS FOR V COMPONENT OF THE WIND TUNNEL MODEL

Poles	Zeros	Gain
0.7755	0.8947	19.06
-0.7343	0.6382	
-0.1697 - 0.6119i	-0.1694 - 0.6063i	
-0.1697 + 0.6119i	-0.1694 + 0.6063i	
-0.2983	-0.7142	
0.0577	-0.1491	

B. DYSCO CH-46 TUNNEL STRIKE MODEL

After several attempts to accurately duplicate the velocity field around the whole rotor disk, it was determined that a separate flowfield would be considered for each rotor

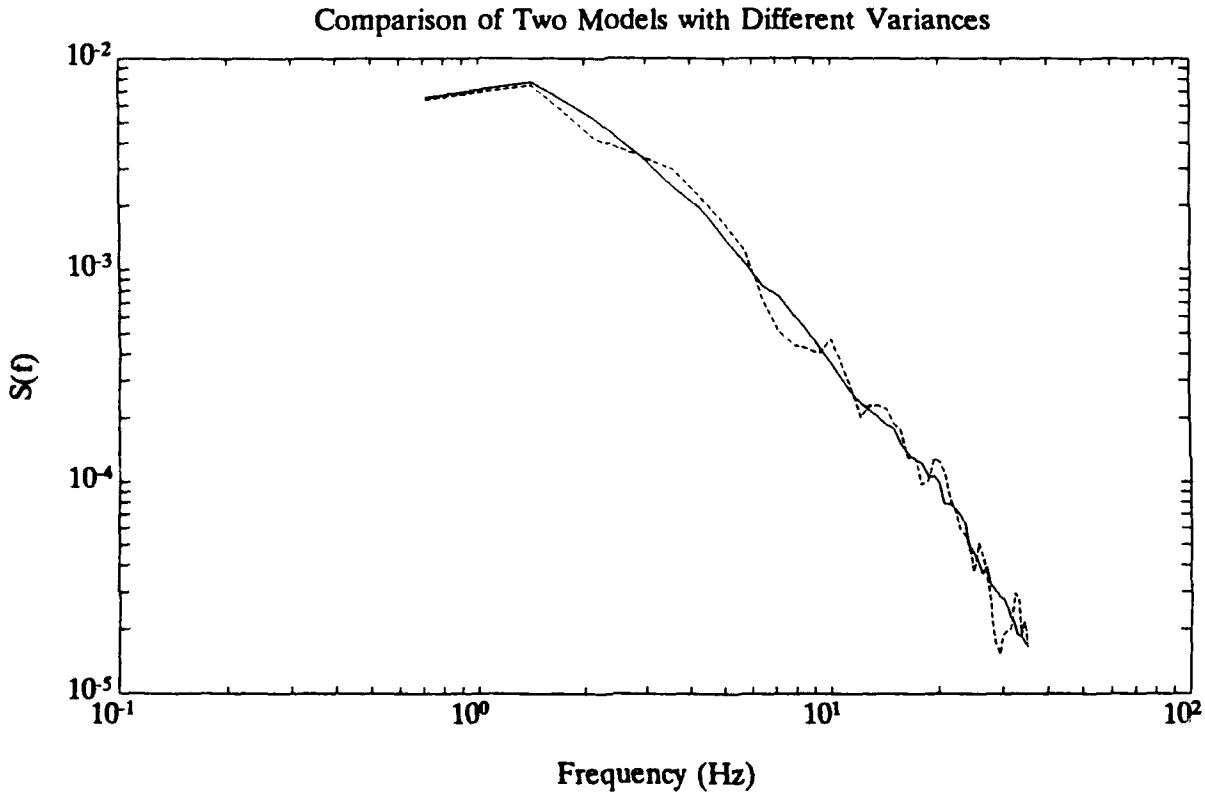

Figure 25. Wind Tunnel U-Spectra Simulation Using PRO-MATLAB.

blade. This assumes that the behavior of the rotor blades are independent of each other, without any interaction via the hub, since the rotor head is fully articulated. It also as-

Table 4. POLES, ZEROS AND GAINS FOR W COMPONENT OF THE WIND TUNNEL MODEL

Poles	Zeros	Gain
0.7541	-0.2436 + 0.7987i	18.5670
-0.2433 + 0.7984i	-0.2436 - 0.7987i	
-0.2433 - 0.7984i	-0.7153	
-0.7376	0.8984	
-0.3243	0.6669	
0.0248	-0.1609	

sumes that the airflow velocity conditions at a particular point in time is constant for the length of the rotor blade. Since the conditions of the velocity field were dependent on the rotor blade position, a history of rotor blade RPM vs. time was required. It was obtained from videotape of a Dynamic Interface flight test conducted aboard an AOR class ship. The time history is illustrated in Figure 26 on page 46.

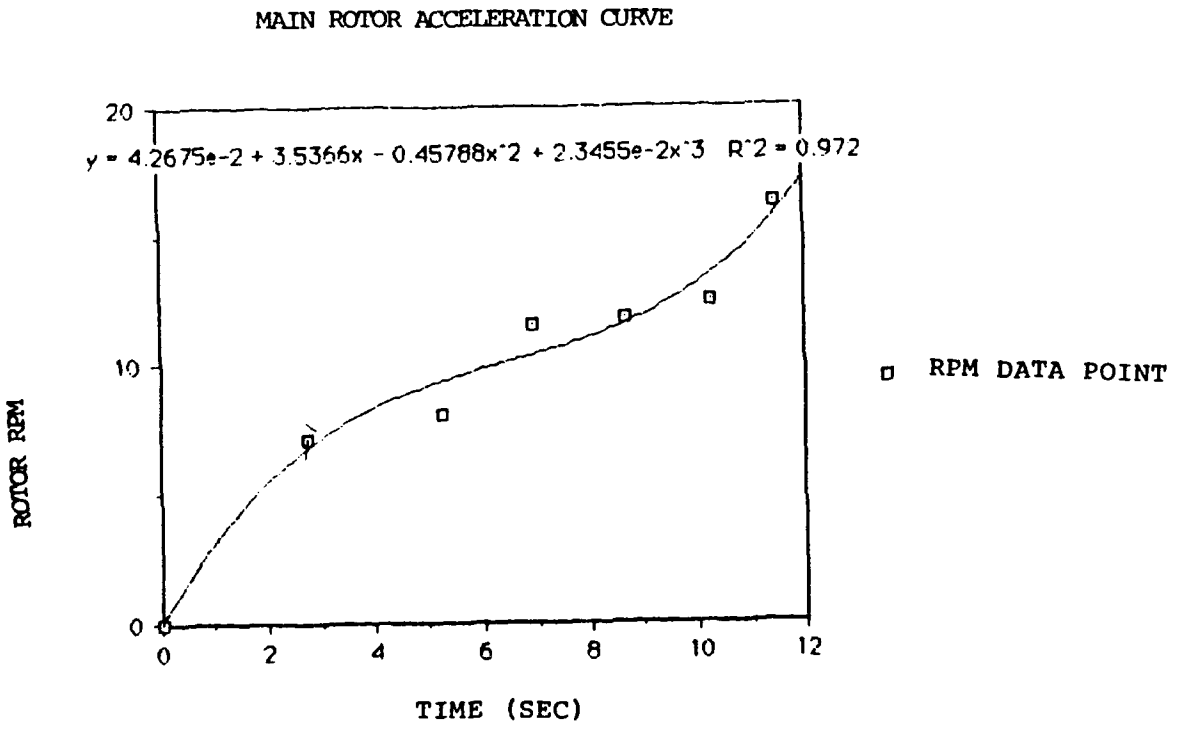

Figure 26. Rotor RPM Time History for Rotor Engagement

By combining this time history with the flowfield measured by Rhoades [Ref. 5], the velocity components relative to the rotor disk for each time step were obtained. This fixes the field in space, and uses only one Reynolds number for the range of velocities each rotor blade will "see." Actual relative velocities (combined effects of mean airflow and rotor blade velocity) are computed by DYSCO. The algorithm for mean velocity components and blade position is based on the velocity measurements obtained for the AOR wind-tunnel model [Ref. 5: p.71.]. The entire program used to determine the velocities, and scale them to the 40 knots simulated in the wind tunnel is listed in Appendix A, along with the results for each rotor blade.

These velocity components were then input to the DYSCO CH-46 model by changing the velocity inputs in the FRA3 module for each time step. The wind values were input using downward flows as positive (+) and upflows as negative (-), consistent

with the DYSCO users manual [Ref. 18: p.56.]. When combined with lift, drag and moment coefficients for a NACA 0012 airfoil, the Runge-Kutta integration in DYSCO could not converge to a solution. After several attempts to correct the divergence, use of DYSCO for the tunnel strike model was abandoned.

C. SIMPLE CH-46 BLADE ELEMENT PROGRAM

Using the methods outlined in Chapter IV, the total vertical forces for each rotor blade where computed with respect to the rotor blade position. These forces are presented in Figure 27, Figure 28, and Figure 29.

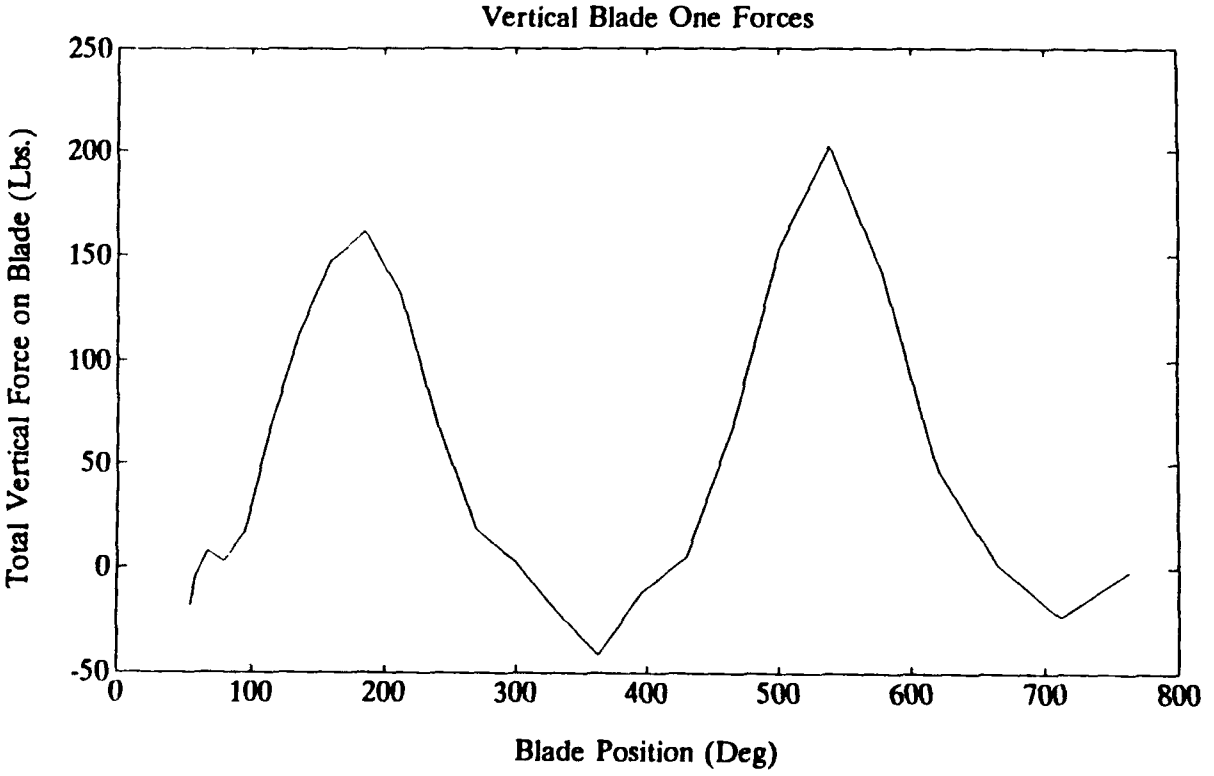

Figure 27. Total Vertical Forces on Blade One.

These results indicate that for blade one, there are large upward forces at the 180° postion and considerably smaller downward forces (less than 50 lbs.) at the 360° posi-

tion. Although this program does not include centrifugal forces on the rotor blade, such forces would limit the affect of the large upward forces on blade displacement. Blade two exhibits similiar behavior, with large (150 lbs.) upward forces at the the 180 ° position and low downward forces at the 360° position. Blade three exhibits forces opposite that of one and two, showing a large upward force near the 360° position, and a small downward force near the 220° position. The distribution of forces agree with the behavior of the blade displacements observed in tunnel strike videos. The shift in forces on blade three are due to the increased rotational velocities when the strong upflow is encountered. Beyond the second revolution, the linear velocities due to the rotation of the blades prevent the net forces from acting in the downward direction. Although the aerodynamic forces appear to be increasing past two revolutions, the resultant force on each blade would move away from the vertical as the centrifugal forces on the rotor blade increased with RPM. The aerodynamic forces correspond with known behavior of the rotor blades in low RPM environments, where the blades tend to rise or "sail" at the 180° position, and dip down when the blade is over the fuselage of the aircraft (360°).

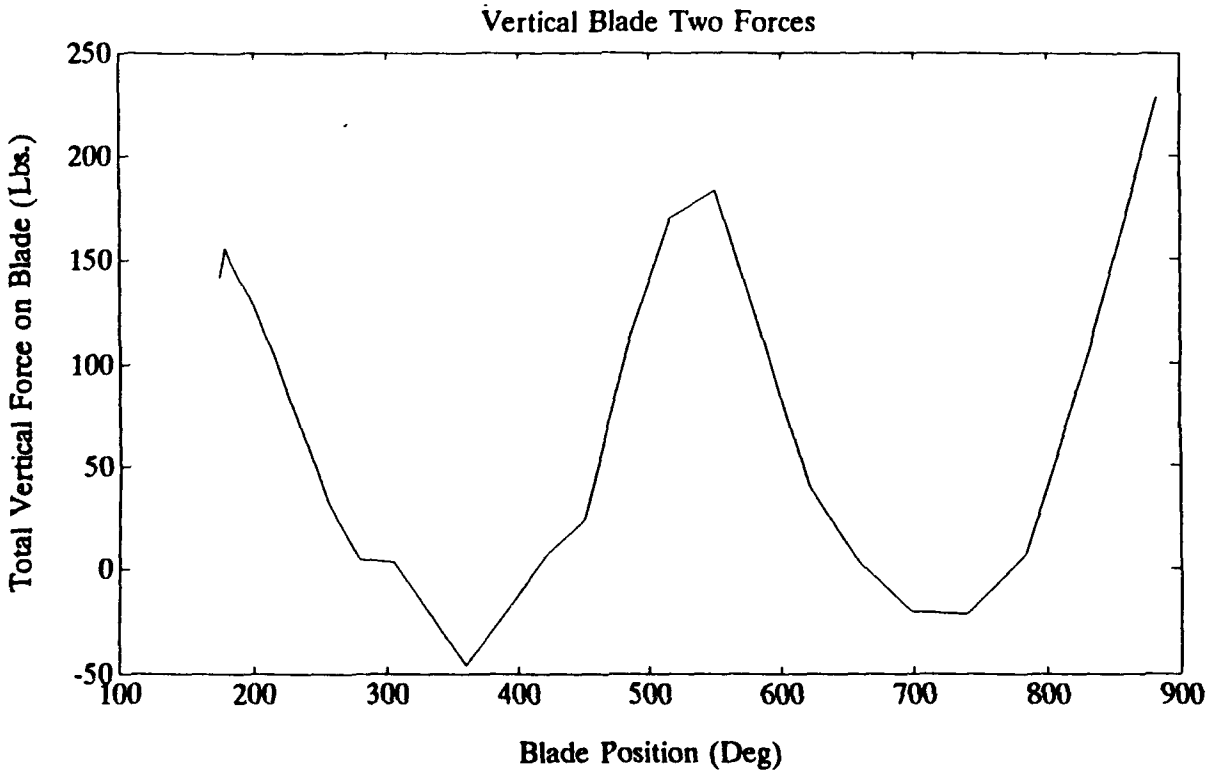

Figure 28. Total Vertical Forces on Blade Two.

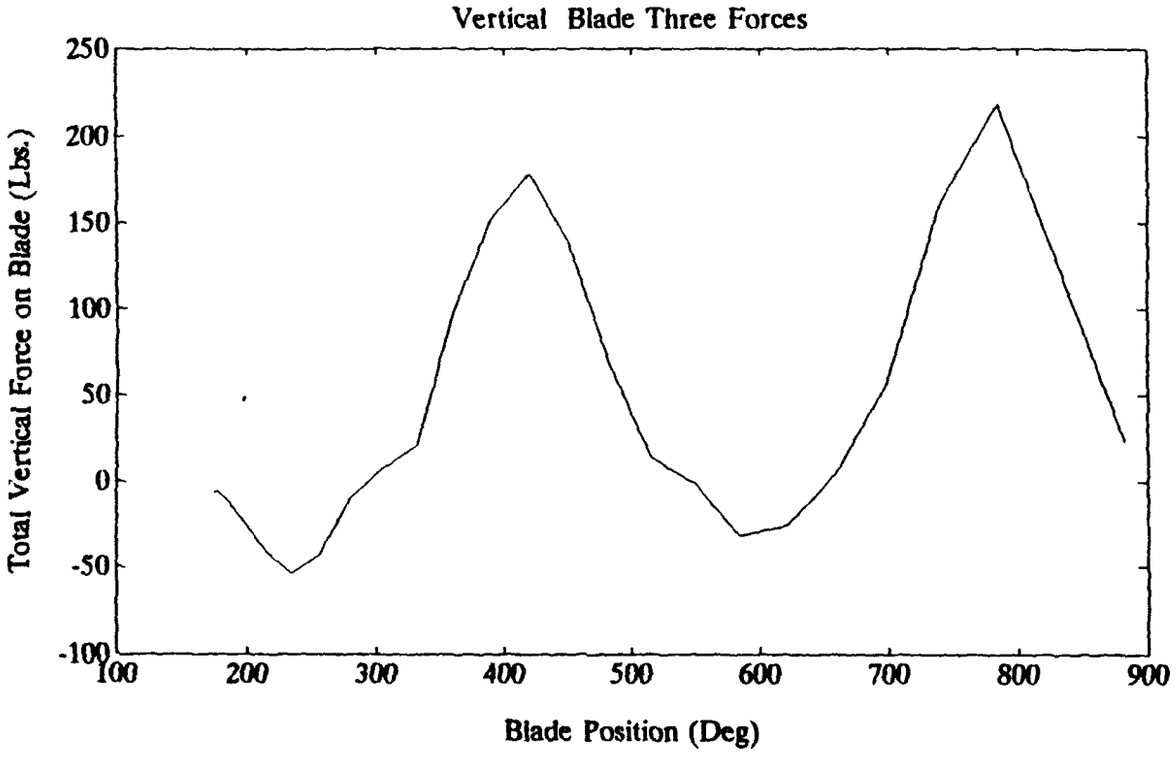

Figure 29. Total Vertical Forces on Blade Three.

V. CONCLUSIONS AND RECOMMENDATIONS

A. AIR-WAKE TURBULENCE MATH MODEL

Initial results show good agreement between predictions of the sixth order math model and the measured data from the wind tunnel model. Higher order transfer functions appear to model the measured turbulence with greater accuracy. Such a high order transfer function would not present computational difficulties in a real-time simulation, since the power spectra could be calculated prior to the running of the helicopter simulator, and the results stored for use as the helicopter passed through the points simulated by the math model. Since each point would have only thirty-nine variables (eighteen poles, eighteen zeros and three gains) for the components of the turbulence, the prior computation would not be time consuming nor utilize a large area for data storage.

This approach requires the measurement of the airwake at numerous points along the prescribed approach paths for each type of helicopter the DD-963 class of ship. Measurements would also have to be made with the wind at various angles to the ship heading. For those measurements already completed, filters must be designed to model the power spectra for each component. As noted in Chapter IV, comparison of the results with Hanson's first order model showed a much smoother curve (with less variance). This results in an overall lower variance than Hanson's model, eliminating the need to reduce the variance of the turbulence velocity components to simulate real-time conditions. The scaling of the frequencies to match the frequencies of the prototype will not affect the coefficients of the transfer functions. The output is simply scaled to match the lower frequencies of the prototype. Thus, the poles and zeros of the transfer functions will not change when applied to the prototype.

The smoothness of the computer model is enhanced with a smaller variance, accomplished by using a larger set of random signals to simulate the white noise. As the number of white noise points increases, the variance approaches zero, thus reducing the scatter in the *PRO-MATLAB* simulation that occurred in the PC simulation. Needing further study are:

Computational compatibility with existing real-time simulators.

Measurement and modeling of additional approach paths to the ship's flight deck.

Pilot evaluation of the turbulence model on a real-time simulator.

Since actual frequencies over 1.0 Hz. are not considered important for most manned air-vehicles, the response of the filters at those higher frequencies are considered to be negligible.

B. CH-46 TUNNEL STRIKE MODELS

In this preliminary analysis, an attempt was made to "produce" a blade strike by exposing the helicopter blade to the mean flow, as measured by a hot-wire anemometer over the flight deck of an AOR model. Due to the extreme divergence occurring during the Runge-Kutta integration scheme in DYSCO, a solution was not obtained. Further study is needed to investigate if the DYSCO routines are suitable for such low Reynolds Number applications. The results of the wind tunnel measurements should also be used in more sophisticated blade analysis programs, such as RACAP and CAMRAD. For the Blade Element Program, progress was made in identifying those areas of upward and downward aerodynamic forces on the rotor blades. The program has shown that measurements of flowfields over model ships in wind tunnels can be applied to estimating the distribution of mean aerodynamic forces on each rotor blade with respect to blade position. Further development of this program should include its validation, incorporation of rotating beam theory, accounting for the blade mass and bending characteristics along with rotor blade flapping. Further measurements of flowfields over various classes of ships should also be made at various yaw angles to analytically investigate those areas of high aerodynamic forces present during rotor engagement and disengagement.

APPENDIX A. CH-46 BLADE ELEMENT PROGRAM

```
      PROGRAM ELEMENT1
C
C ***********************************************
C *  PROGRAM TO DETERMINE VELOCITY FIELD      *
C *  OF AOR FLIGHT DECK AT 90 DEGREES YAW     *
C *  FOR GIVEN ROTOR ENGAGEMENT ACCELL        *
C *  AND FIND LIFT AND DRAG FORCES            *
C *  ON THE ROTOR BLADE USING BLADE  ELEMENTS*
C ***********************************************
C
      DIMENSION TIME(41),U(41),W(41),POS(41),REV(41),PHI(41),RPM(41),
     +VROT(41,10),UM(41),WM(41),AOA(41,10),AOAL(101),CLL(101),CL(41,10),
     +CDL(101),CD(41,10),AOAT(41,10),DRAG(41,10),RSEC(10),TWIST(10),
     +DBLADE(41),AOAAVG(41),AOAD(101),DRAGV(41,10),DBLADV(41),FORCE(41)
      REAL MAG1(41,10),LIFT(41,10),LBLADE(41),LIFTV(41,10),LBLADV(41)
      DOUBLE PRECISION MU, REN1(41,10),RENAVG(41)
      OPEN(UNIT=9,FILE='FLOW1.DAT',STATUS='old')
      OPEN(UNIT=10,FILE='TIMESTEPS.DAT',STATUS='OLD')
      OPEN(UNIT=15,FILE='LCOEFFE.DAT',STATUS='OLD')
      OPEN(UNIT=17,FILE='DCOEFFE.DAT',STATUS='OLD')
      OPEN(UNIT=16,FILE='SECTIONS.DAT',STATUS='OLD')
      OPEN(UNIT=18,FILE='GRAPH1.DAT',STATUS='OLD')
C
C     REV=NO. OF REVOLUTIONS
C     POS=ANGLE OF REFERENCE BLADE IN RADIANS
C     U=VELOCITY COMPONENT TANGENTIAL TO ROTOR DISK
C     W=VELOCITY COMPONENT PERPINDICULAR TO ROTOR DISK
C
      READ(10,*)(TIME(I), I=1,41)
      READ(15,*)(AOAL(J),CLL(J), J=1,101)
      READ(17,*)(AOAD(J),CDL(J), J=1,101)
C
C     COMPUTE BLADE POSITION
C
      DO 100 I=1,41
      REV(I)=.0071*TIME(I)+0.029470*(TIME(I))**2.0-0.002543*(TIME(I))
     +**3.0+0.000098*(TIME(I))**4.0+0.151325
      RPM(I)=4.2675E-02+3.5366*TIME(I)-0.45788*TIME(I)**2.0+2.3455E-02
     +*TIME(I)**3.0
C
C     CHANGE REVOLUTIONS TO RADIANS
C
      POS(I)=REV(I)*2.0*3.141593
      PHI(I)=REV(I)*360.00
C
C  COMPUTE THE TWIST ANGLE AND RADIUS OF EACH BLADE SECTION
C
      DO 25 L=1,10
       RSEC(L)=(L*28.71-28.71/2.0)+18.9
       TWIST(L)=(4.353-0.02779*RSEC(L))
25    CONTINUE
```

```
C
C  COMPUTE THE ROTATIONAL VELOCITY AT EACH BLADE ELEMENT
C
      DO 27 J=1,10
       DO 28 N=1,41
       VROT(N,J)=RPM(N)*2.0*3.1416/60*(RSEC(J)/12.0)
28     CONTINUE
27    CONTINUE
C
C  COMPUTE VELOCITIES HORIZONTAL AND PERPINDICULAR TO ROTOR DISK
C
20    if((PHI(I).GT.0.0).and.(PHI(I).le.90.0))goto 30
      if((phi(i).gt.90.0).and.(phi(i).le.180.0))goto 40
      if((phi(i).gt.180.0).and.(phi(i).le.270.0))goto 50
      if((phi(i).gt.270.0).and.(PHI(I).LE.360.0))GOTO 60
      if(phi(i).gt.360.0)phi(i)=phi(i)-360.0
      goto 20
C
30    U(I)=2.05+(phi(i)/90.0)*(1.83-2.05)
      W(I)=0.94+(phi(i)/90.0)*(0.87-0.94)
      goto 70
C
40    U(I)=1.83+((phi(i)-90.0)/90.0)*(1.80-1.83)
      W(I)=0.87+((phi(i)-90.0)/90.0)*(0.84-0.87)
      goto 70
C
50    U(I)=1.80+((phi(i)-180.0)/90.0)*(1.61-1.80)
      W(I)=0.84+((phi(i)-180.0)/90.0)*(0.53-0.84)
      goto 70
C
60    U(I)=1.61+((phi(i)-270.0)/90.0)*(2.05-1.61)
      W(I)=0.53+((phi(i)-270.0)/90.0)*(0.94-0.53)
70    continue
100   continue
      va=(2.327**2+.37**2)**0.5
      do 200 k=1,41
C       CONVERT WINDTUNNEL COMPONENTS TO SCALED IN FPS
      u(K)=(U(K)/va)*(40*1.688)
      W(K)=(W(K)/va)*(40*1.688)
200   continue
C
C  COMPUTE THE REYNOLDS NUMBER FOR EACH TIME STEP
C
      DO 610 N=1,10
        DO 300 I=1,41
         TERM1=VROT(I,N)-U(I)*COS(POS(I))
         MAG1(I,N)=(TERM1**2.0 + W(I)**2.0)**0.5
         REN1(I,N)=6400*1.6*MAG1(I,N)
300     CONTINUE
610   CONTINUE
C
C  DETERMINE THE ANGLE OF ATTACK FOR EACH TIME STEP
C
      DO 620 N=1,10
      DO 600 I=1,41
      TERM1=VROT(I,N)-U(I)*COS(POS(I))
```

```
      AOAT(I,N)=(ATAN(W(I)/(TERM1)))*(180.0/3.1416)+TWIST(I)
      IF(AOAT(I,N).LT.0)AOAT(I,N)=AOAT(I,N)+180.0
          DO 700 J=1,101
       IF(AOAT(I,N).EQ.AOAL(J))GOTO 900
       IF(AOAT(I,N).LT.(AOAL(J)+0.5).AND.(AOAT(I,N).GT.AOAL(J)))
     +GOTO 910
       IF(AOAT(I,N).GE.(AOAL(J)+0.5).AND.(AOAT(I,N).LT.AOAL(J+1)))
     +GOTO 920
      GOTO 700
900        AOA(I,N)=AOAT(I,N)
           CL(I,N)=CLL(J)
           GOTO 2000
910        AOA(I,N)=AOAL(J)
           CL(I,N)=CLL(J)
           GOTO 2000
920        AOA(I,N)=AOAL(J+1)
           CL(I,N)=CLL(J+1)
           GOTO 2000
700         CONTINUE
2000       DO 750 J=1,101
       IF(AOAT(I,N).EQ.AOAD(J))GOTO 901
       IF(AOAT(I,N).LT.(AOAD(J)+0.5).AND.(AOAT(I,N).GT.AOAD(J)))
     +GOTO 911
       IF(AOAT(I,N).GE.(AOAD(J)+0.5).AND.(AOAT(I,N).LT.AOAD(J+1)))
     +GOTO 921
      GOTO 750
C  901        AOA(I,N)=AOAT(I,N)
901           CD(I,N)=CDL(J)
           GOTO 600
C  911        AOA(I,N)=AOAD(J)
911           CD(I,N)=CDL(J)
           GOTO 600
C   921        AOA(I,N)=AOAD(J+1)
921           CD(I,N)=CDL(J+1)
           GOTO 600
750         CONTINUE
600        CONTINUE
620     CONTINUE
C
C  DETERMINE LIFT AND DRAG FORCES
C
      DO 660 J=1,10
      DO 650 N=1,41
      TERM1=VROT(N,J)-U(N)*COS(POS(N))
      MAG1(N,J)=(TERM1**2.0 + W(I)**2.0)**0.5
      LIFT(N,J)=CL(N,J)*0.5*0.002378*(MAG1(N,J)**2.0)*(28.71/12.0)*1.6
      DRAG(N,J)=CD(N,J)*0.5*0.002378*(MAG1(N,J)**2.0)*(28.71/12.0)*1.6
      LIFTV(N,J)=LIFT(N,J)*ABS(COS(AOA(N,J)*3.1416/180))
      DRAGV(N,J)=DRAG(N,J)*SIN(AOA(N,J)*3.1416/180)
650   CONTINUE
660   CONTINUE
C
C  COMPUTE SUM OF LIFT AND DRAG FOR BLADE ELEMENTS, AVG AOA AND REN
C     LBLADE(1)=0.0
      DBLADE(1)=0.0
      AOAAVG(1)=0.0
```

```
      RENAVG(1)=0.0
      LBLADV(1)=0.0
      DBLADV(1)=0.0
      DO 1500 N=1,41
       DO 1000 I=1,10
       LBLADE(N)=LBLADE(N)+LIFT(N,I)
       DBLADE(N)=DBLADE(N)+DRAG(N,I)
       LBLADV(N)=LBLADV(N)+LIFTV(N,I)
       DBLADV(N)=DBLADV(N)+DRAGV(N,I)
       AOAAVG(N)=(AOAAVG(N)+AOA(N,I))
       RENAVG(N)=(RENAVG(N)+REN1(N,I))/I
1000   CONTINUE
      AOAAVG(N)=AOAAVG(N)/10
      FORCE(N)=LBLADV(N)+DBLADV(N)
1500  CONTINUE
      WRITE(9,10)
10    FORMAT(3X,'TIME(SEC)',2X,'POSITION',2X,'RPM',3X,'AOA AVG',6X,
     +'REN AVG',6X,'LIFT',3X,'DRAG')
      WRITE(9,15)(TIME(I),PHI(I),RPM(I),AOAAVG(I),RENAVG(I),LBLADV(I),
     +DBLADV(I),I=1,41)
15    FORMAT(F8.2,2X,F8.2,2X,F7.2,3X,F7.2,3X,D10.4,4X,2F8.2)
      WRITE(16,*)('BLADE POSITION                    ANGLE OF ATTACK')
      WRITE(16,1600)(PHI(N),(AOA(N,I), I=1,10), N=1,41)
      WRITE(16,*)('BLADE POSITION                    REYNOLDS NUMBER')
      WRITE(16,1700)(PHI(N),(REN1(N,I), I=1,10), N=1,41)
      WRITE(16,*)('BLADE POSITION                RELATIVE VEL. IN FPS.')
      WRITE(16,1800)(PHI(N),(MAG1(N,I), I=1,10), N=1,41)
      WRITE(16,*)('BLADE POSITION                 SECTION LIFT (LBS.)')
      WRITE(16,1800)(PHI(N),(LIFT(N,I), I=1,10), N=1,41)
      WRITE(16,*)('BLADE POSITION                 SECTION DRAG (LBS.)')
      WRITE(16,1800)(PHI(N),(DRAG(N,I), I=1,10), N=1,41)
      WRITE(16,*)('BLADE POSITION       SECTION VERTICAL LIFT (LBS.)')
      WRITE(16,1800)(PHI(N),(LIFTV(N,I), I=1,10), N=1,41)
      WRITE(16,*)('BLADE POSITION       SECTION VERTICAL DRAG (LBS.)')
      WRITE(16,1800)(PHI(N),(DRAGV(N,I), I=1,10), N=1,41)
      WRITE(16,*)('BLADE POSITION                 LIFT COEFFICIENT')
      WRITE(16,1800)(PHI(N),(CL(N,I), I=1,10), N=1,41)
      WRITE(16,*)('BLADE POSITION                 DRAG COEFFICIENT')
      WRITE(16,1800)(PHI(N),(CD(N,I), I=1,10), N=1,41)
      WRITE(18,1900)(POS(N),FORCE(N), N=1,41)
1600  FORMAT(F6.2,2X,10F6.1)
1700  FORMAT(F6.2,2X,10D9.3)
1800  FORMAT(F6.2,2X10F7.1)
1900  FORMAT(2X,F6.2,2X,F9.3)
      END
```

A. AERODYNAMIC VALUES OF BLADE ONE

TIME (SEC)	POSITION (DEG)	RPM	AOA AVG (DEG)	REN AVG	LIFT (LBS)	DRAG (LBS)
.00	54.48	.04	146.16	.4723D+05	-39.28	20.80
.50	58.30	1.70	139.32	.4091D+05	-26.55	22.25
1.00	66.76	3.14	126.72	.3322D+05	-8.12	15.92
1.50	79.27	4.40	100.80	.2909D+05	-.19	2.95
2.00	95.27	5.47	65.16	.3584D+05	3.96	12.34
2.50	114.25	6.39	39.96	.5183D+05	39.40	28.70
3.00	135.77	7.16	27.72	.6979D+05	86.98	26.82
3.50	159.43	7.82	21.24	.8348D+05	128.33	19.21
4.00	184.89	8.36	19.44	.8759D+05	145.38	16.67
4.50	211.86	8.82	18.36	.7811D+05	121.81	10.56
5.00	240.10	9.21	27.72	.5820D+05	53.00	15.67
5.50	269.43	9.55	52.20	.3326D+05	9.69	8.76
6.00	299.72	9.84	118.44	.2204D+05	-5.61	8.13
6.50	330.89	10.13	145.44	.3712D+05	-42.47	21.53
7.00	2.92	10.41	149.40	.4853D+05	-69.70	28.08
7.50	35.82	10.71	140.04	.3711D+05	-36.35	24.80
8.00	69.69	11.04	98.28	.3113D+05	-.87	6.08
8.50	104.66	11.43	43.56	.5626D+05	37.66	29.78
9.00	140.91	11.88	25.92	.8580D+05	122.64	31.38
9.50	178.69	12.43	21.60	.9955D+05	175.47	26.68
10.00	218.28	13.08	22.32	.8584D+05	122.47	19.79
10.50	260.03	13.85	35.28	.5292D+05	33.17	13.70
11.00	304.34	14.76	110.16	.2472D+05	-5.61	7.50
11.50	351.66	15.83	143.64	.3587D+05	-46.29	22.96
12.00	42.49	17.08	122.04	.3014D+05	-15.55	14.38
12.50	97.40	18.52	41.76	.6787D+05	50.25	29.04
13.00	156.98	20.17	20.16	.1170D+06	233.03	25.65
13.50	221.91	22.05	19.44	.1086D+06	208.91	17.46
14.00	292.90	24.17	63.72	.5235D+05	19.35	11.34
14.50	10.72	26.56	120.96	.3294D+05	-25.13	16.43
15.00	96.19	29.23	33.84	.9572D+05	98.09	28.29
15.50	190.19	32.20	15.84	.1536D+06	465.23	17.42
16.00	293.63	35.48	47.16	.8278D+05	64.69	11.68
16.50	47.51	39.10	68.76	.7632D+05	35.98	23.07
17.00	172.86	43.07	14.40	.1862D+06	674.24	14.85
17.50	310.75	47.41	52.56	.1013D+06	91.23	14.42
18.00	102.34	52.14	20.88	.1666D+06	410.12	20.82
18.50	268.81	57.27	15.48	.1682D+06	343.74	4.38
19.00	91.41	62.82	21.60	.1860D+06	503.34	18.12
19.50	291.43	68.81	23.04	.1801D+06	374.32	5.71
20.00	150.24	75.26	11.52	.2717D+06	1030.74	9.53

B. AERODYNAMIC VALUES FOR BLADE TWO

TIME (SEC)	POSITION (DEG)	RPM	AOA AVG (DEG)	REN AVG	LIFT (LBS)	DRAG (LBS)
.00	174.48	.04	28.80	.6566D+05	104.29	37.33
.50	178.29	1.70	28.80	.7021D+05	114.81	41.10
1.00	186.76	3.14	25.92	.7297D+05	114.27	29.86
1.50	199.27	4.40	24.48	.7237D+05	105.65	23.61
2.00	215.27	5.47	24.48	.6685D+05	84.55	19.00
2.50	234.25	6.39	27.72	.5549D+05	54.05	16.54
3.00	255.77	7.16	37.80	.3913D+05	20.45	12.05
3.50	279.43	7.82	78.84	.2340D+05	.99	3.72
4.00	304.89	8.36	127.80	.2468D+05	-11.21	14.59
4.50	331.86	8.82	144.00	.4042D+05	-49.73	28.66
5.00	.10	9.21	150.12	.5154D+05	-75.35	29.28
5.50	29.43	9.55	144.00	.4219D+05	-49.70	28.22
6.00	59.72	9.84	118.08	.2975D+05	-6.71	12.57
6.50	90.89	10.13	61.20	.4180D+05	9.25	15.22
7.00	122.92	10.41	31.68	.6901D+05	76.00	31.56
7.50	155.82	10.71	23.76	.9010D+05	140.78	29.04
8.00	189.69	11.04	21.60	.9392D+05	158.92	24.31
8.50	224.66	11.43	23.76	.7672D+05	96.20	19.10
9.00	260.91	11.88	38.52	.4682D+05	26.17	13.63
9.50	298.69	12.43	108.72	.2340D+05	-3.64	6.45
10.00	338.28	13.08	144.36	.3537D+05	-42.07	21.36
10.50	20.03	13.85	143.28	.3771D+05	-45.74	24.44
11.00	64.34	14.76	97.56	.3340D+05	-1.43	8.55
11.50	111.66	15.83	34.20	.7391D+05	73.55	32.59
12.00	162.49	17.08	20.88	.1101D+06	201.37	26.97
12.50	217.39	18.52	20.16	.1017D+06	172.84	18.77
13.00	276.98	20.17	45.36	.5512D+05	27.25	10.53
13.50	341.91	22.05	128.16	.2857D+05	-25.98	15.39
14.00	52.90	24.17	90.36	.4357D+05	1.43	15.21
14.50	130.72	26.56	22.32	.1196D+06	216.14	28.44
15.00	216.19	29.23	17.28	.1329D+06	328.68	16.67
15.50	310.18	32.20	72.36	.5971D+05	19.78	14.64
16.00	53.63	35.48	68.04	.7175D+05	32.48	21.30
16.50	167.51	39.10	15.48	.1739D+06	580.68	18.20
17.00	292.85	43.07	38.88	.1049D+06	126.35	11.24
17.50	70.75	47.41	39.96	.1207D+06	147.80	22.15
18.00	222.34	52.14	12.60	.1944D+06	601.35	7.28
18.50	28.81	57.27	61.20	.1129D+06	89.31	24.21
19.00	211.41	62.82	11.52	.2324D+06	769.20	7.49
19.50	51.43	68.81	39.24	.1627D+06	304.32	18.68
20.00	270.24	75.26	12.60	.2188D+06	468.15	3.75

C. AERODYNAMIC VALUES FOR BLADE THREE

TIME (SEC)	POSITION (DEG)	RPM	AOA AVG (DEG)	REN AVG	LIFT (LBS)	DRAG (LBS)
.00	294.47	.04	144.00	.3173D+05	-16.72	10.16
.50	298.29	1.70	142.20	.3132D+05	-18.04	12.36
1.00	306.76	3.14	145.44	.3500D+05	-26.96	14.72
1.50	319.27	4.40	149.76	.4189D+05	-42.38	17.26
2.00	335.26	5.47	151.92	.5021D+05	-63.19	22.04
2.50	354.25	6.39	151.92	.5674D+05	-82.68	28.82
3.00	15.77	7.16	149.04	.5304D+05	-75.89	32.24
3.50	39.43	7.82	139.68	.4059D+05	-40.20	30.54
4.00	64.89	8.36	111.60	.2953D+05	-3.29	11.03
4.50	91.86	8.82	59.76	.3984D+05	7.94	13.15
5.00	120.10	9.21	34.20	.6363D+05	64.55	32.42
5.50	149.43	9.55	24.48	.8409D+05	123.69	27.64
6.00	179.72	9.84	21.60	.9239D+05	154.35	24.37
6.50	210.89	10.13	21.96	.8228D+05	118.10	19.13
7.00	242.92	10.41	28.08	.5902D+05	52.12	15.51
7.50	275.82	10.71	61.56	.3151D+05	6.54	7.15
8.00	309.69	11.04	129.60	.2432D+05	-13.14	12.16
8.50	344.66	11.43	148.32	.4149D+05	-54.32	22.83
9.00	20.91	11.88	145.44	.4099D+05	-51.36	25.69
9.50	58.68	12.43	113.40	.2980D+05	-5.82	10.41
10.00	98.27	13.08	47.52	.5475D+05	30.29	26.12
10.50	140.02	13.85	25.20	.9065D+05	131.31	30.82
11.00	184.33	14.76	20.88	.1055D+06	192.17	26.10
11.50	231.65	15.83	23.04	.8355D+05	105.79	17.71
12.00	282.49	17.08	60.84	.4231D+05	13.42	9.73
12.50	337.39	18.52	133.92	.2831D+05	-28.51	17.12
13.00	36.98	20.17	119.52	.3097D+05	-16.96	15.16
13.50	101.91	22.05	36.00	.8161D+05	76.25	31.31
14.00	172.90	24.17	18.36	.1323D+06	325.86	24.19
14.50	250.72	26.56	22.32	.9710D+05	142.56	13.35
15.00	336.19	29.23	105.84	.3812D+05	-12.77	15.36
15.50	70.18	32.20	54.72	.7805D+05	48.42	22.39
16.00	173.63	35.48	15.84	.1645D+06	526.78	19.39
16.50	287.51	39.10	37.08	.9863D+05	108.50	11.38
17.00	52.85	43.07	59.04	.9155D+05	59.16	22.69
17.50	190.75	47.41	13.32	.1971D+06	705.49	11.71
18.00	342.34	52.14	69.48	.9377D+05	50.26	20.66
18.50	148.81	57.27	12.60	.2192D+06	776.24	9.76
19.00	331.41	62.82	53.28	.1295D+06	160.46	16.76
19.50	171.43	68.81	10.80	.2601D+06	990.18	7.42
20.00	30.23	75.26	46.44	.1647D+06	291.69	21.12

D. BLADE ELEMENT RESULTS FOR BLADE ONE

BLADE POSTION (DEG)	ANGLE OF ATTACK (DEGREES) SECTIONS									
	1	2	3	4	5	6	7	8	9	10
54.48	147.6	147.6	147.6	147.6	147.6	147.6	144.0	144.0	144.0	144.0
58.30	140.4	140.4	140.4	140.4	140.4	140.4	140.4	136.8	136.8	136.8
66.76	133.2	129.6	129.6	129.6	126.0	126.0	126.0	122.4	122.4	122.4
79.27	111.6	108.0	108.0	104.4	100.8	100.8	97.2	93.6	93.6	90.0
95.27	75.6	75.6	72.0	68.4	64.8	64.8	61.2	57.6	57.6	54.0
114.25	46.8	46.8	43.2	43.2	39.6	39.6	36.0	36.0	36.0	32.4
135.77	32.4	32.4	28.8	28.8	28.8	25.2	25.2	25.2	25.2	25.2
159.43	25.2	25.2	21.6	21.6	21.6	21.6	21.6	18.0	18.0	18.0
184.89	21.6	21.6	21.6	21.6	18.0	18.0	18.0	18.0	18.0	18.0
211.86	21.6	21.6	21.6	18.0	18.0	18.0	18.0	18.0	14.4	14.4
240.10	36.0	32.4	32.4	28.8	28.8	25.2	25.2	25.2	21.6	21.6
269.43	79.2	72.0	64.8	57.6	50.4	46.8	43.2	39.6	36.0	32.4
299.72	140.4	136.8	133.2	129.6	122.4	118.8	111.6	104.4	97.2	90.0
330.89	154.8	151.2	151.2	151.2	147.6	144.0	144.0	140.4	136.8	133.2
2.92	154.8	154.8	154.8	151.2	151.2	147.6	147.6	147.6	144.0	140.4
35.82	151.2	147.6	147.6	144.0	144.0	140.4	136.8	133.2	129.6	126.0
69.69	122.4	118.8	115.2	108.0	100.8	97.2	90.0	82.8	75.6	72.0
104.66	57.6	54.0	50.4	46.8	43.2	39.6	39.6	36.0	36.0	32.4
140.91	32.4	28.8	28.8	28.8	25.2	25.2	25.2	21.6	21.6	21.6
178.69	25.2	25.2	25.2	21.6	21.6	21.6	21.6	18.0	18.0	18.0
218.28	28.8	25.2	25.2	25.2	21.6	21.6	21.6	18.0	18.0	18.0
260.03	54.0	46.8	43.2	39.6	36.0	32.4	28.8	25.2	25.2	21.6
304.34	144.0	140.4	133.2	126.0	118.8	108.0	97.2	86.4	79.2	68.4
351.66	154.8	154.8	151.2	151.2	147.6	144.0	140.4	136.8	129.6	126.0
42.49	147.6	144.0	140.4	133.2	129.6	122.4	115.2	104.4	97.2	86.4
97.40	64.8	57.6	50.4	46.8	39.6	36.0	32.4	32.4	28.8	28.8
156.98	25.2	25.2	21.6	21.6	21.6	18.0	18.0	18.0	18.0	14.4
221.91	28.8	25.2	21.6	21.6	18.0	18.0	18.0	14.4	14.4	14.4
292.90	126.0	111.6	93.6	75.6	57.6	46.8	39.6	32.4	28.8	25.2
10.72	154.8	151.2	144.0	140.4	133.2	122.4	111.6	97.2	82.8	72.0
96.19	61.2	50.4	43.2	36.0	32.4	28.8	25.2	21.6	21.6	18.0
190.19	21.6	21.6	18.0	18.0	14.4	14.4	14.4	14.4	10.8	10.8
293.63	118.8	93.6	68.4	46.8	36.0	28.8	25.2	21.6	18.0	14.4
47.51	136.8	122.4	104.4	82.8	64.8	50.4	39.6	32.4	28.8	25.2
172.86	21.6	18.0	18.0	14.4	14.4	14.4	10.8	10.8	10.8	10.8
310.75	136.8	111.6	82.8	54.0	39.6	28.8	21.6	18.0	18.0	14.4
102.34	43.2	32.4	25.2	21.6	18.0	18.0	14.4	14.4	10.8	10.8
268.81	43.2	25.2	18.0	14.4	10.8	10.8	10.8	7.2	7.2	7.2
91.41	54.0	36.0	25.2	21.6	18.0	14.4	14.4	10.8	10.8	10.8
291.43	82.8	43.2	25.2	18.0	14.4	10.8	10.8	10.8	7.2	7.2
150.24	21.6	18.0	14.4	10.8	10.8	10.8	7.2	7.2	7.2	7.2

BLADE POSITION (DEG)	SECTION VERTICAL LIFT (LBS.)									
54.48	-3.9	-3.9	-3.9	-3.9	-3.9	-3.9	-4.0	-4.0	-4.0	-4.0
58.30	-3.1	-3.0	-2.9	-2.8	-2.7	-2.6	-2.6	-2.3	-2.3	-2.2
66.76	-1.4	-1.2	-1.1	-1.0	-.8	-.7	-.6	-.5	-.4	-.4
79.27	-.1	-.0	-.0	-.0	.0	.0	.0	.0	.0	.0
95.27	.0	.0	.1	.2	.3	.3	.5	.7	.8	1.1
114.25	2.1	2.4	2.9	3.2	3.7	4.1	4.6	5.1	5.5	5.9
135.77	6.4	7.0	7.3	7.9	8.5	8.6	9.3	9.9	10.6	11.4
159.43	9.5	10.3	10.3	11.1	11.8	12.6	13.5	15.5	16.4	17.4
184.89	9.9	10.7	11.5	12.3	14.3	15.3	16.3	17.3	18.4	19.5
211.86	6.9	7.6	8.3	9.8	10.7	11.6	12.5	13.5	19.7	21.1
240.10	3.0	3.5	4.1	4.4	5.1	5.4	6.0	6.8	7.0	7.7
269.43	.0	.0	.1	.3	.6	.9	1.3	1.7	2.2	2.6
299.72	-1.9	-1.4	-1.0	-.7	-.3	-.2	-.1	-.0	.0	.0
330.89	-6.6	-6.4	-5.7	-5.0	-4.6	-4.1	-3.4	-2.8	-2.2	-1.6
2.92	-10.1	-9.1	-8.3	-8.1	-7.3	-6.9	-6.0	-5.3	-4.7	-3.9
35.82	-6.5	-6.1	-5.3	-4.6	-4.0	-3.3	-2.6	-1.9	-1.3	-.9
69.69	-.5	-.3	-.1	-.0	.0	.0	.0	.0	.0	.1
104.66	.7	1.2	1.7	2.4	3.2	4.0	4.8	5.7	6.6	7.4
140.91	7.9	8.6	9.7	10.9	11.4	12.7	14.0	14.4	15.7	17.1
178.69	11.2	12.5	13.9	14.3	15.8	17.2	18.8	22.1	9	25.8
218.28	7.1	7.7	8.9	10.1	10.6	11.9	13.3	15.9	.6	19.3
260.03	.5	1.0	1.5	2.2	2.9	3.6	4.3	4.9	5.9	6.5
304.34	-2.4	-1.7	-1.0	-.5	-.2	-.0	.0	.0	.0	.1
351.66	-9.0	-7.7	-7.1	-5.9	-5.1	-4.2	-3.2	-2.2	-1.3	-.7
42.49	-5.0	-4.0	-3.0	-1.8	-1.1	-.5	-.2	-.0	.0	.0
97.40	.3	.7	1.6	2.6	4.0	5.3	6.6	8.2	9.6	11.4
156.98	10.6	12.7	13.9	16.2	18.7	23.1	26.2	29.4	32.8	49.4
221.91	7.3	8.7	10.0	12.2	15.7	18.5	21.5	33.5	38.2	43.2
292.90	-.4	-.0	.0	.0	.4	1.3	2.5	3.8	5.2	6.6
10.72	-8.0	-6.5	-5.1	-3.3	-1.7	-.6	-.1	.0	.0	.1
96.19	.5	1.6	3.4	5.5	7.8	10.1	12.4	14.7	18.2	23.8
190.19	12.2	15.7	21.3	26.1	42.5	50.2	58.7	67.8	80.0	90.8
293.63	-.2	.0	.1	1.1	2.9	4.8	7.1	9.6	14.1	25.1
47.51	-2.5	-.6	-.0	.0	.3	1.8	4.5	7.5	10.8	14.2
172.86	14.0	20.7	27.1	46.6	57.6	69.8	85.9	100.9	117.1	134.6
310.75	-1.5	-.1	.0	.8	3.2	6.1	9.0	14.8	20.9	38.0
102.34	2.8	6.4	10.2	14.8	23.0	31.2	55.2	69.9	89.0	107.7
268.81	1.3	3.8	8.0	18.6	29.3	41.5	55.9	48.8	61.3	75.3
91.41	1.2	5.3	9.6	15.3	25.3	48.6	65.4	87.5	110.0	135.1
291.43	.0	1.5	4.9	10.8	25.4	40.5	57.9	78.3	68.5	86.4
150.24	15.4	27.3	55.1	79.3	105.3	135.0	113.4	138.3	165.8	195.8

BLADE POSITION POSITION (DEG)	SECTION VERTICAL DRAG (LBS.)									
54.48	1.9	1.9	1.9	1.9	1.9	1.9	2.4	2.4	2.4	2.4
58.30	2.4	2.3	2.3	2.2	2.1	2.1	2.0	2.4	2.3	2.2
66.76	1.8	2.0	1.8	1.7	1.7	1.6	1.4	1.4	1.3	1.2
79.27	.7	.6	.4	.3	.3	.2	.1	.1	.1	.1
95.27	.4	.6	.8	.9	1.1	1.4	1.5	1.6	1.9	2.0
114.25	2.4	2.7	2.7	3.0	2.8	3.1	2.8	3.1	3.3	2.8
135.77	3.1	3.4	2.6	2.8	3.1	2.1	2.2	2.4	2.5	2.7
159.43	2.3	2.5	1.7	1.9	2.0	2.1	2.3	1.4	1.5	1.6
184.89	1.7	1.8	1.9	2.1	1.3	1.4	1.5	1.6	1.7	1.8
211.86	1.2	1.3	1.4	.9	1.0	1.1	1.1	1.2	.7	.7
240.10	1.8	1.7	1.9	1.6	1.8	1.3	1.4	1.6	1.2	1.3
269.43	.2	.4	.5	.7	.9	1.0	1.2	1.3	1.3	1.2
299.72	1.5	1.4	1.3	1.1	1.0	.7	.5	.3	.2	.1
330.89	1.9	2.4	2.1	1.9	2.2	2.5	2.1	2.2	2.2	2.1
2.92	2.8	2.6	2.3	3.0	2.7	3.3	2.9	2.5	2.8	3.1
35.82	2.4	2.9	2.5	2.8	2.4	2.6	2.6	2.5	2.2	1.9
69.69	1.5	1.2	.8	.5	.3	.1	.1	.2	.5	.8
104.66	1.8	2.2	2.5	2.8	3.0	3.0	3.6	3.4	4.0	3.5
140.91	3.8	3.1	3.5	3.9	2.7	3.0	3.3	2.4	2.7	2.9
178.69	2.7	3.0	3.3	2.4	2.7	2.9	3.2	2.0	2.2	2.3
218.28	2.5	1.8	2.1	2.4	1.8	2.0	2.2	1.4	1.6	1.8
260.03	.9	1.1	1.4	1.6	1.8	1.7	1.5	1.2	1.4	1.1
304.34	1.4	1.3	1.3	1.1	.7	.4	.2	.1	.3	.7
351.66	2.5	2.2	2.6	2.2	2.4	2.5	2.5	2.2	2.2	1.6
42.49	2.4	2.4	2.3	2.4	1.9	1.4	.9	.4	.1	.2
97.40	1.1	1.8	2.3	3.0	3.0	3.2	3.2	3.9	3.4	4.1
156.98	2.5	3.0	2.4	2.7	3.2	2.1	2.4	2.7	3.0	1.7
221.91	2.6	2.1	1.7	2.1	1.4	1.7	2.0	1.2	1.3	1.5
292.90	.9	.4	.1	.4	1.0	1.5	1.9	1.8	1.9	1.6
10.72	2.2	2.4	3.1	2.6	2.3	1.6	.8	.2	.2	1.0
96.19	1.4	2.3	3.1	3.3	3.7	3.6	3.0	2.5	3.1	2.2
190.19	2.1	2.7	1.9	2.4	1.5	1.7	2.0	2.3	.4	.4
293.63	.7	.1	.6	1.3	1.8	1.7	1.7	1.6	1.3	.9
47.51	2.5	1.7	.5	.2	1.3	2.6	3.4	3.6	3.9	3.4
172.86	2.4	1.9	2.5	1.6	2.0	2.4	.4	.5	.6	.7
310.75	1.5	.6	.2	1.4	2.4	2.2	1.5	1.3	1.9	1.3
102.34	2.6	3.1	2.4	2.5	2.1	2.8	1.9	2.4	.4	.5
268.81	1.2	.9	.7	.6	.1	.2	.3	.1	.1	.1
91.41	2.2	3.2	2.3	2.6	2.3	1.7	2.3	.4	.5	.7
291.43	.1	1.4	1.2	1.0	.9	.2	.3	.4	.1	.1
150.24	2.6	2.5	1.9	.4	.5	.7	.2	.2	.3	.3

E. BLADE ELEMENT RESULTS OF BLADE TWO

BLADE POSTION (DEG)	ANGLE OF ATTACK (DEGREES) SECTIONS									
	1	2	3	4	5	6	7	8	9	10
174.48	28.8	28.8	28.8	28.8	28.8	28.8	28.8	28.8	28.8	28.8
178.29	28.8	28.8	28.8	28.8	28.8	28.8	28.8	28.8	28.8	28.8
186.76	28.8	28.8	25.2	25.2	25.2	25.2	25.2	25.2	25.2	25.2
199.27	25.2	25.2	25.2	25.2	25.2	25.2	25.2	25.2	21.6	21.6
215.27	28.8	25.2	25.2	25.2	25.2	25.2	25.2	21.6	21.6	21.6
234.25	32.4	32.4	28.8	28.8	28.8	25.2	25.2	25.2	25.2	25.2
255.77	50.4	46.8	43.2	39.6	39.6	36.0	32.4	32.4	28.8	28.8
279.43	108.0	100.8	93.6	86.4	82.8	75.6	68.4	61.2	57.6	54.0
304.89	140.4	140.4	136.8	133.2	129.6	129.6	122.4	118.8	115.2	111.6
331.86	151.2	151.2	147.6	147.6	144.0	144.0	140.4	140.4	136.8	136.8
.10	154.8	154.8	154.8	151.2	151.2	151.2	147.6	147.6	144.0	144.0
29.43	151.2	151.2	147.6	147.6	147.6	144.0	140.4	140.4	136.8	133.2
59.72	136.8	133.2	129.6	126.0	122.4	115.2	111.6	108.0	100.8	97.2
90.89	82.8	75.6	72.0	68.4	61.2	57.6	54.0	50.4	46.8	43.2
122.92	39.6	36.0	36.0	32.4	32.4	32.4	28.8	28.8	25.2	25.2
155.82	28.8	25.2	25.2	25.2	25.2	21.6	21.6	21.6	21.6	21.6
189.69	25.2	25.2	25.2	21.6	21.6	21.6	21.6	18.0	18.0	18.0
224.66	28.8	28.8	25.2	25.2	25.2	21.6	21.6	21.6	21.6	18.0
260.91	57.6	50.4	46.8	43.2	36.0	36.0	32.4	28.8	28.8	25.2
298.69	140.4	133.2	129.6	122.4	115.2	108.0	97.2	90.0	79.2	72.0
338.28	154.8	154.8	151.2	151.2	147.6	144.0	140.4	136.8	133.2	129.6
20.03	154.8	151.2	151.2	147.6	147.6	144.0	140.4	136.8	133.2	126.0
64.34	129.6	122.4	118.8	111.6	100.8	93.6	86.4	79.2	68.4	64.8
111.66	46.8	43.2	39.6	36.0	36.0	32.4	28.8	28.8	25.2	25.2
162.49	25.2	25.2	21.6	21.6	21.6	21.6	18.0	18.0	18.0	18.0
217.39	25.2	25.2	21.6	21.6	21.6	18.0	18.0	18.0	18.0	14.4
276.98	90.0	75.6	61.2	50.4	39.6	36.0	28.8	25.2	25.2	21.6
341.91	154.8	151.2	147.6	144.0	136.8	129.6	122.4	111.6	97.2	86.4
52.90	136.8	129.6	122.4	108.0	97.2	82.8	72.0	61.2	50.4	43.2
130.72	32.4	28.8	25.2	25.2	21.6	21.6	18.0	18.0	18.0	14.4
216.19	25.2	21.6	21.6	18.0	18.0	14.4	14.4	14.4	14.4	10.8
310.18	140.4	129.6	111.6	90.0	68.4	54.0	43.2	32.4	28.8	25.2
53.63	133.2	118.8	100.8	82.8	64.8	50.4	39.6	36.0	28.8	25.2
167.51	21.6	21.6	18.0	18.0	14.4	14.4	14.4	10.8	10.8	10.8
292.85	111.6	79.2	50.4	36.0	28.8	21.6	18.0	14.4	14.4	14.4
70.75	100.8	75.6	54.0	39.6	32.4	25.2	21.6	18.0	18.0	14.4
222.34	21.6	18.0	14.4	14.4	10.8	10.8	10.8	10.8	7.2	7.2
28.81	144.0	126.0	100.8	72.0	46.8	36.0	28.8	21.6	18.0	18.0
211.41	21.6	18.0	14.4	10.8	10.8	10.8	7.2	7.2	7.2	7.2
51.43	118.8	82.8	54.0	36.0	25.2	21.6	18.0	14.4	10.8	10.8
270.24	36.0	21.6	14.4	10.8	10.8	7.2	7.2	7.2	7.2	3.6

BLADE POSITION POSTION (DEG)	SECTION VERTICAL LIFT (LBS.)									
	1	2	3	4	5	6	7	8	9	10
174.48	10.4	10.4	10.4	10.4	10.4	10.4	10.4	10.4	10.4	10.4
178.29	10.7	10.9	11.0	11.2	11.4	11.6	11.7	11.9	12.1	12.3
186.76	10.5	10.9	10.5	10.8	11.1	11.4	11.8	12.1	12.4	12.8
199.27	8.8	9.2	9.6	10.0	10.5	10.9	11.4	11.8	11.5	11.9
215.27	7.0	6.9	7.4	7.8	8.3	8.8	9.3	9.2	9.7	10.2
234.25	3.8	4.2	4.4	4.8	5.3	5.4	5.8	6.3	6.8	7.3
255.77	.7	.9	1.2	1.6	1.8	2.2	2.5	2.9	3.1	3.5
279.43	-.0	.0	.0	.0	.0	.0	.1	.2	.3	.5
304.89	-2.8	-2.4	-1.9	-1.4	-1.0	-.8	-.4	-.3	-.1	-.1
331.86	-7.5	-6.8	-6.5	-5.8	-5.3	-4.7	-4.1	-3.5	-2.9	-2.5
.10	-10.3	-9.5	-8.7	-8.7	-7.9	-7.1	-6.8	-6.1	-5.5	-4.9
29.43	-7.8	-7.0	-6.7	-5.9	-5.2	-4.7	-4.0	-3.4	-2.8	-2.1
59.72	-2.2	-1.7	-1.2	-.8	-.5	-.2	-.1	-.0	.0	.0
90.89	.0	.0	.1	.2	.4	.7	1.1	1.6	2.2	2.9
122.92	4.1	4.9	5.7	6.4	7.2	8.2	8.7	9.7	10.1	11.1
155.82	10.0	10.4	11.5	12.6	13.8	14.0	15.2	16.5	17.8	19.1
189.69	10.6	11.7	12.8	13.1	14.3	15.6	16.9	19.7	21.3	22.9
224.66	5.7	6.6	7.1	8.0	9.1	9.5	10.5	11.6	12.8	15.2
260.91	.3	.7	1.1	1.6	2.2	2.8	3.4	4.0	4.8	5.2
298.69	-1.6	-1.0	-.6	-.3	-.1	-.0	.0	.0	.0	.1
338.28	-7.5	-6.5	-6.2	-5.2	-4.6	-3.9	-3.1	-2.3	-1.6	-1.0
20.03	-8.1	-7.7	-6.6	-5.9	-5.0	-4.1	-3.3	-2.4	-1.7	-.9
64.34	-1.1	-.5	-.3	-.1	.0	.0	.0	.0	.2	.4
111.66	2.2	3.1	4.3	5.4	6.7	7.9	9.0	10.5	11.4	13.1
162.49	10.9	12.7	13.6	15.5	17.6	19.7	23.8	26.4	29.2	32.0
217.39	7.3	8.9	10.0	11.8	13.7	17.1	19.5	22.1	24.8	37.6
276.98	.0	.0	.2	.8	1.8	2.8	3.7	4.7	6.1	7.2
341.91	-7.3	-6.2	-5.0	-3.6	-2.3	-1.1	-.4	-.1	.0	.0
52.90	-2.5	-1.2	-.4	-.0	.0	.0	.1	.6	1.7	3.3
130.72	7.2	9.2	11.2	14.0	16.1	19.3	24.8	29.0	33.5	52.0
216.19	8.6	10.7	13.7	18.4	22.4	36.4	42.9	50.0	57.6	67.9
310.18	-2.3	-.8	-.1	.0	.1	.8	2.4	4.4	6.5	8.7
53.63	-1.7	-.3	.0	.0	.3	1.7	4.0	6.8	9.4	12.3
167.51	13.2	17.7	24.7	30.9	51.4	61.9	73.3	88.4	102.2	117.0
292.85	-.1	.0	.8	2.8	5.3	7.7	12.6	23.9	32.0	41.3
70.75	.0	.0	1.2	4.2	7.9	11.3	15.6	23.3	30.8	53.4
222.34	9.1	15.5	30.3	41.3	55.9	70.8	87.6	106.1	85.0	99.8
28.81	-4.3	-.9	.0	.1	2.3	6.3	11.1	15.6	24.8	34.3
211.41	12.7	21.7	42.8	60.5	79.5	101.0	84.1	102.1	121.7	143.2
51.43	-.4	.0	1.2	5.9	11.0	17.7	29.5	56.9	79.4	103.0
270.24	2.0	5.7	17.8	31.9	49.0	47.0	63.6	82.6	104.1	64.4

BLADE POSITION POSTION (DEG)	SECTION VERTICAL DRAG (LBS.)									
	1	2	3	4	5	6	7	8	9	10
174.48	3.7	3.7	3.7	3.7	3.7	3.7	3.7	3.7	3.7	3.7
178.29	3.8	3.9	3.9	4.0	4.1	4.1	4.2	4.3	4.3	4.4
186.76	3.8	3.9	2.5	2.6	2.7	2.7	2.8	2.9	3.0	3.0
199.27	2.1	2.2	2.3	2.4	2.5	2.6	2.7	2.8	1.9	2.0
215.27	2.5	1.7	1.8	1.9	2.0	2.1	2.2	1.5	1.6	1.7
234.25	1.8	2.0	1.6	1.7	1.9	1.3	1.4	1.5	1.6	1.7
255.77	1.0	1.1	1.1	1.2	1.4	1.3	1.2	1.4	1.1	1.3
279.43	.3	.2	.1	.1	.2	.3	.4	.5	.7	.9
304.89	2.2	1.8	1.9	1.8	1.7	1.4	1.3	1.1	.8	.6
331.86	2.8	2.5	3.1	2.8	3.2	2.9	3.2	2.8	2.9	2.5
.10	2.9	2.7	2.4	3.2	2.9	2.6	3.2	2.9	3.4	3.0
29.43	2.9	2.6	3.2	2.8	2.5	2.9	3.1	2.7	2.8	2.7
59.72	2.3	2.2	2.0	1.7	1.4	1.2	.8	.5	.3	.2
90.89	.2	.4	.7	1.1	1.4	1.7	2.1	2.3	2.6	2.7
122.92	3.1	3.0	3.4	3.0	3.5	3.9	3.1	3.5	2.4	2.7
155.82	3.6	2.5	2.7	3.0	3.3	2.4	2.6	2.8	3.0	3.2
189.69	2.5	2.8	3.1	2.2	2.4	2.6	2.9	1.8	1.9	2.1
224.66	2.1	2.4	1.7	1.9	2.2	1.6	1.8	2.0	2.2	1.4
260.91	.8	1.0	1.3	1.5	1.3	1.7	1.6	1.4	1.7	1.3
298.69	1.3	1.3	1.1	.8	.5	.3	.1	.1	.3	.6
338.28	2.1	1.8	2.3	1.9	2.2	2.4	2.4	2.3	2.1	1.7
20.03	2.3	2.9	2.5	2.8	2.4	2.5	2.5	2.4	2.1	2.0
64.34	1.9	1.6	1.0	.6	.3	.1	.2	.5	.9	1.5
111.66	2.5	2.9	3.2	3.3	4.1	3.8	3.2	3.8	2.7	3.1
162.49	2.6	3.0	2.3	2.6	3.0	3.3	2.2	2.4	2.6	2.9
217.39	1.8	2.1	1.7	2.0	2.3	1.6	1.8	2.0	2.3	1.3
276.98	.1	.3	.8	1.2	1.3	1.7	1.3	1.1	1.5	1.2
341.91	2.0	2.3	2.4	2.2	2.3	1.9	1.3	.6	.2	.2
52.90	2.5	2.1	1.3	.6	.1	.3	.9	1.8	2.5	3.0
130.72	3.4	3.3	2.7	3.3	2.7	3.3	2.3	2.6	3.0	1.8
216.19	2.1	1.8	2.3	1.7	2.0	1.3	1.5	1.7	2.0	.3
310.18	1.8	1.3	.6	.1	.6	1.5	2.3	2.1	2.3	2.1
53.63	2.2	1.3	.3	.3	1.4	2.5	3.1	4.1	3.4	2.9
167.51	2.2	3.0	2.2	2.8	1.8	2.1	2.5	.4	.5	.6
292.85	.4	.3	1.2	1.7	1.9	1.3	1.1	.8	1.1	1.4
70.75	.2	.6	2.2	3.2	3.8	2.7	2.6	2.1	2.8	1.8
222.34	1.5	1.4	1.0	1.4	.3	.3	.4	.5	.1	.2
28.81	2.6	2.0	.3	.9	2.6	3.8	4.0	2.6	2.3	3.1
211.41	2.1	2.0	1.5	.3	.4	.5	.1	.2	.2	.2
51.43	1.5	.2	2.3	3.6	2.6	3.0	2.7	2.0	.4	.5
270.24	1.2	1.0	.6	.2	.2	.1	.1	.1	.2	.1

F. BLADE ELEMENT RESULTS FOR BLADE THREE

BLADE POSITION POSTION (DEG)	ANGLE OF ATTACK (DEGREES) SECTIONS									
	1	2	3	4	5	6	7	8	9	10
294.47	144.0	144.0	144.0	144.0	144.0	144.0	144.0	144.0	144.0	144.0
298.29	144.0	144.0	144.0	144.0	144.0	140.4	140.4	140.4	140.4	140.4
306.76	147.6	147.6	147.6	147.6	147.6	144.0	144.0	144.0	144.0	140.4
319.27	154.8	151.2	151.2	151.2	151.2	151.2	147.6	147.6	147.6	144.0
335.26	154.8	154.8	154.8	154.8	151.2	151.2	151.2	151.2	147.6	147.6
354.25	154.8	154.8	154.8	154.8	151.2	151.2	151.2	151.2	147.6	147.6
15.77	154.8	151.2	151.2	151.2	151.2	147.6	147.6	147.6	144.0	144.0
39.43	147.6	144.0	144.0	144.0	140.4	140.4	136.8	136.8	133.2	129.6
64.89	126.0	126.0	122.4	118.8	115.2	111.6	104.4	100.8	97.2	93.6
91.86	79.2	72.0	68.4	64.8	61.2	57.6	54.0	50.4	46.8	43.2
120.10	43.2	39.6	36.0	36.0	36.0	32.4	32.4	28.8	28.8	28.8
149.43	28.8	28.8	25.2	25.2	25.2	25.2	21.6	21.6	21.6	21.6
179.72	25.2	25.2	21.6	21.6	21.6	21.6	21.6	21.6	18.0	18.0
210.89	25.2	25.2	25.2	21.6	21.6	21.6	21.6	21.6	18.0	18.0
242.92	36.0	36.0	32.4	28.8	28.8	25.2	25.2	25.2	21.6	21.6
275.82	97.2	86.4	79.2	68.4	61.2	54.0	50.4	43.2	39.6	36.0
309.69	147.6	144.0	140.4	140.4	133.2	129.6	126.0	118.8	111.6	104.4
344.66	154.8	154.8	154.8	151.2	151.2	147.6	147.6	144.0	140.4	136.8
20.91	154.8	151.2	151.2	151.2	147.6	144.0	144.0	140.4	136.8	133.2
58.68	136.8	133.2	129.6	122.4	118.8	111.6	104.4	97.2	93.6	86.4
98.27	68.4	61.2	57.6	50.4	46.8	43.2	39.6	39.6	36.0	32.4
140.02	32.4	28.8	28.8	25.2	25.2	25.2	21.6	21.6	21.6	21.6
184.33	25.2	25.2	21.6	21.6	21.6	21.6	18.0	18.0	18.0	18.0
231.65	32.4	28.8	25.2	25.2	21.6	21.6	21.6	18.0	18.0	18.0
282.49	111.6	97.2	82.8	68.4	57.6	50.4	43.2	36.0	32.4	28.8
337.39	154.8	151.2	147.6	144.0	140.4	136.8	129.6	122.4	111.6	100.8
36.98	147.6	144.0	140.4	133.2	129.6	118.8	111.6	100.8	90.0	79.2
101.91	57.6	50.4	43.2	39.6	36.0	32.4	28.8	25.2	25.2	21.6
172.90	25.2	21.6	21.6	18.0	18.0	18.0	18.0	14.4	14.4	14.4
250.72	39.6	32.4	25.2	25.2	21.6	18.0	18.0	14.4	14.4	14.4
336.19	151.2	147.6	140.4	133.2	118.8	104.4	86.4	72.0	57.6	46.8
70.18	111.6	93.6	75.6	61.2	50.4	39.6	36.0	28.8	25.2	25.2
173.63	21.6	21.6	18.0	18.0	14.4	14.4	14.4	14.4	10.8	10.8
287.51	100.8	72.0	46.8	36.0	28.8	21.6	18.0	18.0	14.4	14.4
52.85	129.6	111.6	90.0	68.4	50.4	39.6	32.4	25.2	21.6	21.6
190.75	21.6	18.0	14.4	14.4	14.4	10.8	10.8	10.8	10.8	7.2
342.34	147.6	136.8	118.8	90.0	61.2	43.2	32.4	25.2	21.6	18.0
148.81	21.6	18.0	14.4	14.4	10.8	10.8	10.8	10.8	7.2	7.2
331.41	144.0	122.4	86.4	54.0	36.0	25.2	21.6	18.0	14.4	10.8
171.43	18.0	14.4	14.4	10.8	10.8	10.8	7.2	7.2	7.2	7.2
30.23	136.8	108.0	68.4	43.2	28.8	21.6	18.0	14.4	14.4	10.8

BLADE POSITION POSTION (DEG)	SECTION VERTICAL LIFT (LBS.) 1	2	3	4	5	6	7	8	9	10
294.47	-1.7	-1.7	-1.7	-1.7	-1.7	-1.7	-1.7	-1.7	-1.7	-1.7
298.29	-2.1	-2.1	-2.0	-1.9	-1.8	-1.7	-1.7	-1.6	-1.5	-1.5
306.76	-3.4	-3.2	-3.1	-2.9	-2.7	-2.6	-2.5	-2.3	-2.2	-2.0
319.27	-5.0	-5.1	-4.9	-4.6	-4.3	-4.0	-4.0	-3.7	-3.5	-3.3
335.26	-7.7	-7.3	-6.9	-6.5	-6.7	-6.3	-5.9	-5.5	-5.4	-5.0
354.25	-10.2	-9.6	-9.1	-8.5	-8.7	-8.2	-7.7	-7.1	-7.0	-6.5
15.77	-9.3	-9.5	-8.9	-8.3	-7.7	-7.5	-6.9	-6.4	-6.0	-5.4
39.43	-6.4	-6.0	-5.4	-4.8	-4.2	-3.8	-3.1	-2.7	-2.2	-1.6
64.89	-1.1	-.9	-.6	-.4	-.2	-.1	-.0	.0	.0	.0
91.86	.0	.1	.1	.2	.4	.6	.9	1.4	1.8	2.4
120.10	3.4	4.1	4.8	5.4	6.1	6.8	7.5	8.0	8.8	9.7
149.43	8.9	9.8	10.1	11.0	12.0	13.0	13.2	14.2	15.3	16.4
179.72	10.9	11.9	12.1	13.2	14.2	15.4	16.5	17.7	20.5	21.9
210.89	7.7	8.6	9.5	9.8	10.7	11.7	12.7	13.8	16.2	17.4
242.92	2.6	3.2	3.7	4.2	4.9	5.3	6.0	6.8	7.2	8.0
275.82	.0	.0	.0	.1	.2	.4	.7	1.2	1.7	2.2
309.69	-3.4	-2.9	-2.3	-1.8	-1.2	-.8	-.5	-.2	-.1	-.0
344.66	-8.6	-7.7	-6.8	-6.5	-5.7	-5.2	-4.4	-3.8	-3.1	-2.4
20.91	-8.2	-8.0	-7.0	-6.1	-5.6	-4.8	-4.1	-3.3	-2.5	-1.8
58.68	-2.3	-1.6	-1.0	-.5	-.3	-.1	-.0	.0	.0	.0
98.27	.2	.5	.8	1.5	2.3	3.1	4.0	4.9	6.0	6.9
140.02	8.0	8.8	10.2	10.9	12.3	13.8	14.4	16.0	17.6	19.4
184.33	11.3	12.9	13.6	15.3	17.0	18.8	22.4	24.6	26.9	29.3
231.65	5.0	5.9	6.7	8.0	8.8	10.2	11.8	14.5	16.4	18.4
282.49	-.0	.0	.0	.1	.4	.9	1.7	2.6	3.5	4.3
337.39	-6.9	-6.1	-5.1	-4.0	-2.9	-1.9	-1.0	-.4	-.1	.0
36.98	-5.8	-4.5	-3.2	-1.9	-1.1	-.3	-.1	.0	.0	.0
101.91	.8	1.8	3.2	4.8	6.5	8.3	10.0	11.5	13.9	15.4
172.90	12.5	14.3	17.1	21.7	25.3	29.2	33.3	51.1	57.4	64.1
250.72	2.3	3.7	5.0	6.9	8.6	11.9	14.9	24.7	29.6	34.9
336.19	-6.4	-4.7	-2.9	-1.4	-.3	-.0	.0	.1	.7	2.1
70.18	-.1	.0	.0	.5	1.9	4.2	6.6	8.9	11.4	15.0
173.63	13.1	17.1	23.5	29.0	47.6	56.7	66.6	77.3	91.6	104.3
287.51	.0	.1	1.0	2.9	5.1	7.2	11.5	15.9	28.5	36.3
52.85	-1.3	-.1	.0	.2	1.7	4.6	8.0	11.1	14.8	20.1
190.75	14.0	21.3	38.6	49.8	62.4	78.9	94.9	112.3	131.2	102.0
342.34	-5.7	-2.4	-.3	.0	.4	2.9	6.6	10.4	15.0	23.3
148.81	12.8	21.1	40.6	54.6	72.9	91.6	112.5	135.5	108.1	126.5
331.41	-3.5	-.4	.0	.9	4.7	8.8	14.4	24.0	46.5	65.1
171.43	18.8	39.3	56.1	78.4	102.0	128.6	106.5	128.6	152.8	179.0
30.23	-2.7	-.1	.2	3.5	9.2	15.6	27.5	55.5	77.2	105.8

BLADE POSITION POSTION (DEG)	SECTION VERTICAL DRAG (LBS.) 1	2	3	4	5	6	7	8	9	10
294.47	1.0	1.0	1.0	1.0	1.0	1.0	1.0	1.0	1.0	1.0
298.29	1.3	1.3	1.2	1.2	1.1	1.4	1.3	1.3	1.2	1.2
306.76	1.6	1.5	1.5	1.4	1.3	1.6	1.5	1.4	1.3	1.6
319.27	1.4	1.9	1.8	1.7	1.6	1.5	1.9	1.8	1.7	2.0
335.26	2.2	2.1	1.9	1.8	2.5	2.3	2.2	2.0	2.6	2.4
354.25	2.9	2.7	2.6	2.4	3.3	3.0	2.8	2.7	3.4	3.1
15.77	2.6	3.5	3.3	3.1	2.8	3.6	3.3	3.0	3.6	3.3
39.43	3.1	3.6	3.3	2.9	3.3	2.9	3.1	2.7	2.8	2.8
64.89	2.4	2.0	1.7	1.4	1.2	.9	.7	.4	.2	.1
91.86	.3	.4	.7	.9	1.2	1.5	1.8	2.0	2.1	2.2
120.10	3.1	3.1	2.9	3.3	3.7	3.2	3.6	2.9	3.2	3.5
149.43	3.2	3.5	2.4	2.6	2.9	3.1	2.2	2.4	2.6	2.8
179.72	2.6	2.9	2.1	2.2	2.4	2.6	2.8	3.0	1.9	2.0
210.89	1.8	2.0	2.3	1.6	1.8	2.0	2.2	2.3	1.5	1.6
242.92	1.6	1.9	1.8	1.5	1.8	1.3	1.4	1.6	1.2	1.4
275.82	.1	.1	.2	.4	.6	.8	1.1	1.1	1.3	1.3
309.69	1.6	1.8	1.8	1.4	1.6	1.3	1.0	.8	.5	.3
344.66	2.4	2.2	1.9	2.4	2.1	2.5	2.1	2.3	2.4	2.4
20.91	2.3	3.0	2.6	2.3	2.7	2.9	2.5	2.6	2.5	2.4
58.68	2.3	2.1	1.8	1.5	1.1	.7	.4	.2	.1	.2
98.27	1.1	1.5	2.0	2.3	2.6	2.9	3.0	3.7	3.6	3.3
140.02	3.8	3.2	3.6	2.6	2.9	3.3	2.4	2.7	3.0	3.3
184.33	2.7	3.1	2.3	2.6	2.9	3.2	2.0	2.2	2.4	2.7
231.65	2.4	2.1	1.6	1.9	1.5	1.7	2.0	1.3	1.5	1.7
282.49	.3	.1	.2	.5	.9	1.3	1.6	1.6	1.7	1.6
337.39	2.0	2.3	2.4	2.4	2.3	1.9	1.7	1.2	.7	.3
36.98	2.8	2.7	2.5	2.5	1.8	1.3	.7	.2	.1	.5
101.91	1.9	2.6	3.0	3.6	4.0	4.0	3.6	2.8	3.3	2.6
172.90	3.0	2.4	2.9	2.0	2.3	2.7	3.0	1.8	2.0	2.2
250.72	1.7	1.8	1.2	1.7	1.5	1.1	1.4	.9	1.0	1.2
336.19	2.4	2.2	2.3	1.8	1.2	.4	.1	.8	1.7	2.5
70.18	.7	.1	.5	1.7	2.7	3.1	4.0	3.2	2.7	3.6
173.63	2.2	2.9	2.1	2.6	1.6	2.0	2.3	2.7	.4	.5
287.51	.2	.4	1.2	1.8	1.8	1.2	1.0	1.4	1.0	1.3
52.85	2.2	.9	.1	1.1	2.5	3.5	3.8	2.6	2.5	3.4
190.75	2.4	1.9	1.3	1.7	2.2	.4	.5	.5	.6	.2
342.34	2.7	2.4	1.1	.1	1.4	2.7	3.2	2.5	2.5	2.1
148.81	2.2	1.9	1.4	1.9	.4	.4	.5	.7	.2	.2
331.41	2.1	1.3	.1	1.7	2.8	2.1	2.4	2.2	1.6	.3
171.43	1.7	1.4	1.9	.4	.5	.6	.2	.2	.2	.3
30.23	2.7	.6	1.0	3.3	3.3	2.6	2.5	1.9	2.7	.5

APPENDIX B. CH-46 ROTOR BLADE PROPERTIES

Blade Station (r/R)	Station Radius (in)	Pitch Inertia (lb.*s*s)	CG Offset (in)	Flapwise Stiffness (lb. in*in)	Chordwise Stiffness (lb. in*in)	Torsional Stiffness (lb. in*in)
0.0167	5.5	5.7	0.0	570.0E06	285.0E06	70.0E06
0.05	4.85	5.7	0.0	160.0E06	285.0E06	70.0E06
0.10	6.90	.51	0.0	81.0E06	345.0E06	70.0E06
0.15	1.15	1.72	0.028	160.0E06	260.0E06	67.0E06
0.20	0.78	1.35	.04	48.0E06	218.0E06	28.0E06
0.25	.65	2.90	-.93	20.0E06	370.0E06	18.0E06
0.30	.52	2.1	-.69	21.0E06	420.0E06	17.0E06
0.35	.505	2.09	-.74	20.0E06	412.0E06	17.0E06
0.40	.499	2.08	-.78	20.0E06	405.0E06	17.0E06
0.45	.48	2.04	-.82	19.5E06	395.0E06	16.9E06
0.50	.45	2.10	-.84	19.5E06	392.0E06	16.5E06
0.55	.42	2.00	-.86	19.5E06	390.0E06	16.2E06
0.60	.42	2.12	-.58	16.0E06	410.0E06	15.5E06
0.65	.42	2.11	-.51	16.0E06	420.0E06	15.2E06
0.70	.42	2.11	-.51	16.0E06	420.0E06	15.2E06
0.75	.42	2.55	-.76	16.0E06	570.0E06	15.2E06
0.80	.41	2.11	-.51	16.0E06	420.0E06	15.2E06
0.85	.45	2.19	-.34	18.0E06	435.0E06	16.5E06
0.90	.50	2.40	.25	15.0E06	440.0E06	16.0E06
0.95	.85	2.35	.33	12.0E06	420.0E06	14.0E06
1.00	1.30	3.10	-.63	18.0E06	755.0E06	15.2E06

APPENDIX C. GENHEL FLOW DIAGRAM

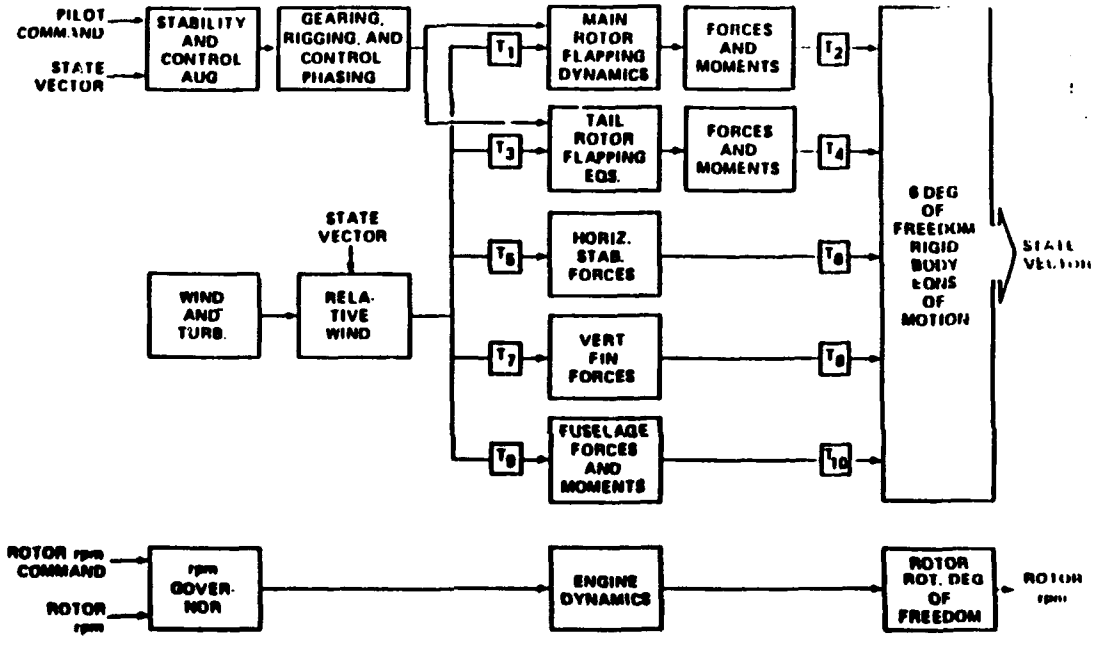

APPENDIX D. MATLAB META FILES

A. U-COMPONENT MODEL FOR WIND TUNNEL

```
mu=[1 .1 -.2 -3.2 -7.2 -8.2]*10
fu=[0 3/1000 35/1000  600/1000 999/1000 1]
[bu,au]=yulewalk(6,fu,mu)
[Au,Bu,Cu,Du]=TF2SS(bu,au);
[Zu,Polesu,Ku]=SS2ZP(Au,Bu,Cu,Du,1)
x=rand(1,4000);
yu=filter(au,bu,x);
pack
Pu=spectrum(x,yu,200,100);
disp('Hit RETURN to see plots');
pause
meta comp_u
spcplotu(Pu,1000);
```

B. V-COMPONENT FOR WIND TUNNEL MODEL

```
clear
mv=[0 .1 -.7 -4.7 -7.2 -10.2]*(10/1.73)
fv=[0 3/1000 35/1000  600/1000 999/1000 1]
[bv,av]=yulewalk(6,fv,mv)
[Av,Bv,Cv,Dv]=TF2SS(bv,av);
[Zv,Polesv,Kv]=SS2ZP(Av,Bv,Cv,Dv,1)
x=rand(1,4000);
yv=filter(av,bv,x);
pack
Pv=spectrum(x,yv,200,100);
disp('Hit RETURN to see plots');
pause
meta comp_v
spcplotv(Pv,1000);
```

C. W-COMPONENT FOR WIND TUNNEL MODEL

```
mw=[0 .1 -.3 -2.7 -4.5 -6.5]*10
fw=[0 3/1000 35/1000  600/1000 999/1000 1]
[bw,aw]=yulewalk(6,fw,mw)
[Aw,Bw,Cw,Dw]=TF2SS(bw,aw);
[Zw,Polesw,Kw]=SS2ZP(Aw,Bw,Cw,Dw,1)
x=rand(1,4000);
yw=filter(aw,bw,x);
pack
Pw=spectrum(x,yw,200,100);
disp ('Hit RETURN to see plots');
pause
meta comp_w
spcplotw(Pw,1000);
```

D. U-COMPONENT FOR PROTOTYPE MODEL

```
mu=[1 .1 -.2 -3.2 -7.2 -8.2]*10;
fu=[0 3/1000 35/1000 600/1000 999/1000 1];
[bu,au]=yulewalk(6,fu,mu)
[Au,Bu,Cu,Du]=TF2SS(bu,au);
[Zu,Polesu,Ku]=SS2ZP(Au,Bu,Cu,Du,1)
x=rand(1,4000);
yu=filter(au,bu,x);
pack
Pu=spectrum(x,yu,200,100);
disp('Hit RETURN to see plots');
pause
meta comp_4u
spcplt4u(Pu,1000/14);
```

E. V-COMPONENT FOR PROTOTYPE MODEL

```
mv=[0 .1 -.7 -4.7 -7.2 -10.2]*(10/1.73);
fv=[0 3/1000 35/1000 600/1000 999/1000 1];
[bv,av]=yulewalk(6,fv,mv)
[Av,Bv,Cv,Dv]=TF2SS(bv,av);
[Zv,Polesv,Kv]=SS2ZP(Av,Bv,Cv,Dv,1)
x=rand(1,4000);
yv=filter(av,bv,x);
pack
Pv=spectrum(x,yv,200,100);
disp('Hit RETURN to see plots');
pause
meta comp_4v
spcplt4v(Pv,1000/14);
```

F. W-COMPONENT FOR PROTOTYPE MODEL

```
mw=[0 .1 -.3 -2.7 -4.5 -6.5]*10;
fw=[0 3/1000 35/1000 600/1000 999/1000 1];
[bw,aw]=yulewalk(6,fw,mw)
[Aw,Bw,Cw,Dw]=TF2SS(bw,aw);
[Zw,Polesw,Kw]=SS2ZP(Aw,Bw,Cw,Dw,1)
x=rand(1,4000);
yw=filter(aw,bw,x);
pack
Pw=spectrum(x,yw,200,100);
disp ('Hit RETURN to see plots');
pause
meta comp_4w
spcplt4w(Pw,1000/14);
```

f is a vector of frequency points, specified in the range between 0 and 1, where 1.0 corrsponds to half the sample frequency (the Nyquist frequency).

m is a vecotr containing the desired magnitude response at the points specified in **f**

b and **a** are row vecotrs containing the **n** + **1** coefficients of the order **n** filter whose frequency-magnitude characteristics match those given in **f** and **m**.

[A,B,C,D] are the state space vectors representing the digital filter transfer function.

[Z,P,K] are the vectors representing the minimum phase zeros, poles and filter gain of the digital filter transfer function.

APPENDIX E. INPUT FOR DYSCO MODULES

```
H46A-1  /MODEL     ON FILE U1

**************************        MODEL H46A-1     **************************

H46 BASELINE

INDEX    COMP     NO.    DATA SET          FORCE    DATA SET

  1      CRE3      2     H46A2             FRA3     WIND
                                    REQUIRED DS/DM= NACA0012/AIRFOIL
  2      CCE0      2     AFT_HEAD          NONE
  3      CFM2      1     H46               NONE
  4      CSF1            GEAR              FSS1     WAVES
  5      CLC1            COUP_G            NONE
  6      CES1            DROOPSTO          NONE
  7      CSF1            BLADE_WG          NONE

*******************************************************************************

*******************************************************************************
                              GLOBAL  VARIABLES

  1 VSOUND    - SOUND VELOCITY       =  1.11700E+03
  2 RHO       - AIR DENSITY RATIO    =  1.00000E+00
*******************************************************************************
```

```
**********          H46A2   /CRE3          **********

H46 AFT ROTOR (3 BLADES:  B2)

*****************************************************************************
INPUT FOR      ROTOR       COMPONENT CRE3.  ROTOR ELASTIC BLADES

  1 JV        - INPLANE DOF          =          YES
  2 JW        - OUTPLANE DOF         =          YES
  3 JP        - TORSION DOF          =          YES
  4 JS        - SHAFT PERTURBED DOF  =          NO
  5 JX        - XHUB(LONG) DOF       =          NO
  6 JY        - YHUB(LAT) DOF        =          NO
  7 JZ        - ZHUB(AXIAL) DOF      =          YES
  8 JAX       - ALFX(ROLL) DOF       =          NO
  9 JAY       - ALFY(PTCH) DOF       =          YES
 10 JAZ       - ALFZ(YAW) DOF        =          NO
 11 NV        - NO. OF INPLANE MODES=             1
 12 NW        - NO. OF OUTPLNE MODES=             2
 13 NP        - NO. OF TORSION MODES=             1
 14 NB        - NO. OF BLADES        =            3
 15 PHL       - PTCH HORN LNGTH (IN)=  8.67000E+00
 16 PHSTA     - PTCH HORN STA (IN)   =  4.30000E+01
 17 NX        - NO. OF STATIONS      =           20
 18 ITYP      - MODE INPUT 1 OR 2    =            2
 19 X         - (REAL) STATIONS
             5.11000E+00  1.42000E+01  4.30000E+01  5.80000E+01
             7.65000E+01  9.18000E+01  1.07100E+02  1.22400E+02
             1.37700E+02  1.53000E+02  1.68300E+02  1.83600E+02
             1.98900E+02  2.14200E+02  2.29500E+02  2.44800E+02
             2.60100E+02  2.75400E+02  2.90700E+02  3.06000E+02
 20 NIP       - INPLANE HINGE STA    =            2
 21 NOP       - OUTPLANE HINGE STA   =            1
 22 NTOR      - PTCH BEARING STA     =            3
 23 CIPP      - IP MODAL DAMPING     =  0.00000E+00
 24 COPP      - OP MODAL DAMPING     =  0.00000E+00  0.00000E+00
 25 CTORR     - TORSION MODAL        =  0.00000E+00
 26 IBIP      - IP BC 1 OR 2         =            1
 27 IBOP      - OP BC 1 OR 2         =            1
 28 IBTO      - TORSION BC 1 OR 2    =            2
 29 NI        - NO. OF IMPLICIT DOFS=             9
 30 NIDOF     - (DOF) IMPLICIT DOF NAMES
           WGT    1  WGT    2  WTIP   0  WGT   12  WGT   22
           WTIP   2  WGT   13  WGT   23  WTIP   3
 31 XSTA      - (REAL) STAS FOR IMPLCT DOFS
             9.83200E+01  1.95600E+02  3.06000E+02  9.83200E+01
             1.95600E+02  3.06000E+02  9.83200E+01  1.95600E+02
             3.06000E+02
 32 DIST      - (REAL) DISTANCE TO EC
             0.00000E+00  0.00000E+00  0.00000E+00  0.00000E+00
             0.00000E+00  0.00000E+00  0.00000E+00  0.00000E+00
             0.00000E+00
 33 IBN       - BLADE NO. FOR IDOFS
                    1         1         1         2         2
                    2         3         3         3
```

```
34 KIP      - IP SPRING RATE       =  0.00000E+00
35 CIP      - IP DAMPING RATE      =  7.85380E+03
36 KOP      - OP SPRING RATE       =  0.00000E+00
37 COP      - OP DAMPING RATE      =  0.00000E+00
38 KTOR     - TORSION SPRING RATE  =  3.57793E+03
39 CTOR     - TORSION DAMPING RATE=  0.00000E+00
40 OM       - RPM                  =  1.70770E+01
41 IC       - ROTATION DIRECTION   =            -1
42 PSIO     - AZIMUTH OF REF BLADE=  7.92710E+01
43 BPCO     - PRECONE ANGLE (DEG)  =  0.00000E+00
44 MHUB     - HUB WEIGHT (LB)      =  0.00000E+00
45 IHUBY    - HUB M.O.I. ABOUT Y-  =  0.00000E+00
46 THO      - ROOT PTCH ANG (DEG)  =  3.00000E+00
47 NONLIN   - NONLIN TERMS         =          NO
48 IU       - UNIFORM BLADE        =          NO
49 M        - (REAL) MASS PER UNIT LENGTH
            5.50000E+00  5.50000E+00  1.00000E+00  8.00000E-01
            6.50000E-01  5.20000E-01  5.05000E-01  4.99000E-01
            4.80000E-01  4.50000E-01  4.20000E-01  4.20000E-01
            4.20000E-01  4.20000E-01  4.20000E-01  4.10000E-01
            4.50000E-01  5.00000E-01  8.50000E-01  1.30000E+00
50 SE       - (REAL) CG OFFSET FROM EA
            0.00000E+00  0.00000E+00  2.50000E-01  2.20000E-01
           -9.30000E-01 -6.90000E-01 -7.40000E-01 -7.80000E-01
           -8.20000E-01 -8.40000E-01 -8.60000E-01 -5.80000E-01
           -5.10000E-01 -5.10000E-01 -7.60000E-01 -5.10000E-01
           -3.40000E-01  2.50000E-01  3.30000E-01 -6.30000E-01
51 SEA      - (REAL) AREA CENTROID OFFSET
            0.00000E+00  0.00000E+00  0.00000E+00  0.00000E+00
            0.00000E+00  0.00000E+00  0.00000E+00  0.00000E+00
            0.00000E+00  0.00000E+00  0.00000E+00  0.00000E+00
            0.00000E+00  0.00000E+00  0.00000E+00  0.00000E+00
            0.00000E+00  0.00000E+00  0.00000E+00  0.00000E+00
52 KM1      - (REAL) MASS ROG ABOUT
            0.00000E+00  0.00000E+00  0.00000E+00  0.00000E+00
            0.00000E+00  0.00000E+00  0.00000E+00  0.00000E+00
            0.00000E+00  0.00000E+00  0.00000E+00  0.00000E+00
            0.00000E+00  0.00000E+00  0.00000E+00  0.00000E+00
            0.00000E+00  0.00000E+00  0.00000E+00  0.00000E+00
53 KM2      - (REAL) MASS ROG ABOUT
            0.00000E+00  0.00000E+00  0.00000E+00  0.00000E+00
            0.00000E+00  0.00000E+00  0.00000E+00  0.00000E+00
            0.00000E+00  0.00000E+00  0.00000E+00  0.00000E+00
            0.00000E+00  0.00000E+00  0.00000E+00  0.00000E+00
            0.00000E+00  0.00000E+00  0.00000E+00  0.00000E+00
54 KA       - (REAL) AREA ROG OF CROSS
            0.00000E+00  0.00000E+00  0.00000E+00  0.00000E+00
            0.00000E+00  0.00000E+00  0.00000E+00  0.00000E+00
            0.00000E+00  0.00000E+00  0.00000E+00  0.00000E+00
            0.00000E+00  0.00000E+00  0.00000E+00  0.00000E+00
            0.00000E+00  0.00000E+00  0.00000E+00  0.00000E+00
55 THP      - (REAL) PRETWIST RATE DEG/IN
            0.00000E+00  0.00000E+00  0.00000E+00  2.90200E-01
           -2.80000E-02 -2.80000E-02 -2.80000E-02 -2.80000E-02
           -2.80000E-02 -2.80000E-02 -2.80000E-02 -2.80000E-02
           -2.80000E-02 -2.80000E-02 -2.80000E-02 -2.80000E-02
```

```
          -2.80000E-02 -2.80000E-02 -2.80000E-02 -2.80000E-02
56 EIY     - (REAL) CHORDWISE EI*10E-6
           2.85000E+02  2.85000E+02  8.00000E+01  2.75000E+02
           3.70000E+02  4.20000E+02  4.12000E+02  4.05000E+02
           3.95000E+02  3.92000E+02  3.90000E+02  4.10000E+02
           4.20000E+02  4.20000E+02  5.70000E+02  4.20000E+02
           4.35000E+02  4.40000E+02  4.20000E+02  7.55000E+02
57 EIZ     - (REAL) BEAMWISE EI*10E-6
           5.70000E+02  1.60000E+02  2.10000E+02  7.00000E+01
           2.00000E+01  2.10000E+01  2.00000E+01  2.00000E+01
           1.95000E+01  1.95000E+01  1.95000E+01  1.60000E+01
           1.60000E+01  1.60000E+01  1.60000E+01  1.60000E+01
           1.80000E+01  1.50000E+01  1.20000E+01  1.80000E+01
58 EA      - (REAL) SECTION EA*10E-6
           0.00000E+00  0.00000E+00  0.00000E+00  0.00000E+00
           0.00000E+00  0.00000E+00  0.00000E+00  0.00000E+00
           0.00000E+00  0.00000E+00  0.00000E+00  0.00000E+00
           0.00000E+00  0.00000E+00  0.00000E+00  0.00000E+00
           0.00000E+00  0.00000E+00  0.00000E+00  0.00000E+00
59 GJ      - (REAL) SECTION GJ*10E-6
           7.00000E+01  7.00000E+01  7.00000E+01  3.40000E+01
           1.80000E+01  1.70000E+01  1.70000E+01  1.70000E+01
           1.69000E+01  1.65000E+01  1.62000E+01  1.55000E+01
           1.52000E+01  1.52000E+01  1.52000E+01  1.52000E+01
           1.65000E+01  1.60000E+01  1.40000E+01  1.52000E+01
60 EB1     - (REAL) CROSS SEC INTEGRAL
           0.00000E+00  0.00000E+00  0.00000E+00  0.00000E+00
           0.00000E+00  0.00000E+00  0.00000E+00  0.00000E+00
           0.00000E+00  0.00000E+00  0.00000E+00  0.00000E+00
           0.00000E+00  0.00000E+00  0.00000E+00  0.00000E+00
           0.00000E+00  0.00000E+00  0.00000E+00  0.00000E+00
61 EB2     - (REAL) CROSS SEC INTEGRAL
           0.00000E+00  0.00000E+00  0.00000E+00  0.00000E+00
           0.00000E+00  0.00000E+00  0.00000E+00  0.00000E+00
           0.00000E+00  0.00000E+00  0.00000E+00  0.00000E+00
           0.00000E+00  0.00000E+00  0.00000E+00  0.00000E+00
           0.00000E+00  0.00000E+00  0.00000E+00  0.00000E+00
62 EC1     - (REAL) CROSS SEC INTEGRAL
           0.00000E+00  0.00000E+00  0.00000E+00  0.00000E+00
           0.00000E+00  0.00000E+00  0.00000E+00  0.00000E+00
           0.00000E+00  0.00000E+00  0.00000E+00  0.00000E+00
           0.00000E+00  0.00000E+00  0.00000E+00  0.00000E+00
           0.00000E+00  0.00000E+00  0.00000E+00  0.00000E+00
63 EC1STA  - (REAL) CROSS SEC INTEGRAL
           0.00000E+00  0.00000E+00  0.00000E+00  0.00000E+00
           0.00000E+00  0.00000E+00  0.00000E+00  0.00000E+00
           0.00000E+00  0.00000E+00  0.00000E+00  0.00000E+00
           0.00000E+00  0.00000E+00  0.00000E+00  0.00000E+00
           0.00000E+00  0.00000E+00  0.00000E+00  0.00000E+00
64 JIL     - INTERNAL LOADS       =          YES
65 NXIL    - NO. OF STATIONS      =           20
66 JIPIL   - INPLANE MOMENTS      =          NO
67 JOPIL   - OUTPLANE MOMENTS     =          YES
68 JTORIL  - TWIST MOMENTS        =          NO
***************************************************************************
```

********** H46 /CFM2 **********

H46 FUSELAGE

****

INPUT FOR STRUCTURAL COMPONENT CFM2. MODAL FUSELAGE

1	RBM	- RIGID BODY MODES =	YES	
2	IXCG	- LONGITUDINAL =	NO	
3	IYCG	- LATERAL =	NO	
4	IZCG	- VERTICAL =	YES	
5	IROLL	- ROLL =	NO	
6	IPTCH	- PITCH =	YES	
7	IYAW	- YAW =	NO	
8	CG	- CG STATION (IN) =	2.94500E+02	
9	NMODE	- NO. OF ELASTIC MODES=	0	
10	NR	- NO. OF ROTORS =	2	
11	NROT	- ROTOR NUMBERS =	1	2
12	XROT	- ROTOR STATIONS =	7.40000E+01	4.76000E+02
13	ZROT	- ROTOR VERTICAL HT =	8.00000E+01	1.28000E+02
14	ASF	- FWD SHAFT ANGLE =	9.50000E+00	7.00000E+00
15	ASL	- LAT SHAFT ANGLE =	0.00000E+00	0.00000E+00
16	IX	- HUB TRAN DOF - LONG =	NO	NO
17	IY	- HUB TRAN DOF - LAT =	NO	NO
18	IZ	- HUB TRAN DOF - AXIAL=	YES	YES
19	IAX	- HUB ANGL DOF - ROLL =	NO	NO
20	IAY	- HUB ANGL DOF - PITCH=	YES	YES
21	IAZ	- HUB ANGL DOF - YAW =	NO	NO
22	NI	- NO. OTHER IMPLCT DOF=	0	
23	MASSL	- FUSELAGE MASS (LB) =	1.94400E+04	
24	IMYF	- PITCH MOI ABOUT CG =	1.16700E+05	

****

```
**********        AFT_HEAD/CCE0        **********

CONTROL RODS FOR H-46 AFT HEAD

********************************************************************************
INPUT FOR CONTROL SYSTEM COMPONENT CCE0.  CONTROL RODS

  1 KROD      - CONTRL ROD STIFFNESS=  3.00000E+03
********************************************************************************


**********        GEAR    /CSF1        **********

LANDING GEAR

********************************************************************************
INPUT FOR COMPONENT CSF1.  FINITE ELEMENT

  1 NCDF      - NUMBER OF DOF         =            2
  2 CDFLI     - DOF NAMES             =     FG     0     AG     0
  3 CM        - (REAL) MASS MATRIX
          NULL MATRIX

  4 CC        - (REAL) DAMPING MATRIX
          NULL MATRIX

  5 CK        - (REAL) STIFFNESS MATRIX
          DIAGONAL MATRIX (DIAGONAL VALUES PRINTED)

     6.50000E+03  6.50000E+03
  6 CF        - FORCE VECTOR          =  0.00000E+00  0.00000E+00
  7 IGR       - GLOBAL REFERENCE      =          NO
********************************************************************************
```

```
**********       COUP_G  /CLC1       **********

RELATE GEAR DOF TO FUSELAGE

*******************************************************************************
INPUT FOR COMPONENT CLC1. LINEAR CONSTRAINTS

  1 NCDF      - NUMBER OF DOF        =            2
  2 CDFLI     - DOF NAMES            =     ZCG 1000      PTCH1000
  3 NCIDF     - # OF CONSTRAINT EQNS=            2
  4 CIDFLI    - IMPLICIT DOF NAMES   =     FG     0      AG      0
  5 COEF      - (REAL) COEFFICIENT MATRIX
          GENERAL MATRIX

    ROW     1
          1.00000E+00  2.64000E+02
    ROW     2
          1.00000E+00 -5.00000E+01
*******************************************************************************


DROOPSTO/CES1      ON FILE U1

**********       DROOPSTO/CES1       **********

DROOP STOP FOR ROTOR HEAD (FLAP STOP)

*******************************************************************************
INPUT FOR COMPONENT CES1. ELASTIC STOP

  1 MCDF      - # OF DOF-EXCEPT BASE=            6
  2 CDFLI     - (DOF) DOF NAMES
          OP  2110  OP  2120  OP  2210  OP  2220  OP  2310
          OP  2320
  3 BASE      - EXISTNCE OF BASE DOF=          YES
  4 CDFLBI    - BASE DOF NAME        =     ZHUB1000
  5 C1        - UPPER DAMPING COEFF  =  0.00000E+00
  6 C2        - LOWER DAMPING COEFF  =  0.00000E+00
  7 K1        - UPPER SPRING COEFF   =  0.00000E+00
  8 K2        - LOWER SPRING COEFF   =  0.00000E+00
  9 DELT1     - UPPER GAP SIZE       =  2.10000E-02
 10 DELT2     - LOWER GAP SIZE       =  0.00000E+00
*******************************************************************************
```

```
*****************       BLADE_WG/CSF1       ***************

Blade weight DOF for CRE3

*************************************************************************
INPUT FOR COMPONENT CSF1. FINITE ELEMENT

  1 NCDF      - NUMBER OF DOF        =             9
  2 CDFLI     - (DOF) DOF NAMES
           WGT    1  WGT    2  WTIP   0  WGT   12  WGT   22
           WTIP   2  WGT   13  WGT   23  WTIP   3
  3 CM        - (REAL) MASS MATRIX
           NULL MATRIX

  4 CC        - (REAL) DAMPING MATRIX
           NULL MATRIX

  5 CK        - (REAL) STIFFNESS MATRIX
           NULL MATRIX

  6 CF        - (REAL) FORCE VECTOR
             0.00000E+00  0.00000E+00  0.00000E+00  0.00000E+00
             0.00000E+00  0.00000E+00  0.00000E+00  0.00000E+00
             0.00000E+00
  7 IGR       - GLOBAL REFERENCE     =          YES
  8 LDC       - (REAL) LOCAL DOF VECTORS
           GENERAL MATRIX

    ROW    1
           0.00000E+00  0.00000E+00  1.00000E+00
    ROW    2
           0.00000E+00  0.00000E+00  1.00000E+00
    ROW    3
           0.00000E+00  0.00000E+00  1.00000E+00
    ROW    4
           0.00000E+00  0.00000E+00  1.00000E+00
    ROW    5
           0.00000E+00  0.00000E+00  1.00000E+00
    ROW    6
           0.00000E+00  0.00000E+00  1.00000E+00
    ROW    7
           0.00000E+00  0.00000E+00  1.00000E+00
    ROW    8
           0.00000E+00  0.00000E+00  1.00000E+00
    ROW    9
           0.00000E+00  0.00000E+00  1.00000E+00
*************************************************************************
```

```
**********       WIND    /FRA3       **********

LOW REYNOLD'S NUMBER AERODYNAMICS FOR NACA0012 AIRFOIL

REQUIRES DS/DM NACA0012/AIRFOIL
NO SEQUENTIAL FILES REQUIRED

********************************************************************************
INPUT FOR FORCE FRA3. ROTOR AERO GENERAL

  1 IEQS      - AERODYNAMICS BY EQS =          NO
  2 INFTAB    - INDUCED VEL BY TABLE=          NO
  3 IUNSTD    - UNSTEADY AERO       =          NO/YES
  4 VAIRH     - (REAL) WIND VELOCITY
              5.22335E+01  0.00000E+00  2.47238E+01
  5 ASTALL    - STALL ANGLE (DEG)   =  1.20000E+01
  6 RFCT      - INDUCED VEL FACTOR  =  1.65000E+00
  7 TIPLOC    - TIP LOSS COEFFICIENT=  9.50000E-01
  8 XH        - HUB EXTENT (IN)     =  1.16000E+01
  9 ALT       - VEHICLE HEIGHT (FT) =  0.00000E+00
 10 K27       - TIP VORTEX COEFF    =  0.00000E+00
 11 CD0       - BLADE DRAG COEFFAT  =  1.00000E-03
 12 Q1C       - Q1C COEFFICIENT     =  1.00000E+00
 13 Q2C       - Q2C COEFFICIENT     =  5.00000E-01
 14 ALAMDA    - NONDIM INDUCED VEL  =  0.00000E+00
 15 NXA       - NO. OF STATIONS     =           10
 16 XAERO     - (REAL) NONDIM AERO STATIONS
              1.00000E-01  2.00000E-01  3.00000E-01  4.00000E-01
              5.00000E-01  6.00000E-01  7.00000E-01  8.00000E-01
              9.00000E-01  1.00000E+00
 17 NUMAF     - NO. AIRFOIL TABLES  =            1
 18 AFTAB1    - NAME AF   TABLE 1   = NACA0012/AIRFOIL
 19 NUMAF1    - NO. OF STATIONS AF 1=           10
 20 STA-AF1   - STATIONS FOR AF 1
                    1         2         3         4         5
                    6         7         8         9        10
 21 XACC      - (REAL) A/C OFFSET FROM E.C.
              0.00000E+00  0.00000E+00  0.00000E+00  0.00000E+00
              0.00000E+00  0.00000E+00  0.00000E+00  0.00000E+00
              0.00000E+00  0.00000E+00
 22 CHORDC    - (REAL) CHORD (IN)
              0.00000E+00  1.10000E+01  1.87500E+01  1.87500E+01
              1.87500E+01  1.87500E+01  1.87500E+01  1.87500E+01
              1.87500E+01  1.87500E+01
 23 NX        - NO. AERO FACTOR STAS=           10
 24 XF        - (REAL) NONDIM FACTOR STAS
              1.00000E-01  2.00000E-01  3.00000E-01  4.00000E-01
              5.00000E-01  6.00000E-01  7.00000E-01  8.00000E-01
              9.00000E-01  1.00000E+00
 25 FL        - (REAL) FACTORS FOR CL
              1.00000E-01  5.00000E-01  7.00000E-01  1.00000E+00
              1.00000E+00  1.00000E+00  1.00000E+00  1.00000E+00
              9.80000E-01  8.90000E-01
? 26 FD        - (REAL) FACTORS FOR CD
              1.00000E-01  5.00000E-01  7.00000E-01  1.00000E+00
```

```
              1.00000E+00   1.00000E+00   1.00000E+00   1.00000E+00
              1.00000E+00   1.00000E+00
 27 FM        - (REAL) FACTORS FOR CM
              1.00000E+00   1.00000E+00   1.00000E+00   1.00000E+00
              1.00000E+00   1.00000E+00   1.00000E+00   1.00000E+00
              1.00000E+00   1.00000E+00
**************************************************************************
```

APPENDIX F. VELOCITY FIELDS OF THE ROTOR BLADES (RHOADES)

ALL VELOCITIES IN M/S

0° YAW

POSITION	MEAN U	RMS U	SKEW U	TURB U	MEAN V	RMS V	SKEW V	TURB V	MEAN W	RMS W	SKEW W	TURB W
AMEN	2.019	0.097	0.141	0.048	0.175	0.088	0.164	0.505	0.108	0.095	0.002	0.882
1	0.836	0.04	-20.969	0.047	-0.001	0.024	-2.756	-17.157	-0.007	0.042	-7.263	-5.994
2	0.841	0.043	-15.672	0.051	-0.003	0.037	-5.438	-11.484	-0.016	0.062	-4.679	-3.962
3	0.846	0.053	-7.016	0.062	-0.005	0.047	-3.766	-9.356	-0.02	0.07	-3.865	-3.537
4	0.858	0.069	-0.999	0.08	-0.031	0.095	-3.055	-3.085	-0.005	0.068	-1.865	-14.934

30° YAW

POSITION	MEAN U	RMS U	SKEW U	TURB U	MEAN V	RMS V	SKEW V	TURB V	MEAN W	RMS W	SKEW W	TURB W
AMEN	1.842	0.107	-0.291	0.058	-0.089	0.097	-0.018	-1.08	0.266	0.105	-0.076	0.395
1	0.858	0.08	0.924	0.094	-0.025	0.109	-2.871	-4.295	0.001	0.073	-0.64	58.584
2	0.845	0.059	-4.267	0.069	-0.002	0.051	-4.571	-20.756	-0.022	0.087	-3.514	-3.859
3	1.36	0.321	0.095	0.236	-0.158	0.237	0.034	-1.631	0.099	0.216	0.017	2.187
4	1.729	0.19	0.118	0.11	-0.094	0.163	0.261	-1.723	0.278	0.125	0.084	0.449

50° YAW

POSITION	MEAN U	RMS U	SKEW U	TURB U	MEAN V	RMS V	SKEW V	TURB V	MEAN W	RMS W	SKEW W	TURB W
AMEN	1.933	0.108	-0.241	0.056	-0.109	0.1	-0.015	-0.917	0.3	0.097	0.013	0.323
1	1.735	0.323	-0.266	0.184	0.166	0.257	0.145	1.35	0.077	0.254	-0.168	3.282
2	1.33	0.372	0.365	0.28	-0.053	0.261	-0.225	-4.893	-0.06	0.271	0.017	-4.556
3	1.79	0.221	-0.556	0.123	-0.133	0.2	0.631	-1.51	0.165	0.164	0.392	0.998
4	1.824	0.174	-0.174	0.096	0.112	0.163	0.325	1.458	0.353	0.129	0.162	0.366

70° YAW

POSITION	MEAN U	RMS U	SKEW U	TURB U	MEAN V	RMS V	SKEW V	TURB V	MEAN W	RMS W	SKEW W	TURB W
AMEN	2.244	0.109	-0.317	0.048	0.167	0.113	0.028	0.674	0.351	0.104	-0.014	0.295
1	2.525	0.268	-0.384	0.106	0.262	0.272	0.172	1.04	0.065	0.207	0.632	3.196
2	2.188	0.297	-0.578	0.136	0.109	0.206	-0.04	2.617	-0.123	0.218	0.135	-1.697
3	2.232	0.241	-0.52	0.108	0.197	0.226	0.176	1.149	0.208	0.208	0.276	0.72
4	2.135	0.207	-0.262	0.097	0.398	0.2	0.081	0.503	0.546	0.178	0.224	0.326

90° YAW

POSITION	MEAN U	RMS U	SKEW U	TURB U	MEAN V	RMS V	SKEW V	TURB V	MEAN W	RMS W	SKEW W	TURB W
AMEN	2.327	0.12	-0.279	0.051	0.062	0.122	0.067	1.978	0.37	0.109	0.074	0.294
1	2.05	0.251	0.411	0.123	-0.221	0.368	0.936	-1.664	0.938	0.196	-0.904	0.208
2	1.606	0.362	-0.015	0.226	-0.016	0.385	0.291	-23.678	0.527	0.309	-0.825	0.586
3	1.803	0.154	-0.209	0.086	0.087	0.356	-0.014	4.092	0.843	0.126	-2.368	0.15
4	1.828	0.137	-0.113	0.075	0.098	0.331	-0.019	3.372	0.871	0.107	-0.45	0.122

110° YAW

POSITION	MEAN U	RMS U	SKEW U	TURB U	MEAN V	RMS V	SKEW V	TURB V	MEAN W	RMS W	SKEW W	TURB W
AMEN	1.709	0.144	0.487	0.084	-0.395	0.116	1.298	-0.292	0.803	0.107	-0.434	0.133
1	1.905	0.247	0.555	0.129	0.371	0.364	-0.845	0.981	0.773	0.218	-1.217	0.281
2	1.771	0.161	-0.683	0.091	0.053	0.328	-0.054	6.184	0.78	0.117	-1.633	0.15
3	1.709	0.123	-0.487	0.069	0.049	0.313	-0.022	6.364	0.863	0.084	-0.475	0.097
4	1.819	0.123	-0.179	0.067	0.145	0.296	-0.235	2.044	0.865	0.101	-0.659	0.117

APPENDIX G. LOOKUP TABLES FOR DYSCO FRA3 MODULE AND BLADE ELEMENT PROGRAM

MACH NO.	AOA (DEG)	LIFT COEFF.	DRAG COEFF.	MOMENT COEFF.
0.060	-180.00	0.000000	0.022000	0.000000
0.060	-176.40	-0.091100	0.049100	0.315800
0.060	-172.80	-0.035400	0.087300	0.417300
0.060	-169.20	0.152700	0.148200	0.384600
0.060	-165.60	0.367900	0.231100	0.305300
0.060	-162.00	0.570700	0.266200	0.290900
0.060	-158.40	0.734400	0.353300	0.315100
0.060	-154.80	0.863200	0.475100	0.349400
0.060	-151.20	0.952600	0.604700	0.383200
0.060	-147.60	0.997300	0.740700	0.415400
0.060	-144.00	1.013100	0.881500	0.445000
0.060	-140.40	1.031500	1.025800	0.470800
0.060	-136.80	1.043500	1.166400	0.491700
0.060	-133.20	1.039100	1.293900	0.507100
0.060	-129.60	1.008400	1.408400	0.519200
0.060	-126.00	0.951200	1.510200	0.528500
0.060	-122.40	0.881500	1.599400	0.535100
0.060	-118.80	0.801000	1.676900	0.539200
0.060	-115.20	0.710900	1.751000	0.541000
0.060	-111.60	0.612300	1.822000	0.540600
0.060	-108.00	0.506600	1.888200	0.538100
0.060	-104.40	0.394800	1.947900	0.533700
0.060	-100.80	0.278400	1.994300	0.527600
0.060	-97.20	0.158400	2.020500	0.519800
0.060	-93.60	0.036200	2.027700	0.510600
0.060	-90.00	-0.087100	2.022000	0.500000
0.060	-86.40	-0.210200	2.007900	0.488400
0.060	-82.80	-0.332000	1.985500	0.476000
0.060	-79.20	-0.451100	1.954300	0.462800
0.060	-75.60	-0.566400	1.915700	0.448700
0.060	-72.00	-0.676600	1.870300	0.433600
0.060	-68.40	-0.780500	1.817600	0.417500
0.060	-64.80	-0.876900	1.756600	0.400400
0.060	64.80	0.887100	1.757600	-0.400400
0.060	68.40	0.795200	1.818000	-0.417500
0.060	72.00	0.696100	1.870100	-0.433600
0.060	75.60	0.591000	1.915500	-0.448700
0.060	79.20	0.480800	1.954300	-0.462800
0.060	82.80	0.366600	1.985500	-0.476000
0.060	86.40	0.249400	2.007900	-0.488400
0.060	90.00	0.130300	2.022000	-0.500000
0.060	93.60	0.010200	2.027700	-0.510600
0.060	97.20	-0.109700	2.020500	-0.519800
0.060	100.80	-0.228400	1.994300	-0.527600
0.060	104.40	-0.344900	1.947900	-0.533700
0.060	108.00	-0.458100	1.888200	-0.538100

0.060	111.60	-0.567100	1.822000	-0.540600
0.060	115.20	-0.670800	1.751000	-0.541000
0.060	118.80	-0.768000	1.676900	-0.539200
0.060	122.40	-0.857900	1.599400	-0.535100
0.060	126.00	-0.939300	1.510200	-0.528500
0.060	129.60	-1.011100	1.408400	-0.519200
0.060	133.20	-1.063600	1.293900	-0.507100
0.060	136.80	-1.089900	1.166400	-0.491700
0.060	140.40	-1.087500	1.025800	-0.470800
0.060	144.00	-1.053800	0.881500	-0.445000
0.060	147.60	-0.986500	0.740700	-0.415400
0.060	151.20	-0.894500	0.604700	-0.383200
0.060	154.80	-0.791600	0.475100	-0.349400
0.060	158.40	-0.688600	0.353300	-0.315100
0.060	162.00	-0.602300	0.266200	-0.290900
0.060	165.60	-0.629600	0.231100	-0.305300
0.060	169.20	-0.722800	0.148200	-0.384600
0.060	172.80	-0.779900	0.087300	-0.417300
0.060	176.40	-0.550600	0.049100	-0.315800
0.060	180.00	0.000000	0.022000	0.000000

APPENDIX H. WAKE TURBULENCE MODELING FILTERS FOR 330° YAW

Pt. 1u	Zeroes	-0.2377	0.6911i	-0.7228	0.0000i	-0.2377	-0.6911i			Data for Point 6w same as 6v.							
K =		0.8765	0.0701i	0.8765	-0.0701i	-0.0214	0.0000i	Pt. 7u	Zeroes	-0.2400	0.6877i	-0.7246	0.0000i	-0.2400	-0.6877i		
22.3112	Poles	0.8900	0.0000i	-0.2381	0.6796i	-0.2381	-0.6796i	K =		0.9101	0.0000i	0.7963	0.0000i	-0.0498	0.0000i		
		-0.7482	0.0000i	-0.3573	0.0000i	0.1041	0.0000i	21.8265	Poles	0.8022	0.0000i	-0.2408	0.6758i	-0.2408	-0.6759i		
Pt 1v	Zeroes	0.8592	-0.0705i	0.8592	0.0705i	0.4642	0.000i			-0.7495	0.0000i	-0.3626	0.0000i	0.0787	0.0000i		
K =		-0.6735	0.0000i	0.4260	-0.2779i	-0.0426	0.2779i	Pt. 7v	Zeroes	-0.2400	0.6877i	-0.7246	0.0000i	-0.2400	-0.6877i		
14.595	Poles	0.8969	0.0000i	0.5154	0.0000i	-0.7068	0.0000i	K =		0.9101	0.0000i	0.7964	0.0000i	-0.0498	0.0000i		
		-0.4426	0.2828i	-0.4426	-0.2828i	-0.1054	0.0000i	21.8265	Poles	0.8023	0.0000i	-0.2408	0.6759i	-0.2408	-0.6759i		
Pt 1w	Zeroes	-0.7021	0.4390i	-0.7021	-0.4390i	-0.5936	0.0000i			-0.7495	0.0000i	-0.3626	0.0000i	0.0787	0.0000i		
K =		0.8762	-0.0394i	0.8762	0.0394i	0.2447	0.0000i	Pt. 7w	Zeroes	-0.2383	0.6905i	-0.7231	0.0000i	-0.2383	-0.6905i		
16.707	Poles	-0.7030	0.4355i	-0.7030	-0.4355i	0.9283	0.0000i	K =		0.8873	0.0000i	0.7094	0.0000i	-0.0264	0.0000i		
		-0.6873	0.0000i	0.2889	0.0000i	-0.1360	0.0000i	21.9524	Poles	0.7015	0.0000i	-0.2388	0.6778i	-0.2388	-0.6789i		
Pt. 2u	Zeroes	-0.2262	-0.6910i	-0.7220	0.0000i	-0.2262	0.6910i			-0.7484	0.0000i	-0.3583	0.0000i	0.0999	0.0000i		
K =		0.7830	0.0000i	0.5852	0.0000i	0.0793	0.0000i	Pt. 8u	Zeroes	-0.2400	0.6877i	-0.7246	0.0000i	-0.2400	-0.6877i		
26.5917	Poles	-0.2252	0.6745i	-0.2252	-0.6745i	-0.7475	0.0000i	K =		0.9101	0.0000i	0.7963	0.0000i	-0.0498	0.0000i		
		0.7088	0.0000i	-0.3566	0.0000i	0.3122	0.0000i	21.8265	Poles	0.8022	0.0000i	-0.2408	0.6759i	-0.2408	-0.6759i		
Pt. 2v	Zeroes	-0.2340	-0.6883i	-0.7271	0.0000i	-0.2340	0.6883i			-0.7495	0.0000i	-0.3626	0.0000i	0.0787	0.0000i		
K =		0.7977	-0.0000i	0.5497	0.0000i	0.0492	0.0000i	Pt. 8v	Zeroes	-0.2400	0.6877i	-0.7246	0.0000i	-0.2400	-0.6877i		
26.6721	Poles	-0.2343	0.6718i	-0.2343	-0.6718i	0.7107	0.0000i	K =		0.9101	0.0000i	0.7964	0.0000i	-0.0498	0.0000i		
		-0.7513	0.0000i	-0.3666	0.0000i	0.2572	0.0000i	21.8265	Poles	0.8023	0.0000i	-0.2408	0.6759i	-0.2408	-0.6759i		
Pt 2w	Zeroes	-0.2377	0.6911i	-0.7228	0.0000i	-0.2377	-0.6911i			-0.7495	0.0000i	-0.3626	0.0000i	0.0787	0.0000i		
K =		0.8765	0.0701i	0.8765	-0.0701i	-0.0214	0.0000i	Pt. 8w	Zeroes	-0.2383	0.6905i	-0.7231	0.0000i	-0.2383	-0.6905i		
22.3112	Poles	0.8900	0.0000i	-0.2381	0.6796i	-0.2381	-0.6796i	K =		0.8873	0.0000i	0.7094	0.0000i	-0.0264	0.0000i		
		-0.7482	0.0000i	-0.3573	0.0000i	0.1041	0.0000i	21.9524	Poles	0.7015	0.0000i	-0.2388	0.6789i	-0.2388	-0.6789i		
	Data for 3 u, 3v, 3w, 4u, 4v, 4w are the same as 2w									-0.7484	0.0000i	-0.3583	0.0000i	0.0999	0.0000i		
Pt. 5u	Zeroes	-0.2400	0.6877i	-0.7246	0.0000i	-0.2400	-0.6877i	Pt. 9u	Zeroes	-0.2400	0.6877i	-0.7246	0.0000i	-0.2400	-0.6877i		
K =		0.9101	0.0000i	0.7964	0.0000i	-0.0498	0.0000i	K =		0.9101	0.0000i	0.7964	0.0000i	-0.0498	0.0000i		
21.8265	Poles	0.8023	0.0000i	-0.2408	0.6759i	-0.2408	-0.6759i	21.8265	Poles	0.8023	0.0000i	-0.2408	0.6759i	-0.2408	-0.6759i		
		-0.7495	0.0000i	-0.3626	0.0000i	0.0787	0.0000i			-0.7495	0.0000i	-0.3626	0.0000i	0.0787	0.0000i		
Pt. 5v	Zeroes	-0.2377	0.6911i	-0.7227	0.0000i	-0.2377	-0.6911i	Pt. 9v	Zeroes	-0.2400	0.6877i	-0.7246	0.0000i	-0.2400	-0.6877i		
K =		0.8765	0.0701i	0.8765	-0.0701i	-0.0214	0.0000i	K =		0.9101	0.0000i	0.7963	0.0000i	-0.0498	0.0000i		
22.3112	Poles	0.8900	0.0000i	-0.2381	0.6796i	-0.2381	-0.6796i	21.8265	Poles	0.8022	0.0000i	-0.2408	0.6759i	-0.2408	-0.6759i		
		-0.7482	0.0000i	-0.3573	0.0000i	0.1041	0.0000i			-0.7495	0.0000i	-0.3626	0.0000i	0.0787	0.0000i		
	Data for Point 5, w as for Point 5, v							Pt. 9w	Zeroes	-0.2383	0.6905i	-0.7231	0.0000i	-0.2383	-0.6905i		
Pt. 6u	Zeroes	-0.2400	0.6877i	-0.7246	0.0000i	-0.2400	-0.6877i	K =		0.8873	0.0000i	0.7094	0.0000i	-0.0264	0.0000i		
K =		0.9101	0.0000i	0.7964	0.0000i	-0.0496	0.0000i	21.9524	Poles	0.7015	0.0000i	-0.2388	0.6789i	-0.2388	-0.6789i		
21.8265	Poles	0.8023	0.0000i	-0.2408	0.6759i	-0.2408	-0.6759i			-0.7484	0.0000i	-0.3583	0.0000i	0.0999	0.0000i		
		-0.7495	0.0000i	-0.3526	0.0000i	0.0787	0.0000i	Pt. 10u	Zeroes	-0.2396	0.6881i	-0.7243	0.0000i	-0.2396	-0.6881i		
Pt. 6v	Zeroes	-0.2378	0.6918i	-0.7225	0.0000i	-0.2378	-0.6918i	K =		0.9007	0.0000i	0.5314	0.0000i	-0.0463	0.0000i		
K =		0.8931	0.0000i	0.4844	0.0000i	-0.0103	0.0000i	21.8721	Poles	-0.2403	0.6763i	-0.2403	-0.6763i	-0.7492	0.0000i		
21.927	Poles	-0.2381	-.6804i	-0.2381	-0.6804i	-0.7480	0.0000i			0.5319	0.0000i	-0.3618	0.0000i	0.0815	0.0000i		
		0.4759	0.0000i	-0.3562	0.0000i	0.1179	0.0000i			Data for Point 10 v same as for 10u							

Pt. 10 w	Zeroes	-0.2386	0.6900i	-0.7234	0.0000i	-0.2386	-0.6900i
K =		0.8571	0.0268i	0.8751	0.0268i	-0.0316	0.0000i
22.0159	Poles	0.8255	0.0000i	-0.2392	0.6783i	-0.2392	-0.6783i
		-0.7486	0.0000i	-0.3592	0.0000i	0.0949	0.0000i
Pt. 11 u	Zeroes	-0.2400	0.6877i	-0.7245	0.0000i	-0.2400	-0.6877i
K =		0.9061	0.0000i	0.7503	0.0000i	-0.0497	0.0000i
21.8425	Poles	0.7537	0.0000i	-0.2408	0.6759i	-0.2408	-0.6759i
		-0.7494	0.0000i	-0.3626	0.0000i	0.0787	0.0000i
Pt. 11 v	Zeroes	-0.2396	0.6881i	-0.7243	0.0000i	-0.2396	-0.6881i
K =		0.9007	0.0000i	0.5314	0.0000i	-0.0463	0.0000i
21.8721	Poles	-0.2403	0.6763i	-0.2403	-0.6763i	-0.7492	0.0000i
		0.5319	0.0000i	-0.3618	0.0000i	0.0815	0.0000i
Pt. 11 w	Zeroes	-0.2386	0.6900i	-0.7234	0.0000i	-0.2386	-0.6900i
K =		0.8571	0.0268i	0.8571	-0.0268i	-0.0316	0.0000i
22.0159	Poles	0.8255	0.0000i	-0.2392	0.6783i	-0.2392	-0.6783i
		-0.7486	0.0000i	-0.3592	0.0000i	0.0949	0.0000i
Pt. 12 u	Zeroes	-0.2400	0.6877i	-0.7246	0.0000i	-0.2400	-0.6877i
21.8265		0.9101	0.0000i	0.7964	0.0000i	-0.0498	0.0000i
	Poles	0.8023	0.0000i	-0.2408	0.6759i	-0.2409	-0.6759i
		-0.7495	0.0000i	-0.3626	0.0000i	0.0787	0.0000i
Pt. 12 v	Zeroes	-0.2400	0.6877i	-0.7246	0.0000i	-0.2400	-0.6877i
K =		0.9097	0.0000i	0.7933	0.0000	-0.0498	0.0000i
21.8279	Poles	0.7989	0.0000i	-0.2408	0.6759i	-0.2408	-0.6759i
		-0.7495	0.0000i	-0.3626	0.0000i	0.0787	0.0000i
Pt. 12 w	Zeroes	-0.2377	0.6911i	-0.7228	0.0000i	-0.2377	-0.6911i
K =		0.8765	0.0701i	0.8765	-0.0701i	-0.0214	0.0000i
22.3112	Poles	0.8900	0.0000i	-0.2381	0.6796i	-0.2381	-0.6796i
		-0.7482	0.0000i	-0.3573	0.0000i	0.1041	0.0000i
Pt. 13 u	Zeroes	-0.2400	0.6877i	-0.7246	0.0000i	-0.2400	-0.6877i
K =		0.9101	0.0000i	0.7964	0.0000i	-0.0498	0.0000i
21.8265	Poles	0.8023	0.0000i	-0.2408	0.6759i	-0.2408	-0.6759i
		-0.7495	0.0000i	-0.3626	0.0000i	0.0787	0.0000i
Pt. 13v	Zeroes	-0.2400	0.6877i	-0.7246	0.0000i	-0.2400	-0.6877i
K =		0.9100	0.0000i	0.7959	0.0000i	-0.0498	0.0000i
21.8267	Poles	0.8018	0.0000i	-0.2408	0.6759i	-0.2408	-0.6759i
		-0.7495	0.0000i	-0.3626	0.0000i	0.0787	0.0000i
Pt. 13w	Zeroes	0.-2386	0.6900i	-0.7234	0.0000i	-0.2386	-0.6900i
K =		0.8571	0.0268i	0.8571	-0.0268i	-0.0316	0.0000i
22.0159	Poles	0.8255	0.0000i	-0.2392	0.6873i	-0.2392	-0.6783i
		-0.7486	0.0000i	-0.3592	0.0000i	0.0949	0.0000i
Pt. 14 u	Zeroes	-0.2400	0.6877i	-0.7246	0.0000i	-0.2400	-0.6877i
K =		0.9101	0.0000i	0.7964	0.0000i	-0.0498	0.0000i
21.8265	Poles	0.8023	0.0000i	-0.2408	0.6759i	-0.2408	-0.6759i
		-0.7495	0.0000i	-0.3626	0.0000i	0.0787	0.0000i

Pt. 14 v	Zeroes	-0.2400	0.6877i	-0.7246	0.0000i	-0.2400	-0.6877i
K =		0.9101	0.0000i	0.7963	0.0000i	-0.0498	0.0000i
21.8265	Poles	0.8022	0.0000i	-0.2408	0.6759i	-0.2408	-0.6759i
		-0.7495	0.0000i	-0.3626	0.0000i	0.0787	0.0000i
Pt. 14w	Zeroes	-0.2396	0.6881i	-0.7243	0.0000i	-0.2396	-0.6881i
K =		0.9007	0.0000i	0.5314	0.0000i	-0.0463	0.0000i
21.8721	Poles	-0.2403	0.6763i	-0.2403	-0.6763i	-0.7492	0.0000i
		0.5319	0.0000i	-0.3618	0.0000i	0.0815	0.0000i
Pt. 15 u	Zeroes	-0.2400	0.6877i	-0.7246	0.0000i	-0.2400	-0.6877i
K =		0.9101	0.0000i	0.7964	0.0000i	-0.0498	0.0000i
21.8265	Poles	0.8023	0.0000i	-0.2408	0.6759i	-0.2408	-0.6759i
		-0.7495	0.0000i	-0.3626	0.0000i	0.0787	0.0000i
Pt. 15 v	Zeroes	-0.2400	0.6877i	-0.7246	0.0000i	-0.2400	-0.6877i
K =		0.9097	0.0000i	0.7933	0.0000i	-0.0498	0.0000i
21.8279	Poles	0.7989	0.0000i	-0.2408	0.6759i	-0.2408	-0.6759i
		-0.7495	0.0000i	-0.3626	0.0000i	0.0787	0.0000i
Pt. 15 w	Zeroes	0.8976	0.0000i	-0.2386	-0.6923i	-0.7221	0.0000i
K =		-0.2386	0.6923i	0.0503	-0.0725i	0.0503	0.0725i
21.8961	Poles	-0.2391	0.6810i	-0.2391	-0.6810i	-0.7477	0.0000i
		-0.3539	0.0000i	0.1100	0.0955i	0.1100	-0.0955i
Pt. 16 u	Zeroes	-0.2400	0.6877i	-0.7246	0.0000i	-0.2400	-0.6877i
K =		0.9101	0.0000i	0.7964	0.0000i	-0.0498	0.0000i
21.8265	Poles	0.8023	0.0000i	-0.2408	0.6759i	-0.2400	-0.6759i
		-0.7495	0.0000i	-0.3626	0.0000i	0.0787	0.0000i
Pt. 16 v	Zeroes	-0.2400	0.6877i	-0.7246	0.0000i	-0.2400	-0.6877i
K =		0.9101	0.0000i	0.7963	0.0000i	-0.0498	0.0000i
21.8265	Poles	0.8022	0.0000i	-0.2408	0.6759i	-0.2400	-0.6759i
		-0.7495	0.0000i	-0.3626	0.0000i	0.0787	0.0000i
Pt. 16w	Zeroes	-0.2387	0.6899i	-0.7235	0.0000i	-0.2387	-0.6899i
K =		0.8705	0.0444i	0.8705	-0.0444i	-0.0319	0.0000i
22.0645	Poles	0.8567	0.0000i	-0.2392	0.6783i	-0.2392	-0.6783i
		-0.7487	0.0000i	-0.3592	0.0000i	0.0946	0.0000i
Pt. 17u	Zeroes	-0.2400	0.6877i	-0.7246	0.0000i	-0.2400	-0.6877i
K =		0.9101	0.0000i	0.7964	0.0000i	-0.0498	0.0000i
21.8265	Poles	0.8022	0.0000i	-0.2408	0.6759i	-0.2400	-0.6759i
		-0.7495	0.0000i	-0.3626	0.0000i	0.0787	0.0000i
Pt.17 v	Zeroes	-0.2396	0.6881i	-0.7243	0.0000i	-0.2396	-0.6881i
K =		0.9007	0.0000i	0.5314	0.0000i	-0.0463	0.0000i
21.8721	Poles	-0.2403	0.6763i	-0.2403	0.6763i	-0.7492	0.0000i
		0.5319	0.0000i	-0.3618	0.0000i	0.0815	0.0000i
Data for Point 17w same as for Point 16w.							

LIST OF REFERENCES

1. Healey, J.V., *Simulating the Helicopter-Ship Interface as an Alternative to Current Methods of Determining the Safe Operating Envelopes.*,Naval Postgraduate School Report, NPS 67-86-003, Monterey, California, September 1986.

2. Fortenbaugh, R.L., *Mathematical Models for the Aircraft Operational Environment of DD-963 Class Ships*, Vought Corp., Dallas, Texas Rep. No. 2-55800/8R-3500, 1978.

3. Department of Defense Military Specification MIL-F-8785C (DoD), *Flying Qualities of Piloted Aircraft*, 1980

4. Hanson, G.D., *Airwake Analysis*, Systems Technology, Inc., Working Paper No. 1198-3, September 1983.

5. Rhoades, M., *A Study of the Airwake Aerodynamics Over the Flight Deck of an AOR Model Ship*, M.S. Thesis, Naval Postgraduate School, Monterey, California , September 1990.

6. Anderson, G. *Mapping the Airwake of a Model DD-963 Along Specific Helicopter Flight Paths*, M.S. Thesis, Naval Postgraduate School, Monterey , California, December 1989.

7. Leone, P.F., "Theoretical and Experimental Study of the Flap Droop Stop Impact Transient Aero-Elastic Response of a Helicopter Rotor Blade", *Journal of the American Helicopter Society*, vol. 9, January 1964.

8. Garnett, T.S., Jr., *Investigation to Study the Aerodynamic Ship Wake Turbulence Generated by a FF 1052 Frigate* Contract No. N00019-75-C-0493, Report D210-11140-1 Boeing Vertol Company, December 1976.

9. Garnett, T.S., Jr., *Investigation to Study the Aerodynamic Ship Wake Turbulence Generated by a DD-963 Destroyer*, Boeing Vertol Report D210-11545-1, August 1979.

10. Nave, Ronald L., *Development and Analysis of a CVA and 1052 Class Fast Frigate Airwake Model*, Final Airtask No. WF-41-400-000, Naval Air Development Center, 30 Sep. 1978.

11. Healey, J.V., "Establishing a Data Base for Flight in the Wakes of Structures", to be published in the AIAA Journal of Aircraft., Jan/Feb 1992.

12. Talbot, P.D., B.E. Tinling, W.A. Decker, R.T.N. Chen, *A Mathematical Model of a Single Main Rotor Helicopter for Piloted Simulation*, NASA TM 84281, September 1982.

13. Wake, B.E., L.N. Sankar, "Solutions of the Navier-Stokes Equations for the Flow About a Rotor Blade", *Journal of the American Helicopter Society*, v.34, pp. 13-23, April 1989.

14. Huber, H., J. Dahl, A. Inglsperger, *Advanced Flight Simulation for Helicopter Development*, AGARD CP 359, 1985.

15. Dahl, H.J., A.J. Faulkner, "Helicopter Simulation in Atmospheric Turbulence", *Vertica*, v.3, pp. 65-78, 1979.

16. Leone, P.F., *Analytic Correlation with Mishap Report of a CH-46D Aft Rotor Blade Tunnel Strike Induced by a Wind Flow Up Through the Aft Rotor Disk During a Start-up Operation While at Sea.*, Boeing Helicopter Company Report 8-7450-PFL-06, April 1982.

17. Johns, M. K., *Flow Visualization of the Airwake Around a Model of a DD-963 Class Destroyer in a Simulated Atmospheric Boundary Layer*, M.S. Thesis, Naval Postgraduate School, Monterey, Ca., September 1988.

18. Berman, A., S. Chen, B. Gustavson, P. Hurst, *Dynamic System Coupler Program (DYSCO 4.1), Volume I: Theoretical Manual*, Kaman Aerospace Corporation, Bloomfield, CT, September 1989.

19. Berman, A., S. Chen, B. Gustavson, P. Hurst, *Dynamic System Coupler Program (DYSCO 4.1), Volume II: User's Manual*, Kaman Aerospace Corporation, Bloomfield, CT., September 1989.

20. Miley, S.J., *A Catalog of Low Reynolds Number Airfoil Data for Wind Turbine Applications*, Texas A&M University, College Station, Texas, February 1982.

21. Freidland, B., *Control System Design*, McGraw-Hill Co., 1986.

22. NAVAIR A1-H46AE-GAI-000, Organizational and Intermediate Maintenance Manual, CH-46D/E, August 1990.

INITIAL DISTRIBUTION LIST

		No. Copies
1.	Defense Technic: Information Center Cameron Station Alexandria, VA 22304-6145	2
2.	Library, Code 52 Naval Postgraduate School Monterey, CA 93943-5002	2
3.	Commandant of the Marine Corps Code TE 06 Headquarters, U.S. Marine Corps Washington, D.C. 20380-0001	1
4.	Department Chairman, Code AA Department of Aeronautics and Astronautics Naval Postgraduate School Monterey, California 93943-5000	1
5.	Dr. J. Val Healey, Code AA/He Department of Aeronautics and Astronautics Naval Postgraduate School Monterey, California 93943-5000	3
6.	Dr. E. R. Wood, Code AA/Wd Department of Aeronautics and Astronautics Naval Postgraduate School Monterey, California 93943-5000	1
7.	Robert D. Moran, Jr. 579-H Wilkes Lane Monterey, Ca. 93940	2